

Aus dem Institut für Neuroanatomie
der medizinischen Fakultät Mannheim
Direktor: Prof. Dr. med. Christian Schultz

in Kooperation mit

dem Laboratoire nationale de la santé
und dem Luxembourg Center of Systems Biomedicine
der Universität Luxemburg

Expression of ErbB4 in astrocytes of human hippocampus
samples and in murine primary astrocyte culture

Inauguraldissertation
zur Erlangung des medizinischen Doktorgrades
der
Medizinischen Fakultät Mannheim
der Ruprecht-Karls Universität
zu
Heidelberg

vorgelegt von:
Simon Uwe Mangold
aus
Villingen-Schwenningen
2022

Dekan: Prof. Dr. med. Sergij Goerd
Referent: Prof. Dr. med. Christian Schultz

Contents

List of abbreviations	1
1 Introduction	4
1.1 Alzheimer's disease	4
1.2 The neuropathology of dementia	5
1.2.1 The biochemical, cellular and clinical phase	7
1.3 Neuroinflammation and glial activation	10
1.3.1 Reactive astrocytes and astrogliosis	11
1.4 Anatomy of the hippocampus	12
1.5 The family of the epidermal growth factor receptors	14
1.6 ErbB4 signalling in AD	16
1.6.1 Neuregulins: important ligands of the ErbB receptors	17
1.7 ErbB4 knock-out mice	19
1.8 Impaired ErbB4-Neuregulin signalling	20
1.9 Proinflammatory pathways linked to ErbB4	21
1.10 ErbB4 and cell growth	22
1.11 Astroglial ErbB4-NRG expression	23
1.12 Aim of this study	24
2 Materials and Methods	25
2.1 Human brain samples	27
2.1.1 Semiquantitative analysis	31
2.2 Cell culture	32
2.2.1 Murine C8-D1A immortalized astrocytes	32
2.2.2 Murine primary astrocytes	33

2.2.3	Human induced pluripotent stem cell (iPCS) astrocyte culture	35
2.2.4	Immunofluorescence	35
2.2.5	Protein extraction, gel electrophoresis and western blotting	36
2.2.6	RNA extraction, cDNA and qPCR analysis	37
2.3	Analysis of immunofluorescence by quantification of pixel intensity	39
2.4	Fiji macro	40
2.4.1	Statistical analysis	42
3	Results	43
3.1	ErbB4 immunofluorescence in control condition	43
3.1.1	Mouse and rat control cortex	46
3.2	ErbB4 immunofluorescence in AD	47
3.3	ErbB4 immunofluorescence in dementia with Lewy bodies (DLB) and Glioblastoma (GB)	53
3.4	ErbB4 immunofluorescence in-vitro	57
3.4.1	Murine C8-D1A immortalized astrocyte culture	58
3.4.2	Murine primary astrocyte culture	59
3.4.3	Human iPSC astrocyte culture	62
3.5	Quantitative analysis	62
3.5.1	Digital fluorescence analysis on human samples	63
3.5.2	Western blot	64
3.5.3	qPCR	66
4	Discussion	67
4.1	ErbB4 overexpression in reactive astrocytes	67
4.2	Correlation of ErbB4 and GFAP	70
4.3	Digital image analysis	74
4.4	ErbB4 and inflammatory pathways	76
4.5	ErbB4 cell specificity and distribution	78

4.6	Regulation of ErbB4 inhibitory signalling	80
4.7	Growth factor receptors and Glioblastoma	82
4.8	ErbB4 in dementia with Lewy bodies	83
4.9	Astrocyte culture and 24 h treatments	84
4.10	Open questions for future ErbB4 expression analyses	87
5	Summary	88
6	Supplemental materials	90
6.1	Primary murine culture treatments	90
6.2	ImageJ Macro	91
	List of Figures	95
	List of Tables	96
	Bibliography	97
	Curriculum vitae	112
	Acknowledgments	113

List of abbreviations

AD	Alzheimer's disease
ADAM	A disintegrin and metalloproteinase
AICD	Amyloid precursor protein intracellular domain
APP	Amyloid precursor protein
CA	Cornu ammonis
CFTR	cystic fibrosis transmembrane conductance regulator
CNS	central nervous system
CERAD	Consortium to Establish a Registry for Alzheimer's Disease
COX2	Cyclooxygenase 2
CSF	cerebrospinal fluid
CTL	control
CYT	cytoplasmic
DG	dentate gyrus
DLB	dementia with Lewy bodies
DSM	Diagnostic and statistical manual of mental disorders
E4ICD	ErbB4 intracellular domain
EGFR	epidermal growth factor receptors
ErbB	erythroblastic leukemia viral oncogene
FAD	familial Alzheimer disease
FL	frontal lobe
FTP	frontotemporal dementia
FPKM	fragments per kilobase of transcript per million fragments mapped

GB	Glioblastoma
GFAP	glial fibrillary acidic protein
GLAST	glutamate aspartate transporter
GLT1	glutamate transporter 1
GOI	gene of interest
GWAS	genome-wide association studies
HER	human epidermal growth factor receptors
ICD	intracellular domain
IHC	immunohistochemistry
iPSC	induced pluripotent stem cells
JM	juxtamembranous
LOAD	late-onset Alzheimer disease
LOAD+P	late-onset Alzheimer disease with psychotic symptoms
LTP	long term potentiation
MACS	magnetic cell sorting
MAPT	microtubule-associated protein tau
MMSE	mini mental status examination
MPFC	medial prefrontal cortex
MW	multi well plate
NFT	neurofibrillary tangles
NRG	neuregulin
PBS	phosphate-buffered saline
PDD	Parkinsons' disease dementia

PFA	paraformaldehyde
PLL	pellet
PV	parvalbumin
ROI	regions of interest
RT	room temperature
RP	recombinant protein
SN	supernatant
SST	somatostatin
TACE	tumor necrosis factor alpha-converting enzyme
TB	total brain
TMD	transmembranous domain
TNF	tumor necrosis factor
WB	western blot

1 Introduction

1.1 Alzheimer's disease

Alzheimer's disease is the most prevalent neurodegenerative disease of the worldwide growing aged population. With a total of 50-70% of all diagnoses of dementia, it is the most common cause of the dementia syndrome. It affected 47 million people around the globe in 2015 and is expected to reach at least 75 million by 2050 [1]. The high economic burden is mostly carried by the family and health care system and is estimated to be 27 fold compared to non-demented people [2].

According to the International classification of disease (ICD) 10 standards (F00-F03), dementia is defined as a syndrome combination of symptoms affecting following brain functions: long-, short-term and episodic memory, disorientation, cognitive decline, changes in personality and speech, impaired judgement, comprehension, emotional regulation, social behaviour and motivation with a minimum duration of six months.

In the Diagnostic and statistical manual of mental disorders (DSM) 5, dementia is redefined as a group of neurocognitive disorders with different causes: Alzheimer's disease (AD), Dementia with Lewy bodies DLB, M. Pick/frontotemporal dementia, vascular dementia, Parkinsons' disease dementia (PDD) and diagnostic criterias like complex attention, executive functions, learning and memory, speech, social cognitions, perceptual and motor functions. AD is categorized in the Late Onset (LOAD, 95% of the cases) and the familial, autosomal, dominant form (FAD, ~5% of the cases) [3].

Characteristic for AD is subtle beginning and continuous progress of dementia, which can be categorized in the Late Onset (LOAD, 95% of the cases) and the familial, autosomal, dominant form (FAD, ~5% of the cases) [3]. The early form usually goes along with loss of higher cognitive functions and a faster progression, whereas the LOAD form progresses slower with impaired consolidation of memory as its main symptom and is supposed to be linked to mutations of different genes Amyloid precursor protein (APP) and APOE, whereas the sporadic form is more associated to genes presenilin 1 and 2 [4], [2].

The progress of AD can clinically be staged in three phases by testing the patients' score of correct answers in the mini mental status examination (MMSE) (<10 / <20 / >20), a standardized survey of 30 tasks and questions to evaluate potential cognitive deficits.

1.2 The neuropathology of dementia

The neuropathological classification of misfolded aggregated proteins, can be divided in two main groups: Gain-of-toxic and loss-of-function. In Gain-of-toxic diseases proteins are misfolded, aggregate, finally leading to cell death with clinical symptoms according to the brain region of the affected cells. Mucoviscidosis serves as an example for loss-of-function where the cystic fibrosis transmembrane conductance regulator (CFTR) gene mutation, misfolding and degradation cause clinical symptoms due to its lack [5].

In prion diseases, like Creutzfeld-Jakob Disease or Kuru, together grouped as gain-of-toxic diseases, misfolded proteins cause other correctly folded proteins to misfold thus forming a self-amplifying cascade that renders other proteins misfolded. As soon as the amount of protein degradation capability is exceeded,

the aggregation becomes toxic and leads to cell-cell transmission and further cell death. Based on this distinct spread mechanisms a potential underlying prion-like pathomechanism for diseases like Huntington disease, Parkinson's disease or frontotemporal dementia has been discussed [6]. In AD the so called neuropathological hallmark of the progressive neurodegenerative disease is characterized by the accumulation of two different peptides: extracellular APP processed to $A\beta$ plaques and intracellular neurofibrillary tangles (NFT) consisting of abnormally phosphorylated tau protein. APP (753–770 amino acids) is cleaved by β - and γ -secretase to form the $A\beta$ peptide with either 40 or 42 aminoacids, depending on the cleavage [7]. The peptide folds into 4-8 β -sheets that aggregate to fibrils that form macroscopically visible plaques. Clearance of these aggregates by microglia and to a lesser extent by astrocytes comes within limits, as these aggregates are highly resistant to cleavage [8].

The tau peptide (352-441 amino acids), encoded by the "Microtubule-associated protein tau" (MAPT) gene on chromosome 17, binds and stabilizes microtubules to regulate axonal dynein/kinesin transport in neurons [9]. In pathological condition, tau hyperphosphorylation through the activity of a variety of different kinases and phosphatases leads to the aggregation of paired helical filaments and finally of NFT, neuropil threads or dystrophic neurites near $A\beta$ plaques [9], [10]. Once it is oligomerized, phospho-tau (P-tau) loses its original function to stabilize the formation of microtubules. It is then able to sequestrate and induce normal tau proteins to misfold and aggregate [10]. Finally this leads to the disruption of microtubules and axonal transport with toxic aggregation of NFT throughout the cell and can even be detected in the CSF of AD patients [4], [11]. The precise mechanism of the interaction of NFT and $A\beta$ plaques is still under discussion, and not yet clearly determined [12].

Activated glia cells form clusters around plaques and apoptotic neurons. The induction of reactive gliosis e.g. around plaques is accompanied by extensive neuroinflammation [13]. Synaptic toxicity, synaptic loss and finally neuronal death lead to cerebral atrophy and dysfunction with the clinical symptoms of dementia [14]. Final stages are macroscopically characterized by brain atrophy most prominent in medial temporal (hippocampus), frontal and occipital lobe [15].

1.2.1 The biochemical, cellular and clinical phase

The progression and complexity of the pathological processes, can be separated into three different phases: The biochemical phase characterized by accumulation of APP/A β and NFT, the following cellular response in the tissue (cellular phase) and the final clinical phase of dementia (see figure 1.1, [14]).

Between the biochemical, proteopathic phase and final, irreversible clinical symptoms lie complex cellular compensatory responses as shown in figure 1.1. As a multifactorial approach, the inflammatory response of microglia and astrocytes to proteopathic stress in self-amplifying, apoptotic cascades is regarded as the most important cause for the neuronal cell death and final clinical stages [14]. Further, the cellular phase reflects the potential cause of different neurological, psychiatric symptoms of AD as a consequence of inflammation and dysbalanced signalling of glia and neurons. As this study later on focusses on the growth factor receptor protein expression of astrocytes in AD, it is first important to understand the different pathological factors which interfere in the early stages of the disease.

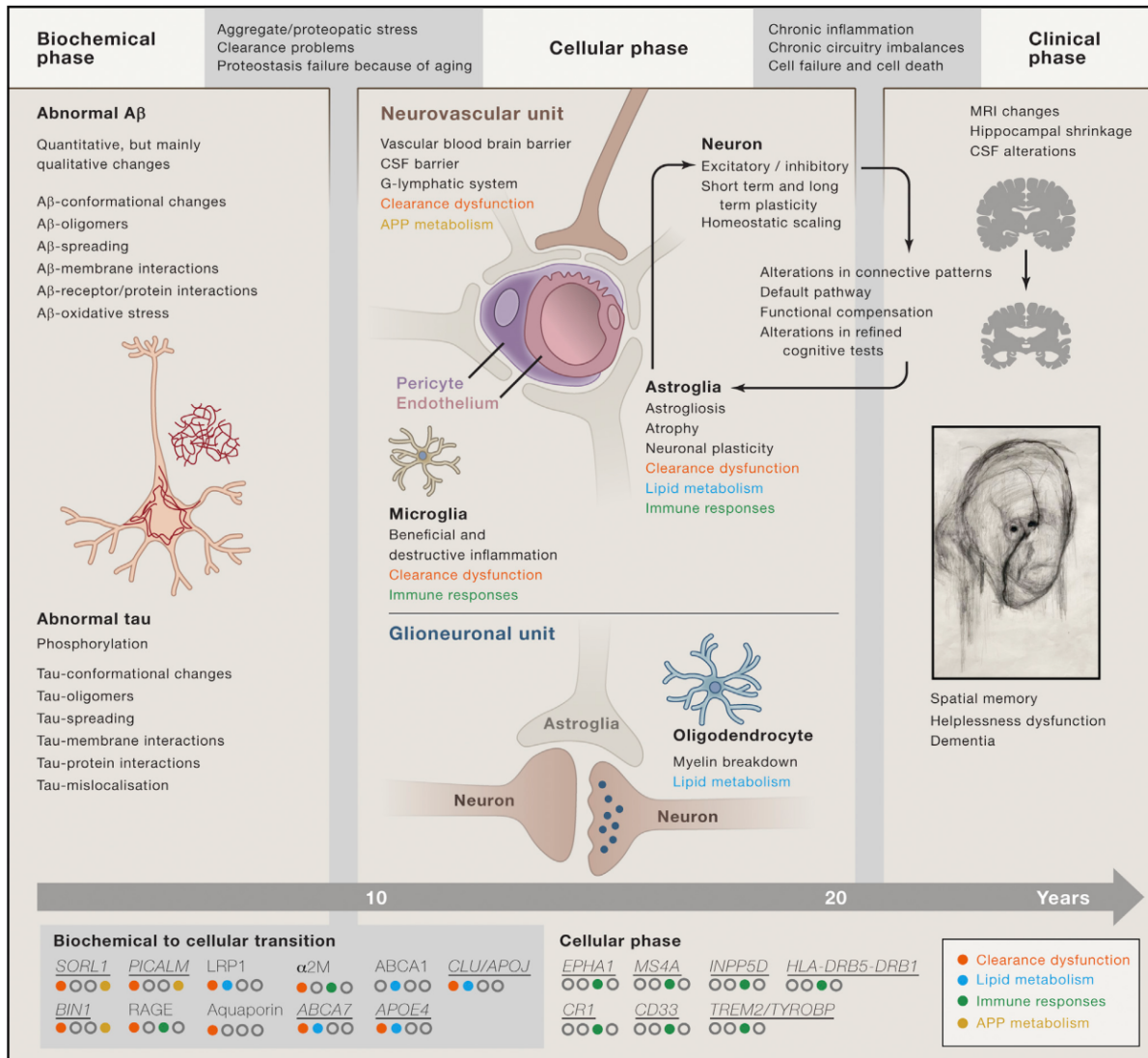


Figure 1.1: The biochemical phase on the left side of the figure with accumulation of phosphorylated tau and $A\beta$ accumulation. On the bottom of the figure, different genetic risk factors are displayed with different functions as indicated by the colored dots on the right bottom. The second phase is located in the middle, where different cell types and their impaired physiology is illustrated. The final phase is illustrated on the right side, with macroscopic changes of the brain and neurological symptoms [14].

Concerning the first biochemical or neuropathological phase, different methods of staging have been established in the past decades. Current guidelines of the National Institute on Aging-Alzheimer’s association for neuropathological assessment propose the "ABC" stage to evaluate the load of (A) $A\beta$, (B) NFT and

(C) neuritic plaques [16]. This includes the previous work of Braak & Braak [15], Thal [17] and the Consortium to Establish a Registry for Alzheimer’s Disease (CERAD) protocol [18], see below table 1.1, and 2.4 applied for human brain samples from this work. The different Thal phases classify the distribution of A β deposition in different brain regions.

A	Thal phase for Aβ plaques [17]	B	Braak & Braak NFT stage [15]	C	CERAD neuritic plaque score [18]
0	0	0	None	0	None
1	1 or 2	1	I or II	1	Sparse
2	3	2	II or III	2	Moderate
3	4 or 5	3	V or VI	3	Frequent

Table 1.1: The summarized ABC score for neuropathological changes in AD, from [16]. The three most established and internationally acknowledged staging methods, including different hallmarks of AD neuropathology (A, B, C) were unified in scores from 0 to 3. Column A: Thal phases of A β plaque distribution, B: Braak & Braak NFT staging, C: CERAD neuritic plaque score.

In the first phase the cortex is affected with preferential involvement of allocortical regions in phase II. Phase three is characterized by deposition in the diencephalon and striatum, together with nuclei of the brain stem in phase four. The final fifth phase includes the occurrence in the cerebellum and other brain areas. The CERAD protocol categorizes the density of neuritic plaques in several regions of neocortex (entorhinal cortex, midfrontal cortex, middle temporal cortex, inferior parietal cortex). The staging by Braak & Braak analyzes the distribution of NFT in different brain areas by the definition of five phases. Phase one and two with affection of the entorhinal cortex, stages III and IV with limbic regions (e.g. the hippocampus), and five and six including the neocortex.

Even though high proteopathic load with high ABC scores correlates with the occurrence of dementia, it is not regarded as a deterministic hypothesis [14], [15]. The translational impact of hypotheses that regard the proteopathic load as monocausal did not end up in successful, therapeutical cures [19]. The German medical guidelines recommend treatment with neurotransmission modulators like choline esterase inhibitors and NMDA receptor antagonist Memantin at severe, later stages of AD (evidence level 1a), although effects remain limited with no effects on the progression [2]. Furthermore high $A\beta$ load and some extent of tau deposition seems to be common for aging [20] and moreover the amount of reactive glia cells is supposed to have a higher correlation to dementia compared to load of $A\beta$ or NFT [21]. This points towards the need to better understand additional e.g. genetic risk factors of glia cells and their different inflammatory responses as a major contribution factor.

1.3 Neuroinflammation and glial activation

As displayed in Figure 1.1 the proteopathic load leads to an inflammatory cellular response, a final stage of cell death which further leads to the induction of inflammatory responses by microglia and astrocytes which lead to cell death and to a cascade of amplified inflammatory responses including IL6, IL1 β , C3/C1q, COX2 and TNF α and apoptotic markers like Cleaved Caspase 3 and Fas9 [22]. These pathological conditions lead to a change of morphology and expression profile of mediating glial cells. In the lower part of figure 1.1, crucial genetic risk factors are displayed to show the broad range of dysbalanced immune response, APP and lipid metabolism and their respective clearance mechanisms, where microglia and

astrocytes are involved. Microglia are able to induce neurotoxic astrocytes [23] and play a major role in the mediation of synapse loss [24].

1.3.1 Reactive astrocytes and astrogliosis

The astrocyte is a highly abundant cell type in the human brain. Developmentally, it originates from the ectoderm, and is derived from the neuroepithelium [25]. As a scaffolding cell it is involved in different pivotal pathways like the genesis and homeostasis of synapses, ion balance and the secretion and recycling of neuro- and gliatransmitters, trophic support for neurons, the formation of the blood-brain-barrier and the glial scar to separate healthy from damaged tissue and the integration and processing of extracellular signalling [26].

In disease conditions astrocytes are able to react in a regulative response. The detrimental or protective effects of this reaction is designated by the terms astrogliosis or reactive astrocytosis. This refers to a change in cellular gene expression which is further reflected in a different composition of translated receptor proteins in the cells membrane, e.g. by glial fibrillary acidic protein (GFAP) up-regulation [27], [28]. The induction of the reactive state of astrocytosis can be mediated by different cytokines e.g. from microglia [23] and many other extracellular, inflammatory molecules like $\text{TNF}\alpha$, IL6 or $\text{IL1}\beta$, which are also upregulated in other neurodegenerative/-inflammatory diseases and hence are used to mimic AD conditions for in-vitro experiments [29].

1.4 Anatomy of the hippocampus

The medial temporal lobe, which contains the hippocampus as an important hub of memory consolidation is often severely affected in AD. Therefore, it is important to have a profound anatomical and physiological knowledge of the different sectors and projections of the hippocampus to better understand the symptoms of dementia in AD.

As part of the phylogenetically older archicortex, the hippocampus consists of two major parts: the dentate gyrus (DG) and the Cornu ammonis (CA). During development, the CA (in grey) and DG (dotted) roll up as U-shapes inside each other (figure 1.2). Each lamina of the archicortex is made up of a group of three layers, divided in six layers in the CA. The hippocampus is folded into the entorhinal cortex, from where most of the neuronal input originates. The vulnerability and therefore rate of neuronal death and gliosis in AD differ between the CA sectors of the hippocampus. Until now, CA1 is supposed to be most vulnerable and CA3 most resistant in cytotoxic conditions like hypoxia and other neuropathological conditions [30]. Therefore it is important to highlight that CA structures differ in their ability to compensate cytotoxic stress, as this thesis in part focuses on the CA1 sector. The CA1 sector, also called the Sommer's sector, is supposed to be an import hub for corticocortical in- and output. Axons from CA1 form most of the output via the alveus that is continued by the fimbria-fornix pathway.

Further circuits throughout the brain consolidate short- to longterm memory as a part of the Papez' circuit. In figure 1.3 the pathways between the different brain

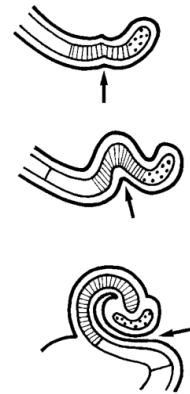


Figure 1.2: The hippocampus during cerebral development. Arrow points towards medial part [30].

regions are illustrated, providing a connection to the hippocampus to almost all brain areas. A: (1) hippocampus → (2) fornix → (3) mamillary bodies → (4) mammillothalamic tract → (5) thalamus → (6) cingulate gyrus → (7) cingulum → (8) parahippocampal gyrus and perforant pathway).

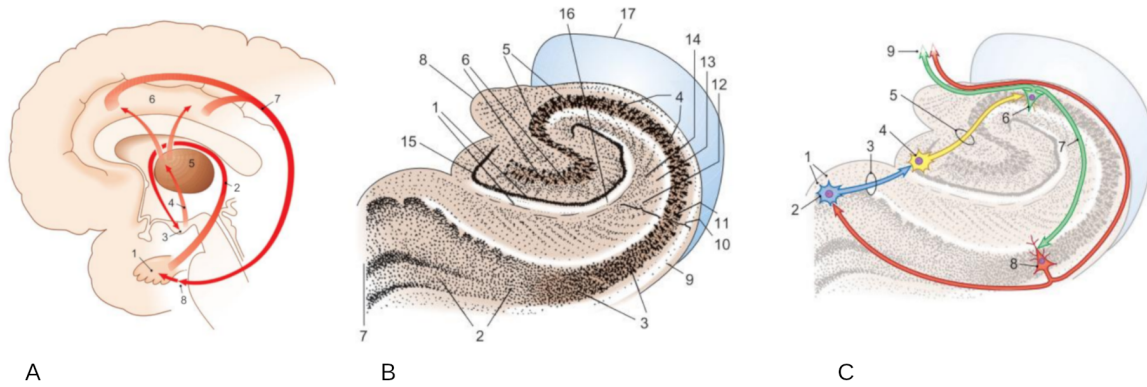


Figure 1.3: Archicortex of the hippocampus, coronal section, picture A, Papez' circuit, 1: Hippocampus, 2: Fornix, 3: Mamillary bodies, 4: Mammillothalamic tract, 5: Thalamus, 6: Cingulate gyrus, 7: Cingulum, 8: Parahippocampal gyrus, 9: Perforant pathway. Picture B: layers of the hippocampus, 1: Dentate gyrus, 2: Subiculum, 3: CA1, 4: CA2, 5: CA3, 6: CA4, 7: Entorhinal cortex, 8: hippocampal fibers, 9: Alveus, 10: Stratum oriens, 11: Stratum pyramidale, 12: Stratum moleculare, 13: Radiate layer, 14: Lacunar layer, 15: Granular layer, 16: Molecular layer, 17: lateral ventricle. Picture C, projections of hippocampal neurons: 1: Entorhinal cortex, 2: Pyramidal cells of the parahippocampal gyrus, 3: Perforant pathway, 4: granular cells, dentate gyrus, 5: mossy fibers, 6: pyramidal cells of CA3, 7: projections between CA3 and CA1, 8: pyramidal neuron in CA1, 9: hippocampal fibers, [31].

Memory consolidation as described above is the result of a neuronal network that loops, connects, amplifies and inhibits afferent excitations from and to the cortex. It is differentiated in a direct, perforant path and a polysynaptic path. Pyramidal cells from the entorhinal cortex of the parahippocampal gyrus (Figure 1.3, C, 2) project to the subiculum through the perforant pathway (3) into the hippocampus to the molecular layer where they contact distal dendrites from the granule cells of the dentate gyrus (4). Their efferent projections reach the pyramidal cells in CA3 sector (6) via the mossy fibers (5). These pyramidal cells from CA3 connect

to CA1 passing via the Schaffer collaterals, which project back to the entorhinal cortex through the subiculum thus establishing an excitatory loop. The repetition and amplification of stimuli by this loop leads to changes of synaptical receptor protein expression as a major prerequisite for neuronal plasticity and learning, referred to as long term potentiation (LTP) [31], [32]. Efferent projections from pyramidal neurons of CA1-3 leave the hippocampus as fimbria-fornix pathway shaping the fornix to connect back to other brain regions via the Papez' circuit [31].

Taken together, the hippocampus constitutes a hub for a vast number of neuronal projections to and from different cortical regions connected through the CA sectors of the hippocampus, emerging to the complex phenomenon of memory. This detailed description displays the high number of different neuronal and glial subpopulations in the CA sectors which demonstrates the importance of a profound anatomical knowledge of the hippocampus regarding this study.

1.5 The family of the epidermal growth factor receptors

Amongst the risk factors for AD, altered expression rates of the epidermal growth factor receptors (EGFR), also called the erythroblastic leukemia viral oncogene (ErbB) receptors or human epidermal growth factor receptors (HER) and its ligands were reported [33]. The ErbB growth factor receptors belong to the family of receptor tyrosine kinases. The abbreviation ErbB derives from the discovery of an oncogenic retroviral protein of the avian erythroblastosis virus to infect chicken cells. As the gene of the oncogenic, viral protein was found out to be homologous

to the gene of the epidermal growth factor receptors, the synonymous term ErbB has been introduced [34].

In total, there are four different receptor protein isoforms: EGFR1/ HER1 (ErbB1), HER2 (ErbB2), HER3 (ErbB3) and HER4 (ErbB4). Except from haematopoietic cells the ErbB proteins are expressed in cells originated from mesoderm and ectoderm. They are located in the basolateral compartment of the epithelium mediating mesenchymal-epithelial interactions. Invertebrates like *C. elegans* and *drosophila* carry a single ErbB-like receptor that can be activated by a single ligand [35].

The protein structure of ErbB receptors can be divided into three different domains: a ligand-binding cystein-rich ectodomain, a single-pass type 1 transmembranous (juxtamembranous) domain and a terminal intracellular domain containing a tyrosine kinase and its autophosphorylation sites. After ligand binding, the activated receptors undergo a conformational change and untether their dimerization arm to form hetero- or homodimers in different combinations. This formation allosterically activates the ki-

nases to autophosphorylate both c-terminal domains. For ErbB3 (no intracellular

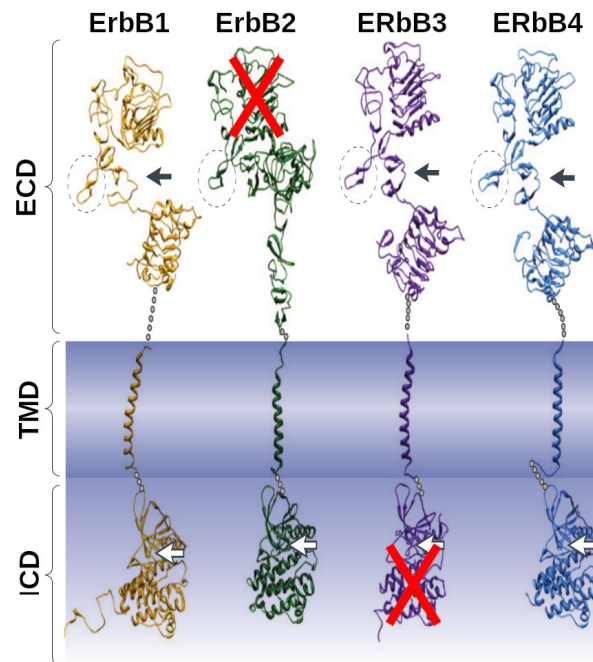


Figure 1.4: Extra-/intracellular (ECD/ICD) and transmembranous domains (TMD), black arrows: ligand binding sites, white arrows: autophosphorylation sites, dashed circles: dimerization loops. Red crosses: no ligand binding site for ErbB2, and lack of downstream activity for ErbB3.

tyrosine kinase activity) and ErbB2 (weak ligand binding site) a heterodimer formation with ErbB1 or ErbB4 are essential to successfully activate a downstream signalling cascade. The phosphorylated tyrosine residues can bind different adapter proteins to further activate downstream pathways Ras/ERK, PI3K/Akt, PLC- γ 1, Src, Shc and STAT [36], [37].

Until now two non-canonical pathways have been identified: endosomal internalization for ErbB1 [38] and ErbB2 [39] and proteolytic cleavage for ErbB4 [40].

1.6 ErbB4 signalling in AD

As the fourth member of the Epidermal growth factor receptors, it is expressed in different tissues including brain, testis, skeletal muscle, heart and kidney. Therefore the receptor is important for a variety of different cell types and functions in each organ. The molecular weight of the whole, uncleaved receptor amounts to 180 kDa. After ligand binding, dimerization and autophosphorylation, proteolytic cleavage by extramembranous shedding by A disintegrin and metalloproteinase (ADAM) 17 also called tumor necrosis factor alpha-converting enzyme (TACE) leads to the release of the N-terminal ectodomain that contains the ligand binding site.

Interestingly, the remaining 80 kDa membrane anchored carboxy-terminal part gets cleaved by the intramembrane protease complex, called γ -secretase complex, which releases the ErbB4 intracellular domain (E4ICD), containing autophosphorylated residues. As the Presenilin subunit of the γ -secretase is also involved in the degradation of Amyloid precursor protein (APP) it is important to highlight this potential common element of downstream pathways of AD pathology and ErbB4 signalling.

The ErbB4 receptor is the only member of the ErbB growth receptor family, where the juxtamembranous (JM) isotype a (JM-a) of ErbB4 can be cleaved by the γ -secretase [41]. Alternative splicing leads to four different ErbB4 proteins: cytoplasmic (CYT) 1 and 2, JM-b and JM-a. Not all isoforms undergo the cleavage by the γ -secretase, as only the c-terminal region of isoform JM-a CYT-2 and CYT-1 contain the E4ICD unit which is able to dimerize and translocate to the nucleus to regulate transcription [42], [43]. This allows further nuclear translocation to bind promoters and alter the expression of different genes. This underlines the potential impact on malfunctional gene transcription through impaired ErbB4 signalling.

Further, the multitude of different receptor isoforms that forward different downstream pathways underlines the complexity of growth factor receptor signalling and illustrates the multiplicity of potential targets/isoforms e.g. for designing expression analysis experiments.

1.6.1 Neuregulins: important ligands of the ErbB receptors

ErbB4-Neuregulin signalling is complex and includes a variety of different functions throughout different brain areas. ErbB4 is the only member of the epidermal growth factor receptor family that can bind Neuregulins and at the same time initiate a downstream signal after homodimerization (see table 1.2).

NRGs are a family of structurally related polypeptides, each of which contains an epidermal growth factor (EGF)-like domain, distinguished into Neuregulin 1 to 6 [44]. NRG1 binds to ErbB3 and ErbB4 and potentially ErbB2 if it has bound to ErbB3 or ErbB4. As the kinase activity of ErbB3 is impaired, downstream pathways for ErbB2 and ErbB3 are dependent on heterodimers with each other or

ErbB4. As ErbB4 can also form homodimers with itself to forward NRG signal, it is supposed to be the main binding partner of NRG1 [33]. Impaired NRG1 signalling after ErbB4 deletion highlights the importance of ErbB4 for NRG1 signalling [45].

The ErbB ligands specifically bind to their respective receptor, as shown in the overview of table 1.2 from Linggi et al. [46]. However, there exists a certain discrepancy between different authors regarding specificity, as discussed by Iwakura et al [47].

	ErbB1	ErbB2	ErbB3	ErbB4
EGF	+	-	-	-
TGF α	+	-	-	-
HB-EGF	+	-	-	+
Amphiregulin	+	-	-	-
Betacellulin	+	-	-	+
Epigen	+	-	-	-
Epiregulin	+	-	-	+
Neuregulin-1	-	-	+	+
Neuregulin-2	-	-	+	+
Neuregulin-3	-	-	+	+
Neuregulin-4	-	-	-	+
Neuregulin-5	-	-	-	+
Neuregulin-6	-	-	+	-

Table 1.2: Specificity of ErbB receptors and ligands [46]. As illustrated in figure 1.4, no ligands have yet been discovered for ErbB2 due to inexistent extracellular binding sites. ErbB4 has a the highest number of eight binding partners, ErbB1 with seven and ErbB3 with four ligands.

Previous findings related to ErbB4-NRG signalling in different diseases or experimental conditions could highlight its importance in different neurophysiological pathways like neurodevelopment, LTP, regulation of inhibitory pathways, motor functions and cell growth [45], [48]–[50]. Being enriched in the postsynaptic density (PSD) associating with AMPA through PSD95, the complex in-

terplay of ErbB ligands with different neurotransmitters regulate the expression of neurotransmitter transporters glutamine synthase, glutamate aspartate transporter (GLAST) and glutamate transporter 1 (GLT1) [51] and act on septal cholinergic and mesencephalic dopaminergic neurons through glia cells [52], that all are crucial for memory related pathways and therefore of specific importance for AD research [44].

Scar-forming astrocytes overexpress NRG6 that can bind to ErbB3 and thus heterodimerize and stimulate ErbB4 on astrocytes around plaques or apoptotic neurons [53]. Further, β -site APP-cleaving enzyme that produces the amyloid precursor protein, has been shown to regulate the proteolytic processing of NRG1 and its effect on neuroprotection and myelination [54] which could be blocked by ErbB4 siRNA inhibition [55].

1.7 ErbB4 knock-out mice

Between 10 and 11 days after fertilization ErbB4 knock-out (KO) mice die during mid-embryogenesis from heart failure due to the lack of myocardial trabeculae [56]. ErbB4 KO mice with reintroduction of transgenic ErbB4 expression are able to survive and show behavioural deficits [57] with anxiety-like behaviour, fear conditioning and hyperactivity in the open field test [58]. Mice with Cre-inducible ErbB4 in mesencephalic Tyrosin-Hydroxylase positive neurons show deficits in learning, spatial and working memory related behaviour that could be restored by tamoxifen administration [50]. Due to its role in neuro-/gliogenesis, the number of GFAP+ cells in the developing cerebral cortex of KO mice was reduced by 46% [59]. Interestingly, these behavioural studies on KO mice demonstrate a possible connection between ErbB4 expression and different neurological impairments.

Nevertheless, concerning the implication for a transfer towards ErbB4 signalling in AD, conclusions from behavioural observations from mice to human neurological symptoms of dementia should be drawn with caution.

1.8 Impaired ErbB4-Neuregulin signalling

To investigate a potential link between neurological symptoms of AD and ErbB4-Neuregulin signalling in the hippocampus, recent publications have been studied. The multiplicity of different pathways and targets of the Neuregulin ligands and their respective effect concerning AD is challenging to recapitulate. AD related, suspected pathways therefore include memory and LTP, motor function and spatial orientation, inhibition and regulation of behaviour and emotion with a majority of studies related to psychotic symptoms and schizophrenia.

30–60% of LOAD patients show multiple psychotic symptoms (LOAD+P). The inheritability of LOAD+P is estimated to be around 61% and to be associated with a more severe, earlier form of cognitive decline and further progression of dementia [60], [61]. This underscores the importance of genetic risk factors involved in pathways associated with psychotic symptoms during the progression of AD. Amongst these different risk factors, polymorphisms for ErbB4 ligand NRG1 were reported to be associated with psychotic symptoms, delusions and hallucinations for LOAD+P patients [62].

Concerning memory related pathways, it seems that NRG1 is important for the functionality of the regulation of LTP excitation, as the mutation of the NRG1 gene was reported to be associated to LTP dysregulation in AD pathology [63]. This could be partially confirmed for murine in-vivo experiments as microdialysed NRG1 added into dorsal hippocampus reversed LTP at CA1 glu-

tamatergic synapses. At the same time motor functions were restored via the Dopamine receptor 4 that activated and rapidly increased extracellular Dopamine concentration [49]. Another in-vivo study demonstrated a potential beneficial effect of NRG1 by using a neuroinflammatory, encephalopathic mouse model which measured disrupted hippocampal NRG1 levels at the beginning. The dysregulated LTP together with the observed cognitive impairment, could be restored after NRG1 was administrated [64].

Confirming the beneficial inhibitory effect, the overexpression of NRG1 was shown to prevent the occurrence of seizures in epilepsy patients by promoting inhibitory GABAergic neurotransmission [65]. This inhibitory characteristic of NRG1 has likewise been reported for its binding partner. Recently, it has been demonstrated that ErbB4 activity regulates the formation of inhibitory projections and synapses via the expression and activity of AMPA/ NMDA receptors of GABAergic neurons [66]–[68] and further via the secretion of GABA from parvalbumin interneurons [69].

1.9 Proinflammatory pathways linked to ErbB4

Amyloid protein deposition and subsequent plaque formation interferes with the activity of growth and differentiation molecules such as members of the NRG family. Colocalization of the expression profiles of ErbB4 and their Neuregulin ligands of the glial cells were associated with neuritic plaques [70]. The neuroprotective effects of NRG1 administration was demonstrated by antagonising apoptosis [71]. Further, it induces neurite extension and arborization in cultured neurons [72] and has anti-apoptotic, neuroprotective effects via PI3K/Akt pathway [71]. In a mouse model of chronic cerebral hypoperfusion used to mimic inflamma-

tory, neurodegenerative conditions, ErbB4 correlated with the apoptotic marker Cleaved-Caspase-3. And further, in the RNA sequence data of Ben Barres, reactive, neuroinflammatory astrocytes in aged mice upregulate ErbB4 expression, as illustrated in figure 4.2 [73]. These studies demonstrate the profound role of ErbB4 in neuroinflammatory pathways.

1.10 ErbB4 and cell growth

As a growth factor receptor, ErbB4 is expressed in different cancer types. In the past, the ErbB network has been intensively studied revealing a variety of therapeutic targets especially for breast cancer. Interestingly, for prostate, renal, and pancreatic cancer, ErbB4 expression is downregulated, whereas in medulloblastomas, thyroid, gastric, breast and colon cancer it is upregulated. This different ErbB4 expression in neoplasia is assumed to be linked to a different expression pattern of the four ErbB4 isoforms in the respective tissue types, that act via different downstream signalling pathways [74]. Concerning astroglial brain tumours, ErbB4 expression seems to be lower for Glioblastoma (GB) compared to non-neoplastic control brains [75] and to be higher in low-grade gliomas as compared to GB [74]. As a potential hypothesis, upregulation of ErbB4 is suspected to act as a tumor suppressor of malignant transformation with pro-apoptotic effects against aggressive brain tumours. Mechanistically, the cleavage of the intracellular 4ICD unit acts as a BCL-2 homology, 3-only protein in the mitochondrion and leads to programmed cell death via cytochrome c efflux [76]. The effect could be confirmed for in-vivo conditions by the transfection of an activating, mutated ErbB4 allele in breast, prostate and ovarian cancer cell lines which lead to an enhanced autophosphorylation as well as other pro-apoptotic effects.

1.11 Astroglial ErbB4-NRG expression

Expression of NRG I in astrocytes increases as a response to neuronal activity [77] and lipopolysaccharide (LPS) treatment [78]. Around areas from induced rat brain injury activated astrocytes upregulate Neuregulin I expression; a finding reproducible with in-vitro astrocyte cultures and forskolin treatment, an inducer of reactive astrogliosis [79]. The NRG1 expression by reactive astrocytes can also be observed during the formation of a glial scar mediated via autocrine and paracrine signalling [80]. Concerning the inflammatory responses of ErbB4 for reactive astrocytes in AD, immunopositive GFAP and ErbB4 astrocytes were observed around neuritic plaques [70]. Additionally, in different pathological conditions in a mouse model of spinal cord injury, both ErbB4 and GFAP in astrocytes were found to be colocalized [81].

Sardi et al. could show that the cleaved E4ICD unit inhibits GFAP expression in wild type mice [48]. This is supposed to play a crucial role for early neurodevelopment to favor neurogenesis by suppressing GFAP and promoting subsequent astrocytogenesis. Since astrocytogenesis depends on the translocation of the E4ICD, altered activity of Presenilin/ γ -secretase could affect ErbB4 JM-a processing [82].

Taken together, NRG1-ErbB4 signalling in astrocytes is involved in multiple pathways correlating with inflammation, injury and repair mechanisms. Of note, the relatively low number of references (only 13 results of the pubmed search "GFAP + ErbB4") demonstrates the lack of studies concerning ErbB4 expression in reactive astrocytes.

1.12 Aim of this study

The aim of this study was to further investigate ErbB4 expression in the human hippocampus with a focus on reactive astrocytes. As the involvement of dysbalanced astroglial ErbB4 signalling in AD is still unclear, this work seeks to address the following questions:

1. Is the overexpression of ErbB4 in AD associated with reactive astrocytes?
2. Is ErbB4 associated with pro- or antiinflammatory markers?
3. How is the expression of ErbB4 distributed throughout the hippocampus?
4. Can the expression of ErbB4 be regarded as cell specific, as previously argued [57], [70]?
5. How is the astroglial expression of ErbB4 in other diseases and therefore different pathological conditions when compared to AD?
6. Are the results from immunofluorescence on human brain sections reproducible in-vitro?
7. Does the stimulation of astrocyte cultures with ErbB4 receptor ligands lead to an ErbB4 activation?
8. Does the receptor stimulation lead to pro- or antiinflammatory responses?

2 Materials and Methods

Antibody	Host/Target	[conc.]	Manufacturer	Reference number
Primary antibodies				
α -Tubulin	mouse	1/5000	Abcam	ab7291
β -Actin	Rabbit	1/1000	Abcam	ab8227-50
C1q	Rabbit	1/200	Dako	A0136
Cleaved Caspase-3	Rabbit	1/200	R&D Syst.	AF835
Cox2	Rabbit	1/500	Sigma	HPA001335
ErbB3	Rabbit	1/500	Abcam	ab93739
ErbB4	Rabbit	1/200	Thermofisher	ab32375
ErbB4 (N-term.)	Mouse, clone Ab77	1/250	Thermofisher	MA5-12888
ErbB4 (C-term.)	Rabbit, clone HFR1	1/200	Thermofisher	MA1-861
Phospho-ErbB4	Rabbit, polyclonal	1/250	Abcam	ab61059
Phospho-Erk	Rabbit	1/2000	Abcam	ab08115
GFAP	Guinea-pig, polyclonal	1/500	Synaptics	173004
Iba1	Rabbit	1/500	Wako	019-19741
Iba1	Goat	1/500	LSBio	LS-B2402
Secondary antibodies				
AlexaFluor®405	Donkey anti-mouse	1/200	Jackson	715-475-150
AlexaFluor®405	Donkey anti-guineapig	1/200	Jackson	706-475-148
AlexaFluor®488	Donkey anti-mouse	1/400	Jackson	715-545-150
AlexaFluor®488	Donkey anti-rabbit	1/400	Jackson	711-545-152
AlexaFluor®555	Donkey anti-rabbit	1/400	Jackson	AB 162543
AlexaFluor®647	Donkey anti-chicken	1/200	Jackson	703-605-155
AlexaFluor®647	Donkey anti-guineapig	1/200	Jackson	706-605-148
AlexaFluor®647	Donkey anti-rabbit	1/200	Jackson	711-605-152
HRP	horse anti-rabbit	1/2000	Cell signaling	7074
HRP	horse anti-mouse	1/2000	Cell signaling	7076S
IRDye800CW®	Donkey anti-mouse	1/10000	LI-COR	926-32212
IRDye680LT®	Donkey anti-rabbit	1/10000	LI-COR	26-68023

Table 2.1: Antibody data sheet

Product	Species	[conc.]	Manufacturer	Reference number
Treatments				
EGF	human	100 ng/ml	Sigma	SRP6253-10 ug
NRG1b1	human	100 ng/ml	Novus Biologicals	H8916-10 ug
NRG4	human	100 ng/ml	Sino Biological	12183-HNCE-5
TNF- α	human	50 ng/ml	Sigma	H8916-10 ug
Cells				
C8-D1A immortalized astrocytes	mouse	-	ATCC	CRL-2541
iCell iPSC derived astrocytes	human	-	Fujifilm	ASC-100-020-001-PT
MACS® - magnetic cell sorting				
CD11b microbeads	mouse	-	Miltenyi Biotec	130-093-634
MACS column	-	-	Miltenyi Biotec	130-042-401
MACS system	-	-	Miltenyi Biotec	130-042-302 / 130-090-976
Culture medium				
BSA	bovine	-	Sigma	A3059
DMEM F-12	-	-	Lonza	BE04-687FV1
DMEM	-	-	Gibco	41965-039
FBS	bovine	-	Gibco	10270-106
HEPES	-	-	Sigma	SLBC4362
N-2 Supplement	-	100X	Gibco	17502048
Laminin	human	10 μ g/ml	Sigma	L2020
PBS	-	pH 7.4	Sigma	P3813
Penicillin Streptomycin	-	10 000 U per 10 mg/ml	Gibco	15140-122
Poly-L-Lysine	-	1:1000	Sigma	P1274

Table 2.2: Cell culture - used materials

Product	description	Manufacturer	Reference number
Protein extraction and quantification			
Femto Kit	chemiluminescent detection	Thermofisher	34094
Protease inhibitors	1%/well	Thermofisher	78440
Protein Assay Kit	protein quantification	BIO-RAD	5000001
RIPA lysis buffer	120 μ l / well	Fisher Scientific	89900
TGX agarose gels	precast, 4-15% gradient	BIO-RAD	4561086
Transblot Turbo Transfer Kit	gel electrophoresis, transfer	BIO-RAD	17001915
RNA extraction and quantification			
innuPREP DNA/RNA Mini Kit	extraction kit	analytikjena	845-KS-20800
IM-Prom-II RT System	Reverse transcription	Promega	A3800
iQ5 qPCR Kit	Fluorophore, polymerase, buffers, nucleotides	BIO-RAD	170-8860/75

Table 2.3: Protein and RNA quantification, used materials

Both IgG isotype control and a staining with secondaries only on a human hippocampus sample turned out negative with unspecific staining. To test the interaction of primary antibodies as a possible artefact, stainings with different antibodies/epitopes for GFAP and ErbB4 could reproduce the observed GFAP⁺/ErbB4⁺ immunoreactivity. ErbB4 only stainings showed ErbB⁺ cells with astrocyte morphology, therefore no interaction could be detected.

2.1 Human brain samples

Human brain samples from table 2.4 were obtained from the Douglas-Bell Brain Bank of Canada as part of the McGill University Health Centre in a collabora-

tion with the University of Luxembourg. All performed experiments on human samples were approved by the Ethics Review Panel of the University of Luxembourg. In average, the age of the samples was 83,3 years, with a male to female ratio of 1:1.7 and a mean postmortem time of 22.1 hours. For AD samples, the average neuropathological ABC score (see table 1.1) was A = 2, B = 2.8, C = 2.5. According to clinical observations and neurohistopathological examinations of the McGill University, samples were classified as non-demented control (CTL).

The samples were first rinsed in phosphate-buffered saline (PBS) and incubated in 30% sucrose solution in PBS for 36 hours at 4 °C. Samples were then embedded in M-1 embedding matrix (Thermo Scientific, Waltham, MA) and cut into 50 μ m thick coronal slices on a sliding freezing microtome. After cryosectioning, slices of samples were stored in a cryoprotectant solution containing ethylene glycol (30%) and glycerol (30%) in 0.05 M phosphate buffer (PB, pH 7.4) until processed for immunostaining.

The following protocol of immunohistochemistry was used: (1) 24 hours UV light treatment to prevent autofluorescence. (2) PBS containing 0.5% Triton-X 100 treatment for permeabilization for 30 minutes at room temperature (RT). (3) PBS containing 2% horseserum and 0.5% Triton-X 100 treatment for 2 hours for blocking unspecific epitopes. (4) Primary antibody in PBS containing 0.5% Triton-X 100 and 2% horseserum, incubation for 72 hours at 4 °C, with different concentrations for each antibody (table 1). (5) Washing 3 times for 10 minutes with PBS at RT. (6) Incubation of secondary antibody for 2 hours at RT in PBS containing 0.5% Triton and secondary antibodies (table 1) covered in aluminium foil (7). Two washings for 10 minutes in PB at RT in aluminium foil. (8) One washing with PB containing 1% Triton. (9) One washing with PB.

The confocal Microscope Zeiss LSM-71 with a 20x objective was used for acquisition. Laser (488 nm, 555 nm, 647 nm) strength, amplification, and resolution were manually adjusted to the amount of emission of applied antibodies. Larger tile scan overviews were performed as maximum intensity projections based on 10 z-stacks (1 μ m each step).

Brain tumor samples were deparaffinied with Xylene and rehydrated via the ethanol series (100% - 70%, each 3 minutes), incubated in cresyl violet for 5 minutes, rinsed in distilled water, incubated 3 minutes each in 95%/100% ethanol and cleared in xylene 2 times for 5 minutes and mounted with permanent mounting medium. For immunohistochemistry, samples were heated 20 minutes at 50 °C, then samples were rehydrated with the ethanol series as above. Then the samples were boiled with antigen retrieval solution for 15 minutes and cooled in citrate buffer for 20 minutes. Afterwards, blocking and antibody incubation steps were performed as described.

Case	ID	Age	Sex	Diagnosis	PMD (h)	ABC Stage
1	1669	87	M	AD	21.8	A2B3C2
2	1631	87	M	AD	10.8	N/A
3	1565	83	M	AD	43.3	B3
4	1523	86	M	AD	27.3	A2B3C2
5	1504	91	M	AD	25	A2B3C2
6	1494	85	M	AD	31.1	A2B3C3
7	1296	80	M	AD	15.5	B4
8	1780	90	M	AD	26.1	A3B2C3
9	1939	90	M	AD	32	A2B2C3
10	1763	83	M	AD	16.8	N/A
11	1326	82	M	AD	11.5	A2B3
12	1923	87	F	AD	17	A1B2C2
13	1534	96	F	AD	26.5	B3
14	1352	83	F	AD	15	N/A
15	1501	83	F	AD	25	A2B3C3
16	1725	77	F	AD	24.3	B3
17	1839	74	F	AD	27.6	-
18	1696	81	F	DLB	8.58	-
19	1629	83	F	DLB	17.8	-
20	975	77	F	DLB	19.5	-
21	1671	82	M	DLB	22	-
22	1573	64	M	DLB	17.3	-
23	488	86	F	CTL	5.8	-
24	808	80	F	CTL	17.5	-
25	1117	82	F	CTL	32.6	-
26	1547	95	F	CTL	23.8	-
27	1895	55	F	CTL	21.1	-
28	1443	83	F	CTL	35.8	-
29	1374	89	F	CTL	23.6	-
30	1582	85	M	CTL	26.8	-
31	1709	93	M	CTL	18	-
32	1881	89	M	CTL	32	-
33	1419	80	M	CTL	13	-
34	1582	85	M	CTL	26.8	-
35	1389	89	M	CTL	32.3	-
36	2003	81	M	CTL	72h (autopsy)	-
37	AMKE36	51	M	GB	postop.	-
38	AMKE37	72	F	GB	postop.	-

Table 2.4: Human brain samples, paraformaldehyde (PFA) fixed

2.1.1 Semiquantitative analysis

A semiquantitative analysis of ErbB4/GFAP proteins on different samples was carried out with parameters for different characteristics of IHC micrographs as shown in table 2.5. Morphological criteria were quantified in frequency of ErbB4 immunoreactivity in each image as percentage of cells with nucleic, cell body and proximal processes, the amount of GFAP positive area that colocalizes with ErbB4 and the GFAP overall intensity. Total number of samples was n=31, with groups AD (n=17) and control (n=14). Different confocal images per sample from CA1 sector of ErbB4 and GFAP staining were evaluated. Mann-Whitney-U tests and visualisation with Box-Whisker plots with interquartile range for non-parametric ordinal/interval scale were performed with R 4.0.4 and ggplot2 package on resulting data.

Grade	1	2	3	4	5
Frequency	0-1%	1-25%	25-50%	50-75%	>75%
Intensity	sparse		medium		high
Coloc.	sparse		medium		high

Table 2.5: Semiquantitative grading scale for IHC

For the statistical analysis a Mann-Whitney-U-Test for non normal distributed interval and ordinal scale was calculated to determine if there were differences between AD and control for occurrence of ErbB4 staining as nucleic and cell body or proximal processes, and colocalization (with ErbB4) and intensity of GFAP fluorescence. Means for interval scale for frequency (cell body, nucleic) and medians for ordinal scale for intensity (colocalization, fluorescence) were calculated.

Murine whole brain samples

Murine control brains (p100 C57BL/6 mice, p300 Wistar rats) were anesthetized with halothane, decapitated, post-fixed with PFA 2% (wt/vol) and cryosectioned in coronal slices at 30 μm . Blocking, staining and mounting steps were performed according to IHC protocol on free floating samples from section 2.1.

2.2 Cell culture

The overview (see supplemental table 6.1) shows the different experiments on different astrocytic cell types (immortalized, primary, iPSC) with cell counts and treatments with duration, amount, reagents and which kind of extraction was done afterwards. All used reagents are shown in table 2.2.

2.2.1 Murine C8-D1A immortalized astrocytes

8-D1A astrocytes (type 1 clone, ATCC CRL-2541) were cultured in the incubator at 37 °C, 5% CO_2 in DMEM (Dulbecco's Modified Eagle's Medium, gibco 30-2002) containing 10% fetal bovine serum, as well as 1% Pen Strep (Thermo Fisher Catalog No. 15070063) as antibiotics (table 6.1). After thawing, cells were centrifuged for 5 minutes at 10 000 g at 4 °C. The pellet was resuspended in DMEM medium and transferred for passaging in 25 ml flask. Once cells reached confluency they were detached with Trypsin-EDTA 2% and transferred either to a 12 multiwell plate for protein extraction or to coverslips for further immunostaining. After different treatments, cells were washed with PBS. For cell lysis and total protein extraction see section 2.2.5.

2.2.2 Murine primary astrocytes

All animal experiments were carried out according to the 2010/63/EU European Union Directive and internal ethical committee regulations. The protocols were approved by the Animal Experimentation Ethics Committee (AEEC) of the University of Luxembourg. All efforts were made to minimize suffering. Newborn mice were decapitated.

For mixed glial cultures from newborn C57BL/6J mice from Charles River (France) we used the culture medium DMEM (Gibco), together with 10% FBS (Gibco) and 1% antibiotics (10 000 U/ml Pen - 10 000 μ g/ml Strepto). After dissectioning the head of the 1 to 3 days old mice, the 2 hemispheres of the brain were separated and the cerebellum and the meninges were removed in a petri dish with PBS 1X.

With a 18 G and 21 G needle the brain was mechanically dissociated. Then 30-40 ml of culture medium was added and centrifuged at 1100 rpm for 10 minutes at 4 °C. After removal of the supernatant the cells were mixed with some media and transferred to a 75 cm^2 flask coated with poly-L-Lysine (Sigma). Following incubation at 37 °C, 5% CO_2 of 5 to 7 days, the media was removed and one washing step with PBS was performed to remove debris.

After 14-16 days mixed glial cultures were confluent and after one washing step with PBS, Trypsin-EDTA 2% was added to dissociate the cells, then put in the incubator (37 °C, 5% CO_2). Equal volume amount of media was then added to inhibit the Trypsin. After centrifugation of the suspension at 1100 rpm for 10 min at 4 °C the supernatant was removed.

Magnetic cell sorting - purification of astrocytes cultures

To limit the analysis to the response of astrocyte cultures after pro-inflammatory treatments, microglial cells were removed from the mixed glial cultures by magnetic cell sorting (MACS; Miltenyi Biotec). The pellet was first resuspended with 20-30 ml of MACS buffer (Sigma). The suspension was then filtered with a 70 μm filter. After centrifugation at 1100 rpm for 10 minutes at 4 °C the supernatant was removed and 90 μl per 10 million of cells MACS buffer at 4 °C were added.

Then 10 μl of CD11b antibody coated microbeads (Miltenyi) per 10 million cells were added and put in the tube at 4 °C in the fridge for 10 minutes, then resuspended and put back at 4 °C for another 10 minutes. After incubation, 2 ml of MACS buffer for each 10^7 cells was added. The suspension was then centrifuged at 1100 rpm for 10 minutes at 4 °C, the supernatant was then removed and 500 μl of MACS buffer at 4 °C added.

The columns (Miltenyi) of the magnetic system (MidiMACS/ QuadroMACS separators) were then first filled with each 3ml of MACS buffer at 4 °C. Then the cell suspension was applied on the rinsed column to magnetically pull microglia out of the mixed glial culture to the magnetic column and let astrocytes pass through it. After that, 3 washing steps with MACS buffer each 3 ml were performed.

The residing astrocytes in the solution were then centrifuged at 1100 rpm for 10 minutes at 4 °C, the supernatant was removed and then the pellet was solubilized with complete culture medium. To achieve a purified astrocyte culture (less than 0.5% microglia cells) the MACS steps from above were repeated after incubating the cells for days to reach confluency.

2.2.3 Human induced pluripotent stem cell (iPSC) astrocyte culture

Human induced pluripotent stem cells (iPSC) derived astrocytes (No.#11 in table 6.1) were purchased from Fujifilm as iCell[®] astrocytes and stored in liquid nitrogen at -150 °C until further use. Twelve well plates were coated with laminin by incubation for 1 hour (laminin concentration 10 µg/ml) at 37 °C prior to the transfer of cells and washed with PBS afterwards. Complete culture medium DMEM/F-12,HEPES (97 ml), FBS (2 ml) and N2 supplement (1 ml) was then added. The vial with cells was thawed in the incubator for 10 minutes and centrifuged at 300 g for 5 minutes to remove the freezing solution. Afterwards the cell pellet was resuspended in 3 ml of maintenance medium.

Total amount of 1.35 million cells were counted and for 12 well a seeding density of 100 000 cells/well in 0.5 ml was distributed in all 12 wells and for immunocytochemistry analyses 10 wells of a 96 well plate were used with a density between 10 000 and 20 000 cells in 0.1 ml. Well plates were then incubated at 37 °C/5% CO₂. Half of medium was changed every 2 days. After 72 hours, total proteins of cells in 12 well plates were extracted as described in section 2.2.5 and cells in 96 well plates were fixed with 4% PFA and incubated with antibodies as described in section 2.2.4.

2.2.4 Immunofluorescence

The astrocytic cell cultures (less than 0.5% microglia) with approximately 700.000 cells per well were treated for 24 h as indicated, see table 6.1. After 24 hours the media was removed. The cells were then fixed for 20 minutes with a 4% PFA

dilution in PBS at RT and washed 2 times with pre-cooled PBS at 4 °C. For immunocytochemistry analyses, one coverslip of each condition was treated at RT with following steps: one hour permeabilization step with PBS containing 0.5% Triton, 2 hours blocking unspecific epitopes with PBS (Thermofisher) containing 2% HS and 0.5% Triton, 3 washings with PBS 10 minutes each and 2 hours with different primary antibodies. After 3 washing steps with PBS, secondary antibodies were added and incubated for 2 hours. After 3 additional washings for 10 minutes with PBS (Gibco) the coverslips were mounted on slides using antifade mounting medium.

2.2.5 Protein extraction, gel electrophoresis and western blotting

The purified astrocyte cultures were treated for 24 hours. After 24 hours the media was removed and 150 μ l RIPA lysis buffer (Fisher) with 1% Protease inhibitor and 1% Phosphatase inhibitors (Thermofisher) were added to each well which were then scraped. The solution was then centrifuged for 10 minutes at 1100 rpm at 4 °C to separate debris from proteins. The supernatant was then removed from the pellet and stored at -20 °C. Protein content was determined using the Bio-Rad Protein Assay Kit according to the manufacturer's protocol. For denaturation of proteins, 2X Laemmli loading buffer (4% SDS, 10% 2-mercaptoethanol, 20% glycerol, 0.004% bromophenol blue, 0.125 M Tris-HCl, pH 6.8) was used. The samples were then heated at 90 °C for 5 minutes for further degeneration.

To be able to compare the different conditions, an equal amount of protein was then added to the gel containing a gradient of 4 to 15% of SDS. and migration with buffer (25 mM Tris, 190 mM glycine, 20% ethanol, diluted in H₂O) was

performed for 45 minutes. The proteins on the gels were transferred along the applied current onto the nitrocellulose membranes with wet transfer for 2 hours at RT with 20% ethanol.

The membranes were then blocked for 2 hours at RT under agitation with FBS 3%. Afterwards, incubation with primary antibodies in PBS + Tween 0.1% and BSA 3% for 24 h at RT, subsequently with secondary antibodies (in PBS + Tween 0.1% and BSA 3%) for 2 hours at RT on agitation. They were then washed 3 times for 10 minutes in PBS-tween 0.1%. For chemiluminescent detection the membranes were incubated in 500 μ l of each reagent of Femto kit substrate for 5 minutes prior to detection. For immunofluorescent detection, after incubation for 2 hours with IRDye secondaries, membranes were washed 3 times in PBS-tween 0.1% prior to acquisition.

2.2.6 RNA extraction, cDNA and qPCR analysis

For RNA extraction of the samples in 12 well plates, the innuPREP RNA Mini Kit (analytikjena) was used. Reverse Transcription was done with the IM-Prom-II Reverse Transcription System (Promega).

To have single stranded RNA, a mix of total RNA and 1 μ g RNase free water (9 μ l, Promega), and 1 μ l of OligodT was heated at 70 °C for 5 minutes. Samples were then put on ice for 5 minutes. For the reverse transcription a buffer mix (see table 2.3) of 8 μ l RT buffer was used, 6 μ l MgCl₂ (25mM), 2 μ l dNTP mix (10mM), 1 μ l RNAsine inhibitors, 2 μ l reverse Transcriptase and 11 μ l RNase free water (all from Promega kit).

After a short centrifugation at RT for 1 minute at 10 000 g the reverse transcription was done in following steps: annealing (5 minutes, 25 °C), elongation (60 minutes, 42 °C), inactivation of the enzyme (15 minutes, 70 °C). The complementary DNA (cDNA) was then kept at -20 °C. For the qPCR analyses, primers were designed with PrimerBLAST and NucleotideBLAST from NCBI to span exon-exon junctions to increase specificity. For the following PCR, materials from the iQ5 kit of Bio-Rad was used.

First, 1 μl of cDNA in 3 μl of water was put into each well. 8 μl SYBR Green (nucleotides, polymerase 50 U/ml, 6 mM MgCl_2 and 20 nM fluorescent) 0.8 μl of forward and reverse primers (12.5 μM) and 6.4 μl of RNAase free water were then added. To eliminate bubbles and to pull down the liquid to the bottom of the well, the plates were centrifuged at 1000 g for 2 minutes.

The PCR steps with a total of 40 cycles were as follows: 3 minutes at 95 °C for the activation of the enzyme, 10 seconds at 95 °C for denaturation, 30 seconds at the annealing temperature according to the primers. For establishing the melt curves the probes were treated for 1 minute at 95 °C, 1 minute at the specific melt temperature of the primer and cycles for 30 seconds increasing to a final 95 °C.

The concentration of the nucleic acid (in this case cDNA) of each gene of interest (GOI), targeted by a primer, is antiproportional to the number of cycles needed until the fluorescence of SYBR green fluorophore (highest when bound to DNA) reaches a predefined threshold.

Normalization for each gene was done by subtracting Ct value of housekeeping gene RPL27 from GOI $\Delta\text{Ct} = \text{Ct}_{GOI} - \text{Ct}_{Ref}$. Expression of each gene as $\Delta\Delta\text{Ct} =$

$\Delta Ct_{CH} - \Delta Ct_{GOI}$ was calculated for each technical replicate and plotted on figure 3.19 as log2 fold relative to control. High $\Delta\Delta Ct$ values indicate upregulation of gene, low values downregulation. No statistical analysis due to small size of biological replicates (n=1) was performed.

Gene	Forward	Reverse
ErbB4	AGTGGTTTTGCCTATGCCTGA	ACAGATGGACAACAAATTCAGT
NRG4	ACACTATACTCTGCTTGATTCCCTC	CTTCCCCCGTGGGTAAATAGA
ErbB1	ACACGCGCTAGTTTACCAGT	CATGAAATGAAGACAGGAACACA
NRG1	CAGTACCCACCCGGAAGAAC	TCCGAGCTGGAGAAGGGAAG
IL6	TCCTACCCCAATTTCCAATGCT	TAACGCACTAGGTTTGCCGA
GFAP	CACGAACGAGTCCCTAGAGC	GCAAGTGCCTCCTGGTAACT

Table 2.6: Nucleotide sequences of used primers

2.3 Analysis of immunofluorescence by quantification of pixel intensity

The set of the included samples for the digital analysis amounted to a total of $n = 16$, with Control ($n = 7$) and AD ($n = 9$). The age of cases ranged between 55 and 96 ($\mu = 83.63$, $SD = 9.2$, $\mu_{CTL} = 85.8$, $\mu_{AD} = 82.3$), with a gender ratio of 56% male to 44% female (see table 2.4). The multi-tile images covering a total area of $1118 \mu m^2$ were obtained with Zeiss confocal microscope.

The 20X objective was positioned at the CA1 sector between the stratum radiatum (4) and stratum oriens (2) as demonstrated on the red box in figure 2.1. A tissue depth of $z = 10$ stacks with a thickness of $1 \mu\text{m}$ per stack was set for each sample to cover approximately one cell layer.

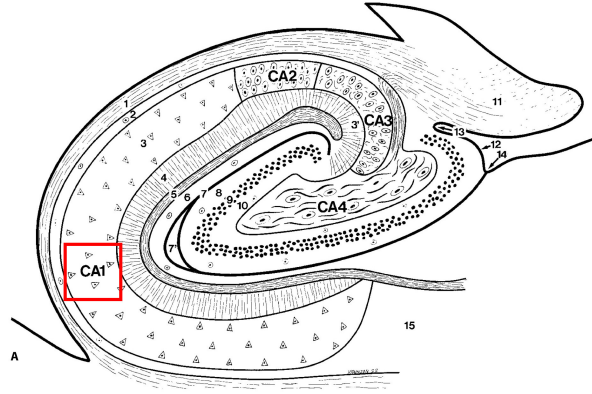


Figure 2.1: Exemplary coronal plane of the human hippocampus. Red square: area of the images for digital analysis. Drawing from Duvernoy et al. [30]

2.4 Fiji macro

To quantify the level of fluorescence intensity for the analysis of images from IHC experiments, Fiji (ImageJ with scientific plugins) and its macrolanguage were used. For GFAP and ErbB4 expression analysis in astrocytes, a mask around astrocytes cell body was created via the GFAP channel. This was done by the k-means plugin from ij-tools [83] by the detection of GFAP pixel clusters that were further "Converted to Mask". This mask contains the calculated clusters as so called "regions of interest" (ROI) that are stored in a database of the software (ROI manager).

This ROI manager contains the coordinates of these regions as a mask that can be "hold" onto the images like a template. After the template was created, the raw images were opened to apply the ROI (mask). Measurements on these defined areas achieve the desired output of separating cells from background. Different sizes can then be measured under respective regions.

To quantify the amount of fluorescent intensity under the area, in a way that it is proportional to the amount of expression or amount of protein of the cell, integrated density was used. Where integrated density is defined as "the sum of the values of the pixels in the image or selection. This is equivalent to the product of area and mean gray value" [84], [85]. In case of varying sizes - like the soma of astrocytes in different conditions - the sum of all pixel values (which is also defined to be proportional to size) "collects" all pixel values under the area and can therefore be seen as proportional to the abundance or expression of protein.

The following sequence was performed on all samples: Z-stacks of each image were split in stacks (n=10) and saved to folder. To create a mask to measure, the GFAP channel was used for following preprocessing steps: background subtraction with radius of 50, despeckle, median with radius of 2, which were equally applied to all images. Intensity thresholds for creating the mask have been globally adjusted once for each stack/image.

Next, by using k-means clustering from ImageJ Plugins toolkit [83] each pixel was initially randomly assigned to image seeds distributed by k-means++ algorithm [86]. According to the pixels vector values in space and intensity (RGB value), proximity to each random seed was iteratively summarized and minimized to reallocate and finally find cluster centroids with local optima. Clusters were then transferred to the ROI manager to serve as a cell mask that is held on the original, unprocessed GFAP and ErbB4 images. The whole macro code is attached (see section 6.2), with explanatory comments highlighted in green.

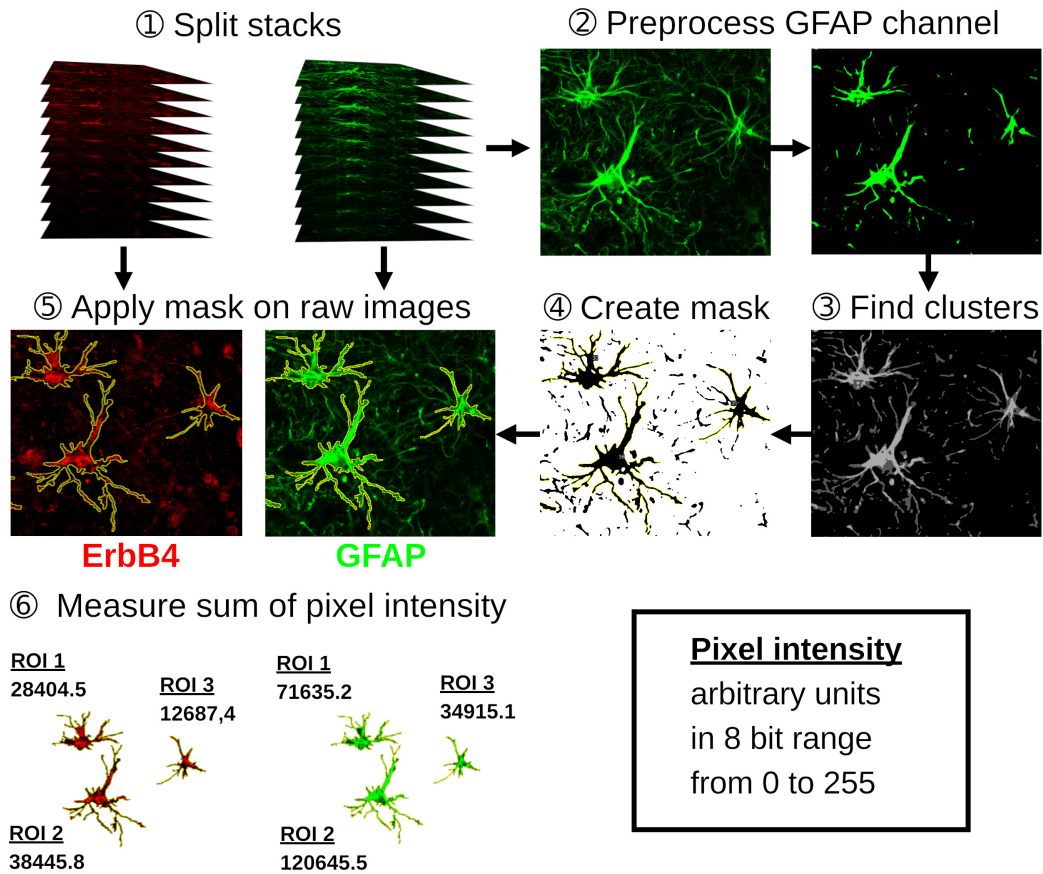


Figure 2.2: Sequence of analysis with Fiji macro from step 1 to 6. The generated mask with ROI as astrocytes from the GFAP channel is applied on the original image for step 6, the measurement of fluorescent intensity.

2.4.1 Statistical analysis

Statistical analysis between groups (AD vs. Control) and correlation between protein expression (ErbB4 and GFAP) was done with SPSS. Unpaired t-test was conducted to test differences in GFAP and ErbB4 intensities between AD and control groups. The precondition for a t-test is a Gaussian normal distribution of the data, which was recommended to be confirmed with a Shapiro-Wilk test (small sample size $n < 30$) on a significance level of $\alpha = .05$. Pearson's r correlation coefficient was calculated between groups of ErbB4 and GFAP for a two sided t-test on a significance level of $\alpha = .05$.

3 Results

3.1 ErbB4 immunofluorescence in control condition

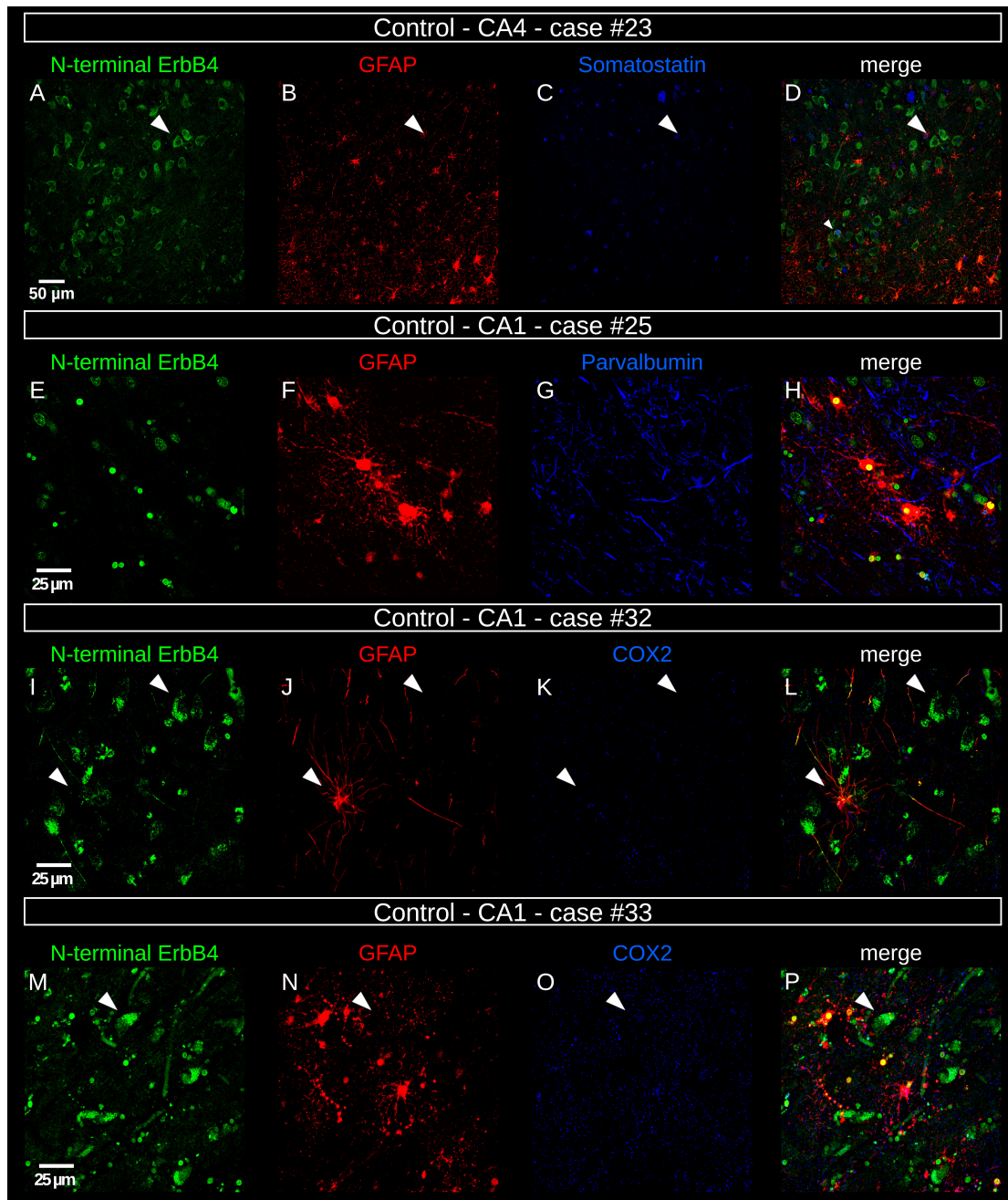


Figure 3.1: Human hippocampus, control condition, cases No.#23 (A - D), No.#25 (E - H), No.#32 (I - L), No.#33 (M - P). Columns: N-ErbB4, GFAP, SST/PV interneuronal marker, COX2 proinflammatory marker.

Control hippocampi stainings in figure 3.1 from page 43 show different interneuronal somatostatin (SST), parvalbumin (PV), and Cyclooxygenase 2 (COX2) inflammatory marker. Morphological features of astrocytes in physiological, resting state can be well observed in picture F and J with thin processes and eutrophic cell body. The low signal for COX2 in pictures K and O indicate a low inflammatory activity. ErbB4 is present in putative neurons with triangle-like cell body (white arrowheads in pictures A, L, M). No ErbB4 staining in GFAP⁺ cell bodies or proximal processes in pictures D, H, L, P. The observed nuclear-like staining for astrocytes appears to be present in pictures H and P, to a weaker extent in picture L.

In figure 3.2 (sample No.#29) with ErbB4, GFAP and Parvalbumin staining and close-up view in image D on a Parvalbumin⁺ neuron, shows clear distinguishable layers of the CA1 sector. Strong GFAP immunoreactivity along a blood vessel in the center of the image. In contrast to control, ErbB4 seems unspecific and primarily nuclear-like (arrowhead in picture E). No ErbB4 signal for GFAP⁺ cell bodies or processes. Concomitant with AD is the high density of ErbB4⁺ nuclei along the dentate granule cell layer. One Parvalbumin⁺ neuron is indicated with arrowheads, counterstaining the nuclei with ErbB4. Compared to AD condition, the morphological features of astrocyte reactivity seems to be less prominent with smaller cell bodies and thinner processes.

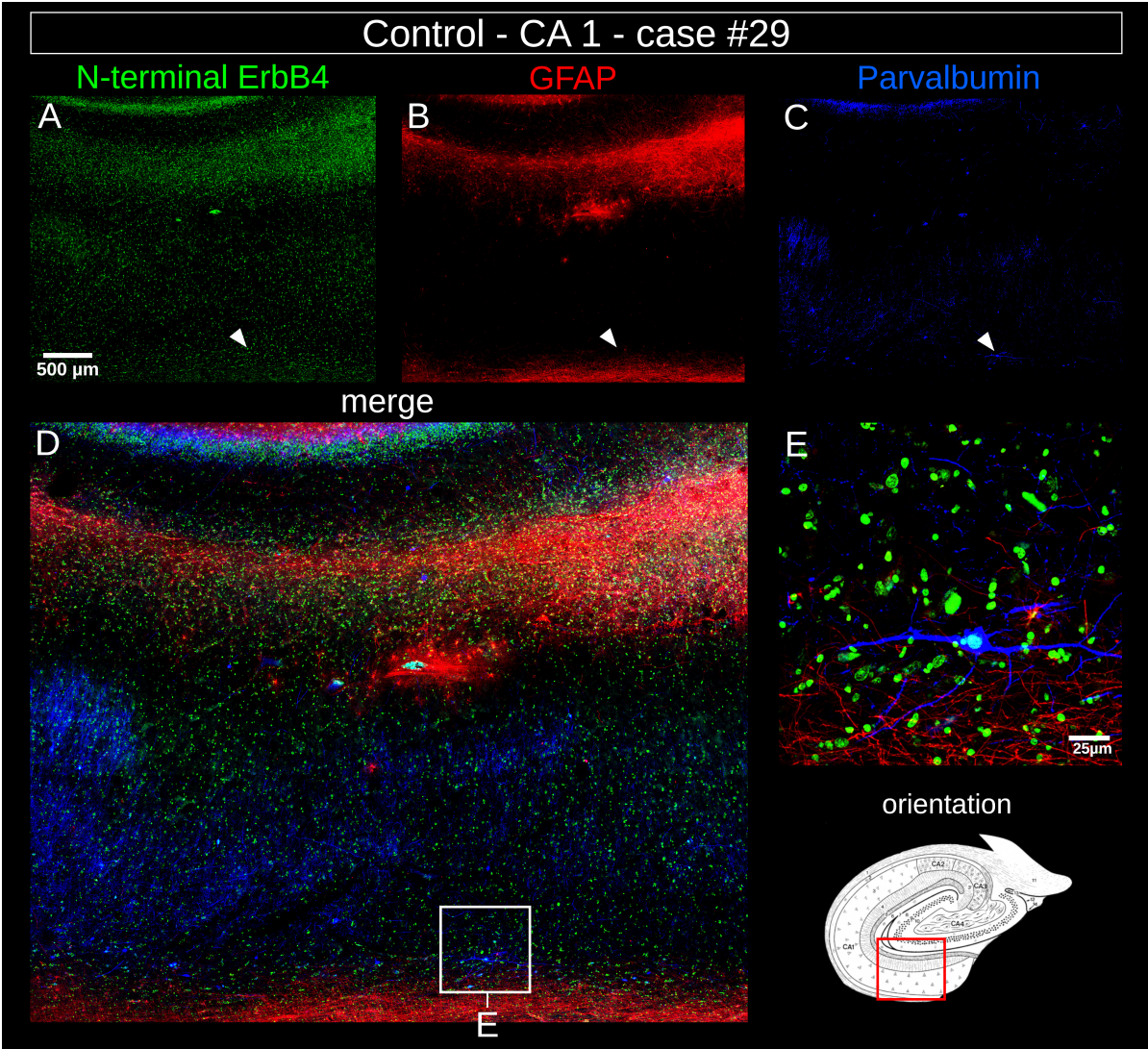


Figure 3.2: Human hippocampus, control condition, case No.#29., CA1 sector. A: ErbB4, B: Cleaved-Caspase 3, C: Iba1, D: merge, E: close-up view.

3.1.1 Mouse and rat control cortex

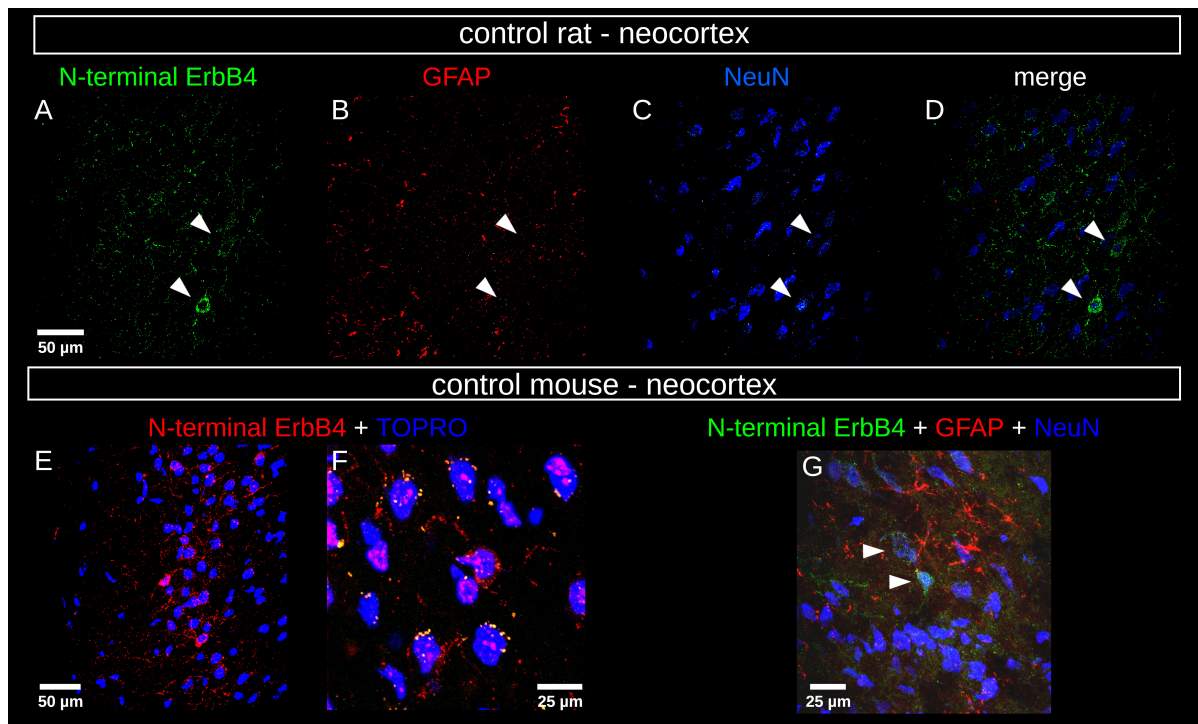


Figure 3.3: Control neocortex of rat and mouse. A: N-ErbB4, B: GFAP, C: NeuN, D: merge, E: N-ErbB4 + TOPRO nuclear dye, G: N-ErbB4, GFAP, TOPRO nuclear dye.

In the whole brain coronal sections of mouse and rat neocortex, some ErbB4⁺/NeuN⁺ neurons from merged region D are indicated with white arrowheads and demonstrate a triangle-like shaped cell body. The GFAP staining appears quite low with few dots in B, possibly due to poor IHC (antibody binding/loss of epitope). Despite weak GFAP immunoreactivity the lower series of pictures shows a similar cell body shape for ErbB4 signal, that could be most compatible with neuronal cell body shape. Overall GFAP appears less colocalized with ErbB4 and with a lower signal strength (E - G) compared to NeuN. Single immunostaining to exclude a possible antibody interaction, with ErbB4 primaries only (images E + F) could confirm the observed neuron-like staining of images G and D.

3.2 ErbB4 immunofluorescence in AD

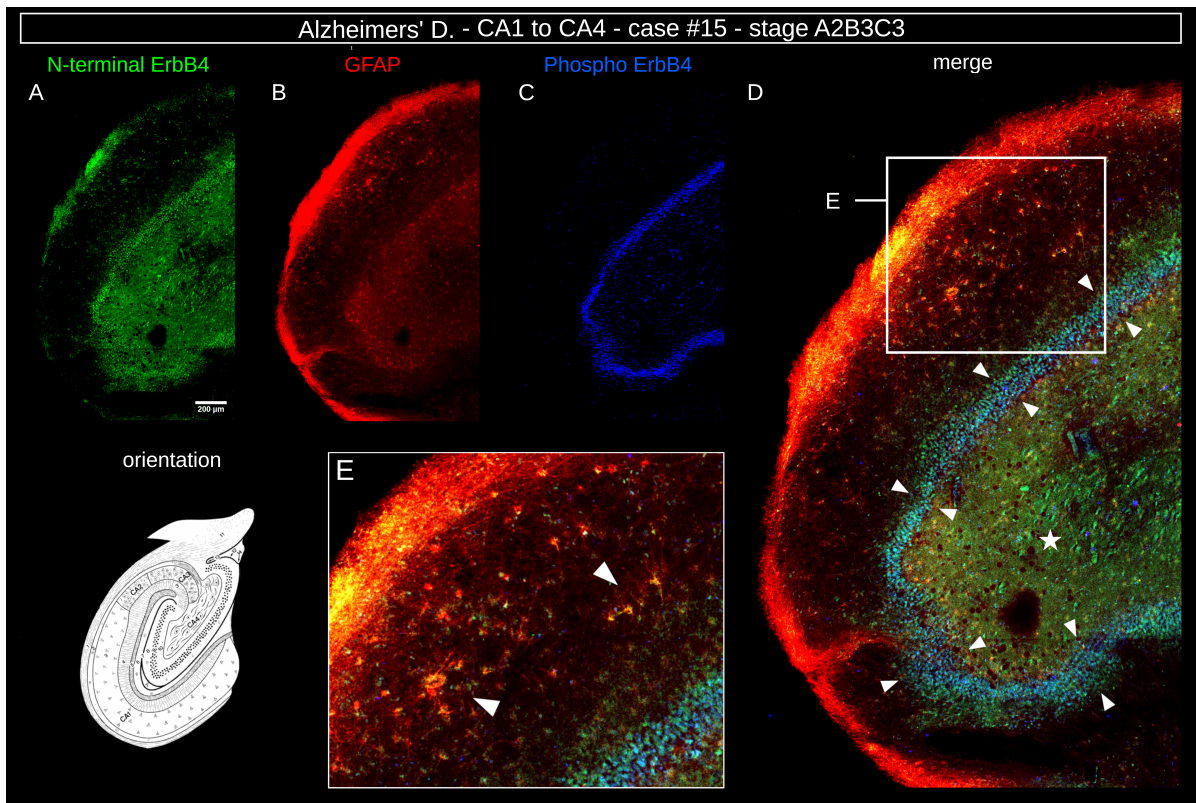


Figure 3.4: Human hippocampus, AD, CA1 - CA4 sectors, DG, case No. #15, stage A2B3C3. A: ErbB4, B: GFAP, C: P-ErbB4, D: merge, arrowheads: dentate granular layer, ☆ in D: CA4 sector, E: close up view, arrowheads: clusters of astrocytes.

Figure 3.4 (case No.#15) with a triple staining of Phospho-ErbB4, ErbB4 and GFAP, from case No.#15 (staged A2B3C3) demonstrates a representative example for ErbB4 expression in AD hippocampus. For orientation, the anatomical scheme [30] is shown in the left part of the figure. From the GFAP staining the outer borders of the alveus and the stratum oriens of the sample can be estimated. In the magnified region E, clusters of astrocytes positive for ErbB4 and GFAP, are shown in CA1 sector, as indicated by the arrowheads. Colocalization with ErbB4 seems to be present mostly on proximal cell body and in parts of the proximal processes. White arrows in the merged section D indicate strong

nuclear-like expression of Phospho-ErbB4 and ErbB4 (A) in the dentate granule cells. The CA4 sector (★) with low signal to noise ratio, shows high Erbb4 and GFAP signal, also with high reactivity along the GD. Signal from Phospho-ErbB4 is morphologically round, and most probably nuclear, potentially associated with granular cells. Interestingly, P-ErbB4 expression is limited to the dentate gyrus.

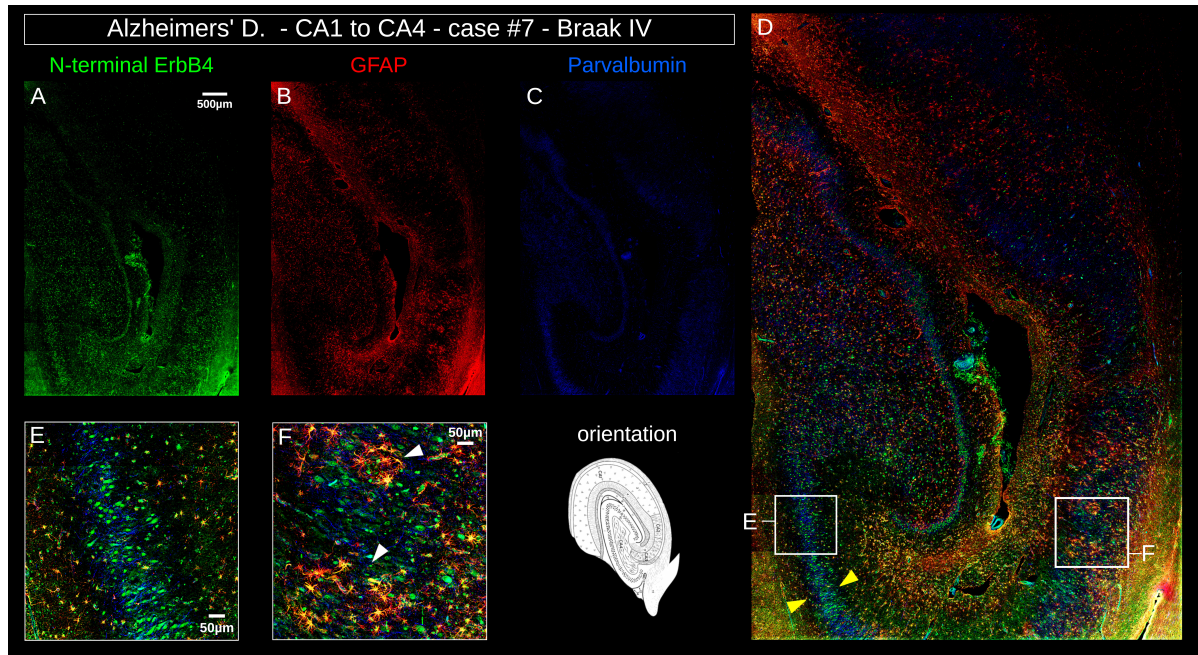


Figure 3.5: Human hippocampus, AD, CA1 - CA4 sectors, DG, case No.#7, Braak 4. A: ErbB4, B: GFAP, C: Parvalbumin, D: merge, arrowheads: dentate granular layer, E + F: close up views, arrowheads: cluster of astrocytes.

The overview in figure 3.5 (case No.#7, staged Braak 4) on CA sectors 1 to 4 shows a triple staining of ErbB4, GFAP, and Parvalbumin. Magnified regions show parts of CA3 and GD. Arrowheads on magnified region F point to histopathological hallmarks of putative neuritic plaques with clusters of astrocytes. High level of astrocytic reactivity with hypertrophic proximal processes and cell bodies. GFAP

channel shows different clusters of astrocytes, most prominent in ventral and dorsal CA3 and on the transition to CA4.

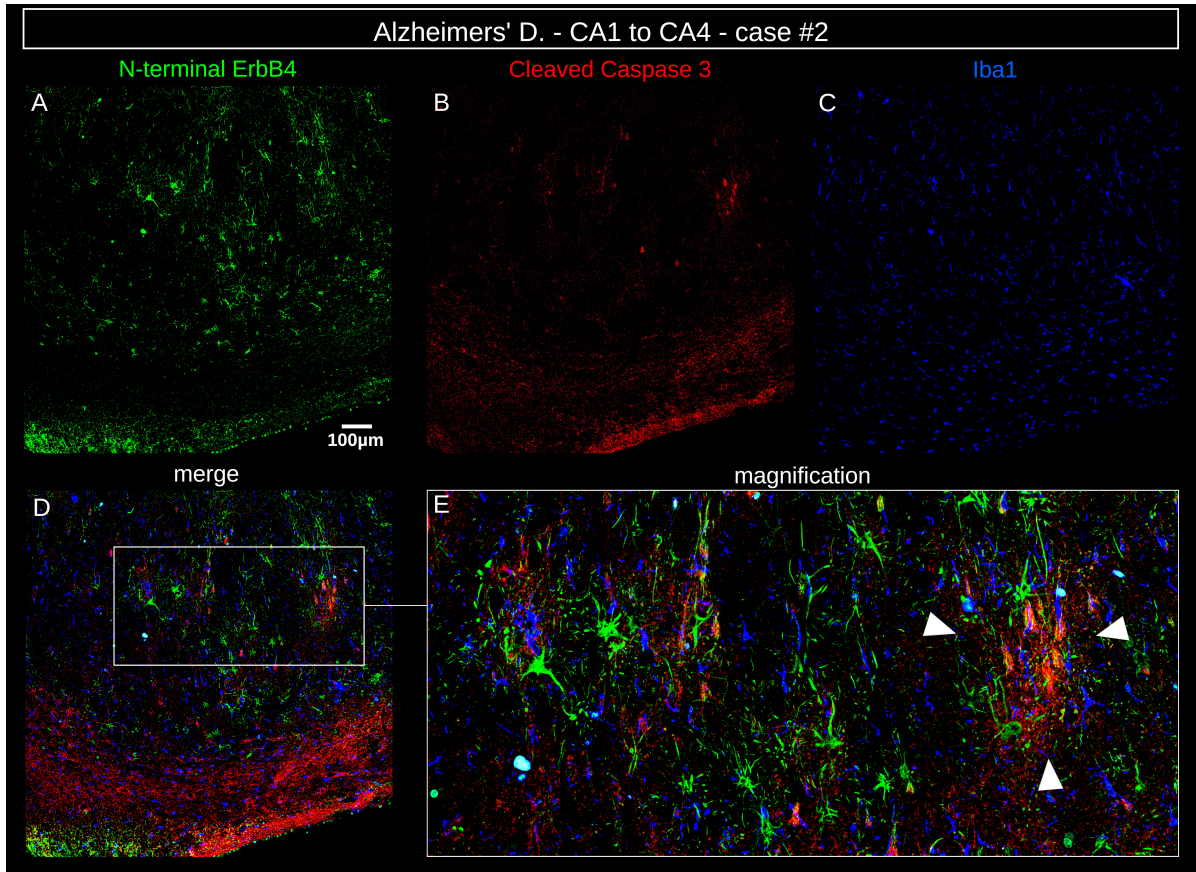


Figure 3.6: Human hippocampus, AD, CA1 sector, case No.#2, no staging available. A: ErbB4, B: Cleaved-Caspase 3, C: Iba1, D: merge, E: close-up view, arrowheads: cluster of astrocytes.

ErbB4 signal is present in nuclei of neurons almost throughout the entire hippocampus, with enhancement in the granular and pyramidal layer of CA1 as observed in figure 3.4 from page 47. Magnified regions show strong ErbB4 immunoreactivity on neurons and glial cell bodies. Some putative ErbB4⁺/GFAP⁻ neurons are surrounded by clusters of astrocytes as shown in region F. Parvalbu-

min staining looks similar to Phospho-ErbB4 from figure 3.4 along nuclei of the neurons in the dentate granule layer.

Figure 3.6 (case No.#2) shows a large part from the CA1 sector. ErbB4 appears as an almost GFAP-like signal where multiple clusters of astrocytes in the pyramidal layer and stratum oriens can be seen. Reactive astrocytes with long spiny processes and along strong immunoreactivity for Cleaved-Caspase 3, an indicator for apoptotic cell death, inside acquired CA1 sector. The triangle shaped morphology of Cleaved-Caspase 3⁺ cell bodies indicate that these cells most probably correspond to apoptotic neurons surrounded by reactive astrocytes. Thus, there seems to be a high level of codistribution between ErbB4⁺ regions and Cleaved-Caspase 3⁺ regions. In E these areas with apoptotic neurons surrounded by ErbB4⁺ astrocytes and Iba1⁺ microglia are magnified. ErbB4 immunoreactivity seems to be limited to astrocytes, although some microglia show a nuclear-like staining. The previously observed round, nuclear-like signal for ErbB4 is limited to some single cells on the lower end of the image.

In figure 3.7 inflammatory markers COX2, C1q, Cleaved-Caspase-3 in AD condition partially colocalize with ErbB4. Pronounced ErbB4 immunoreactivity accumulates around plaque-like cluster of Iba⁺ cells as indicated with the red circles in images D and H. Further, images A, E, I and M show ErbB4 positivity for the soma and proximal processes, counterstaining for GFAP, as demonstrated in image H (red circle) and image P (arrow). Remarkably, GFAP⁺ astrocytes that are not associated to the plaques, seem to be immunonegative for ErbB4, as indicated with arrowheads in pictures E - H.

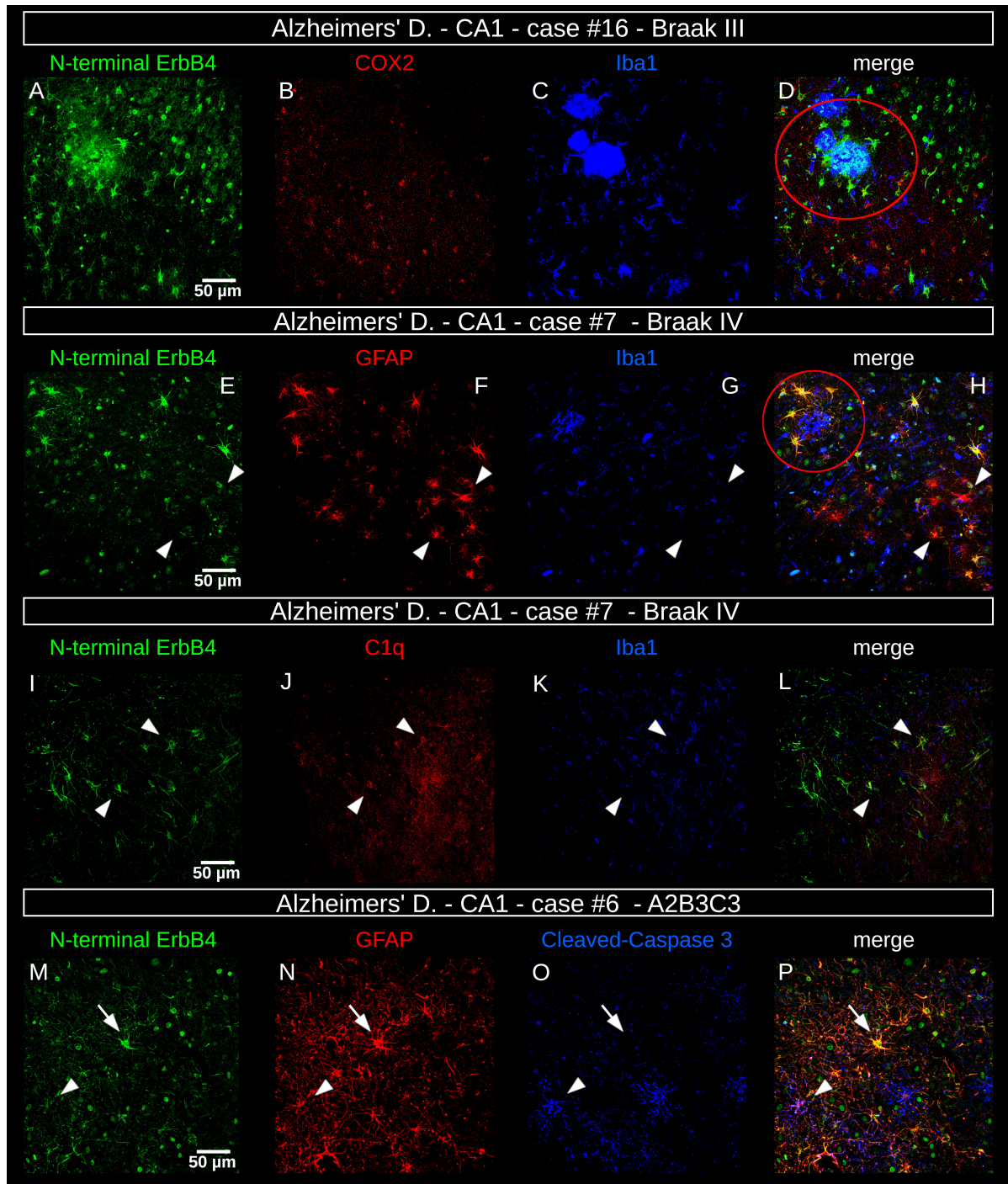


Figure 3.7: Human hippocampus, AD, case No.#16, stage Braak III (CA1 sector, images A - D), case No.#7, stage Braak IV (CA1, images E - L), case No.#6 stage A2B3C3 (CA1, M - P). Red circles around plaque-like Iba1⁺ clusters of reactive microglia.

In nearly all images, ErbB4 stains for some additional nuclei, probably neurons. Interestingly, there is no COX2 staining around the plaque in picture B. No visible ErbB4 signal was found for Iba1⁺ microglial cells in picture C, G and K. Arrowheads in picture I, J, K and L indicate an immunopositivity for the proinflammatory marker C1q complement factor together with ErbB4 surrounded by multiple Iba1⁺ cells. Only weak nuclear-like signal for ErbB4 in picture I. Apoptotic marker (arrowheads in picture M - P) show the positivity for GFAP, Cleaved-Caspase-3 and ErbB4 around the cell body. In summary the shown inflammatory microenvironments could be characterized by reactive astroglial cells, strongly expressing ErbB4 and clustering around plaques.

As ErbB4 is able to dimerize with other members of the EGFR family, the pattern of binding partners ErbB4 and EGFR, were analyzed in figure 3.8. As an addition to the previous figure, a distinct image with Parvalbumin⁺ cells on can be seen on sample AD1669. Strong reactivity of clustered astrocytes can be observed in picture B, F and J. Arrowheads in pictures A - D and E - H show some smaller cell, nuclear-like parts that are positive for both ErbB4 and ErbB3/EGFR. Overall nucleic signal for both dimerizing partner, with less strength in signal and no staining in cell body or proximal processes. Distinct nucleic signal of ErbB4 in picture I, costaining with Parvalbumin⁺ cells as indicated with white arrows in pictures I - L, which confirms that ErbB4 is expressed in interneurons.

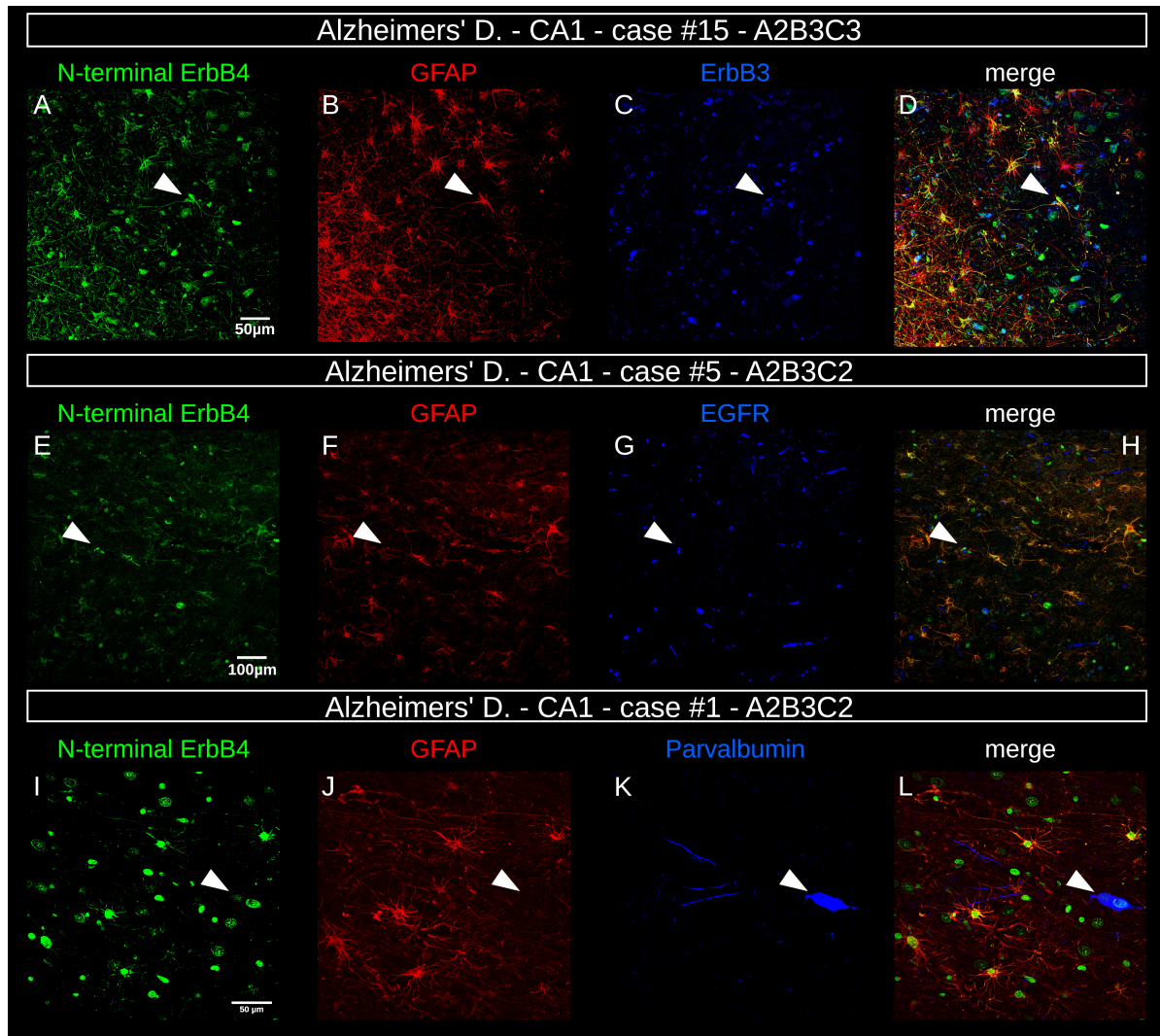


Figure 3.8: Human hippocampus, AD, case No.#15 (CA1 sector, images A - D), case No.#5 (CA1, images E - H), case No.#1 (CA1, images I - L). Immunostaining: N-ErbB4, GFAP, ErbB4 dimerization partners ErbB3, EGFR and interneuronal marker PV.

3.3 ErbB4 immunofluorescence in DLB and GB

Addressing the question number #7 (section 1.12) in order to investigate the expression of ErbB4 during inflammatory responses to different pathological conditions, DLB and GB samples were analyzed. In figure 3.9 two images from samples with DLB are shown to observe the colocalization of ErbB4, interneuronal

marker Parvalbumin and GFAP. Reactive astrocytes form several clusters, possibly around a plaque-like structure, as indicated with the arrowheads highlighting GFAP⁺/ErbB4⁺ double positive cells in images A to D.

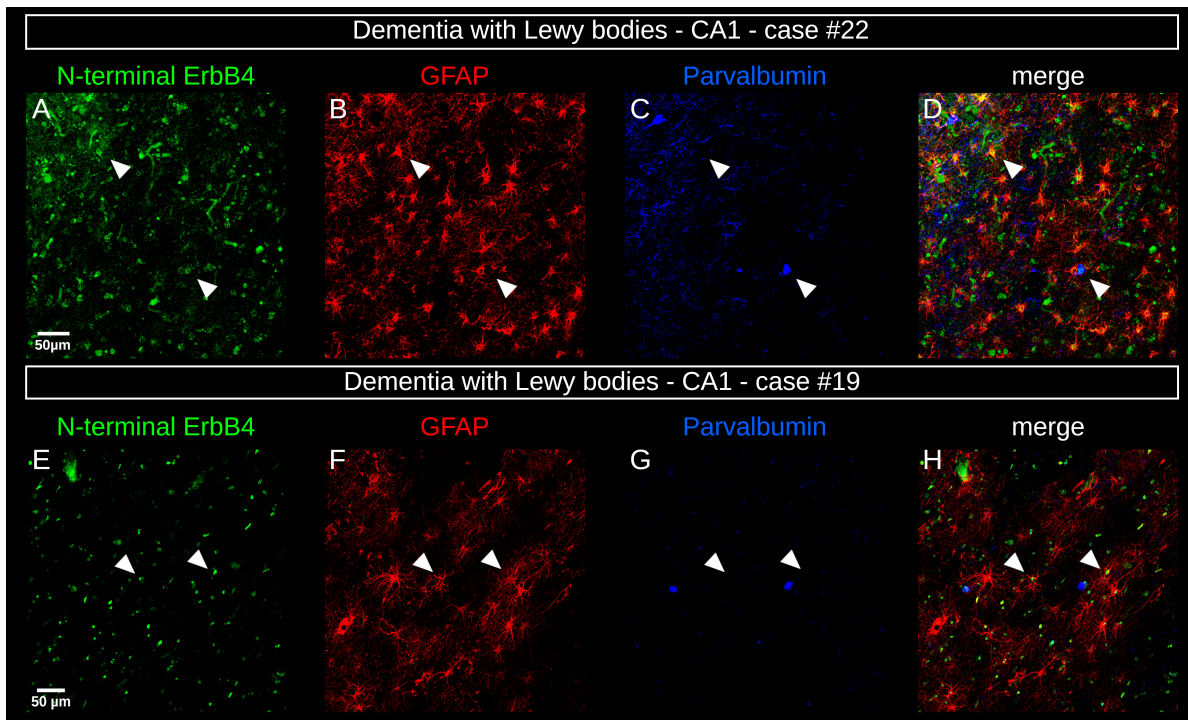


Figure 3.9: Human hippocampus, DLB, case No.#22 (CA1 sector, images A - D), case No.#19 (CA1, images E - H), Immunostaining: N-ErbB4, GFAP, PV.

For images E to H, ErbB4 seems to be weaker and more nuclear-like, with no immunopositivity for the soma and the processes for astrocytes. Concerning the observation of interneurons expressing ErbB4 from previous AD and CTL samples, there seems to be no visible colocalization of Parvalbumin positive nuclear-like staining in image G, neither for GFAP nor ErbB4.

Figures 3.10 and 3.11 display the results from Glioblastoma brain tumor cases #37 and #38. Nissl stainings were also analyzed as overviews together with double immunohistochemistry (ErbB4 and GFAP) and TOPRO[®] nuclear staining.

Magnified regions of interest are outlined with rectangular boxes. The arrowheads indicate ErbB4⁺ astrocytes, with strong signal in cell body and processes.

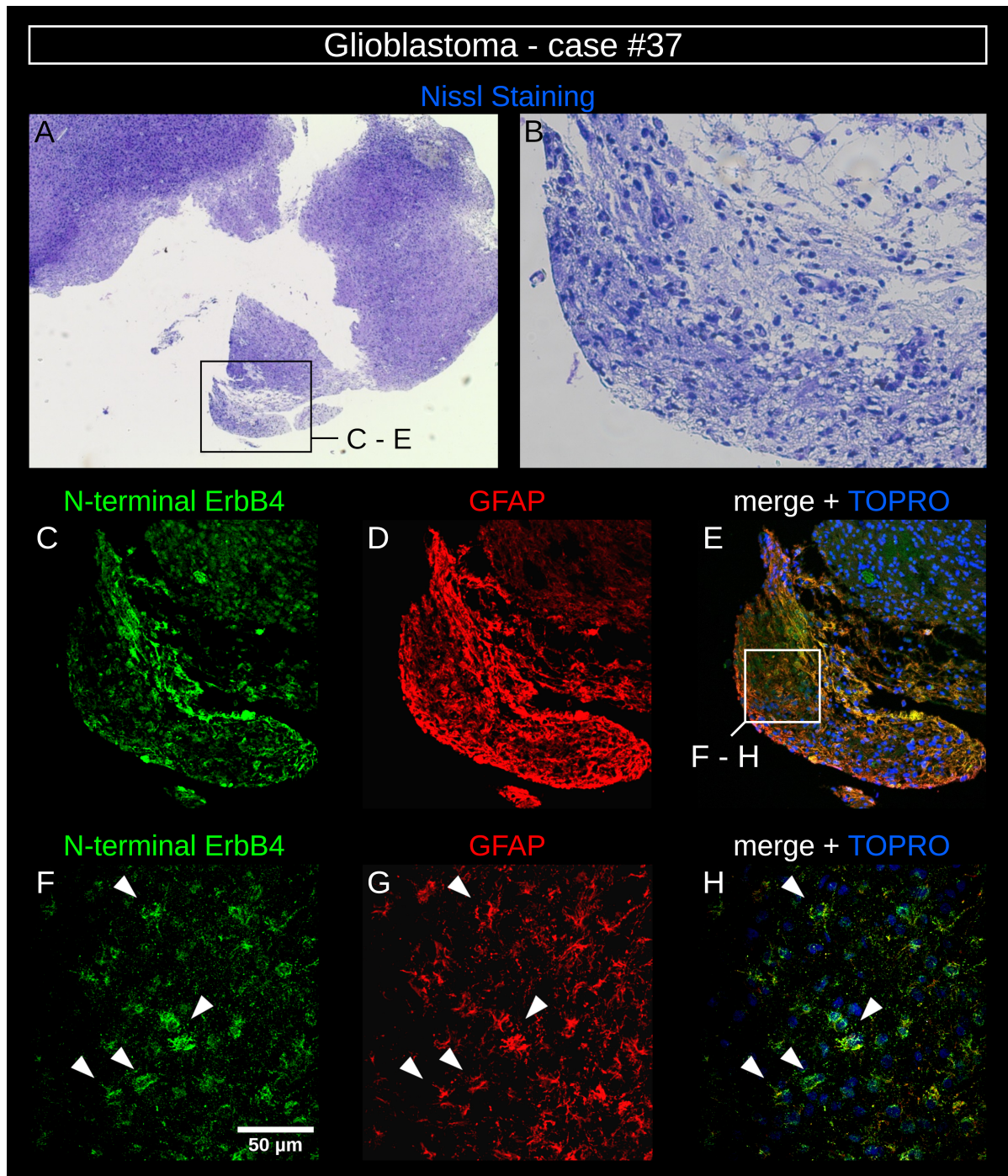


Figure 3.10: Glioblastoma brain tumor, case No.#37, Nissl stainings (A, B), box in A around close-up view of immunostainings (C - E), and from area E (F - H), arrowheads with ErbB4⁺ and GFAP⁺ astrocytes.

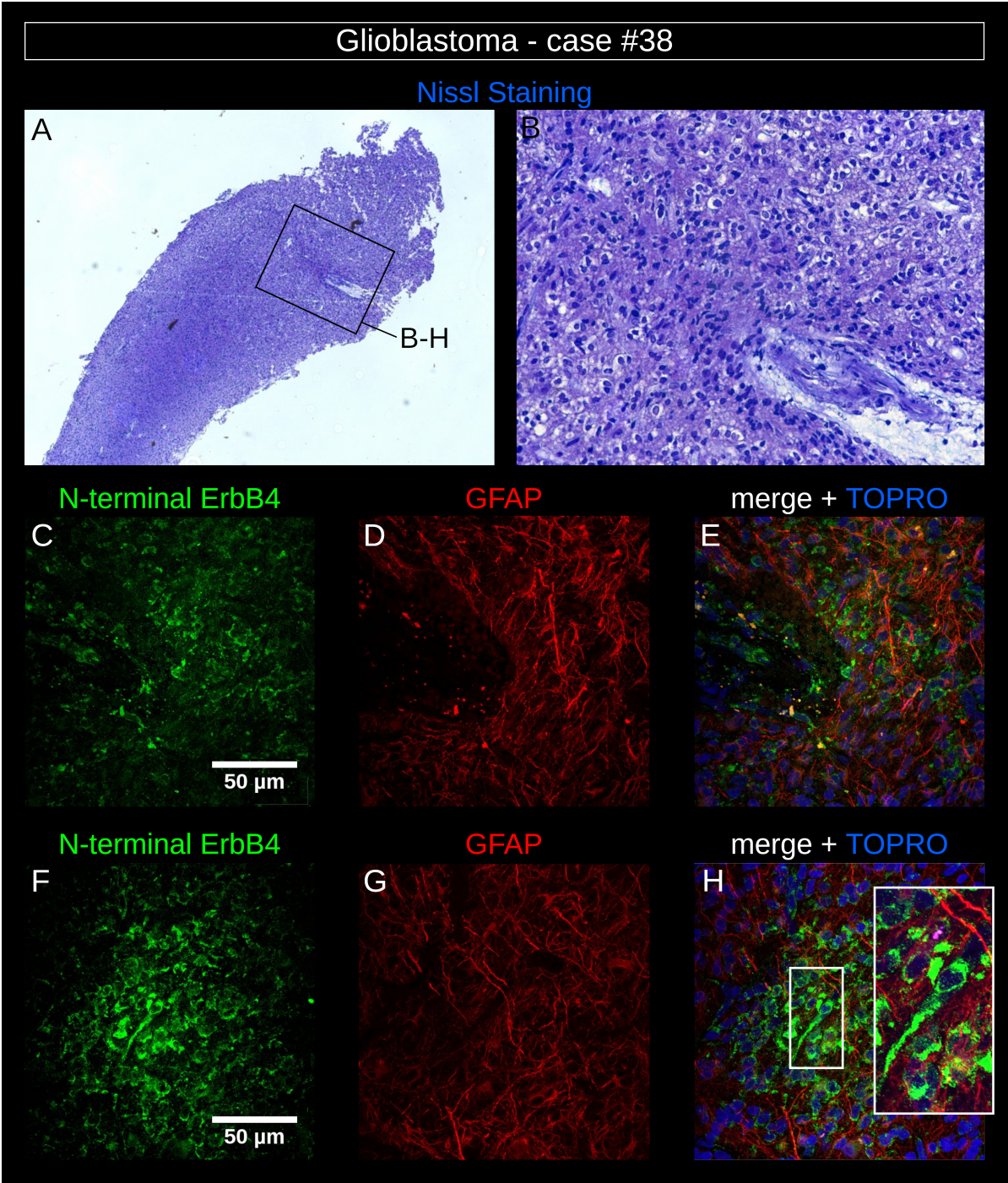


Figure 3.11: Glioblastoma brain tumor, case No.#38, Nissl stainings (A, B), box in A around close-up view of image B. Close-up view of image H with ErbB4⁺/GFAP⁺ astrocytes.

Figure 3.11 shows images taken from Glioblastoma sample No.#38. with high cell density and picture E + H with decent colocalization of both GFAP and ErbB4, which seems mostly perinuclear and on the proximal cell body including some processes. ErbB4 seems to be expressed in the soma of astrocytes in GB tissue, including activated and dividing astrocytes. Compared to AD an overall lower nuclear-like signal can be observed.

3.4 ErbB4 immunofluorescence in-vitro

Based on the results from human brain sections, the question No.#6 was addressed to investigate whether the findings of ErbB4 positive astrocytes were reproducible in-vitro. Astrocyte cultures and treatments would additionally allow a protein and RNA expression analysis, which human brain sections could not provide due to PFA fixed tissue. To date, no publication exists concerning the stimulation of ErbB4 in astrocyte cultures with receptor ligands and proinflammatory $\text{TNF}\alpha$. Therefore question No.#7 and concerning the effect of culture treatments, was addressed after the astrocyte culture model has been established. The easy accessible and fast dividing murine immortalized C8-D1A astrocytes turned out to be a suitable cell line. Next, we utilized primary murine astrocytes of newborn mice, as this culture system resembles the in-vivo system more closely. Subsequently, question No.#8 was addressed by the extraction of protein and RNA after treatments for the analysis of putative anti- or proinflammatory responses. To reassure that the ErbB4 antibody equally renders a specific epitope binding for the murine culture model, negative controls with only secondary antibodies and IgG isotype control turned out negative.

3.4.1 Murine C8-D1A immortalized astrocyte culture

The immunostaining from figure 3.12 on C8-D1A astrocyte cultures was done with two antibodies for ErbB4 (N-terminal extracellular domain and the activated, phosphorylated tyrosine domain), the astroglial marker GFAP and nuclear dye DAPI.

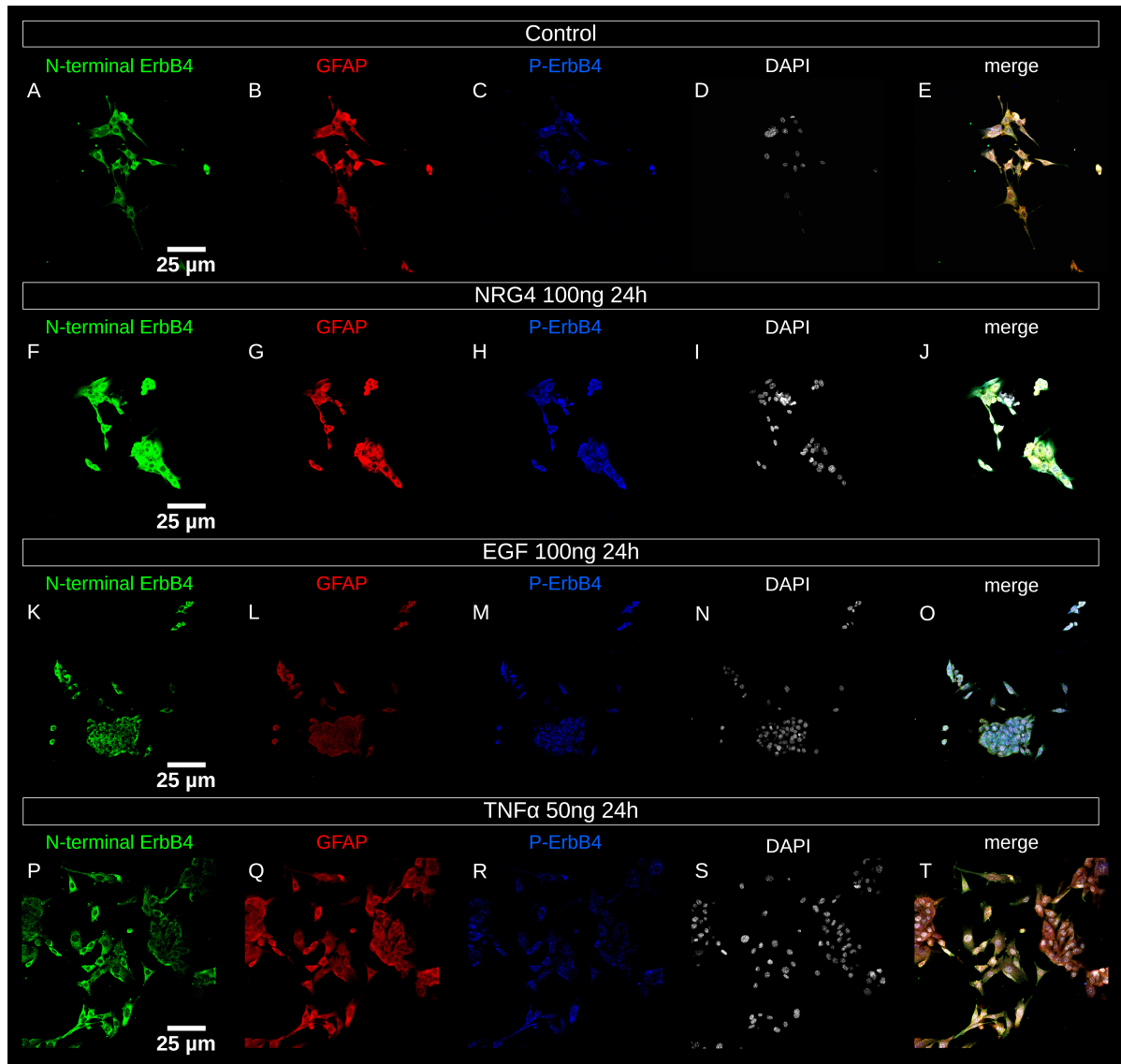


Figure 3.12: Immunofluorescence on C8-D1A immortalized astrocyte culture. Antibodies: N-ErbB4, Phospho-ErbB4 and GFAP and nuclear dye DAPI. A - E: Control condition, 24 h treatments in images F to J (NRG4), K to O (EGF) and P to T (TNF α).

From top to bottom, each row displays different 24 h treatment with respective ligand and its effect on the immunofluorescence (see headers above images). Different treatment conditions with ErbB4-specific receptor ligand NRG4, ErbB1-specific receptor ligand EGF and proinflammatory $\text{TNF}\alpha$.

In control condition of figures A - E, groups of astrocytes with few short and spiny processes with no full confluent cell layer is illustrated. ErbB4 and GFAP seem to be mainly expressed in the cells membrane, whereas the signal for Phospho-ErbB4 seems more pronounced around the nucleus. In images F - I, immunofluorescence after treatment with ErbB4 specific ligand NRG4 was performed. The expression of all three proteins appears increased, with no visible cell processes for the dense group of cells. Images K - L show the effects of EGF receptor ligand, which is specific for ErbB1 receptor but is able to dimerize with ErbB4.

Compared to control no specific upregulation for neither ErbB4, GFAP nor P-ErbB4 can be observed, possibly due to no direct activation of EGF on ErbB4. The change of immunofluorescence after $\text{TNF}\alpha$ treatment in images P - T is surprisingly small and can be compared to control. Overall, the treatment with receptor ligand NRG4 seems to induce the highest expression change for ErbB4, GFAP and Phospho-ErbB4.

3.4.2 Murine primary astrocyte culture

Figure 3.13 shows stainings with ErbB4, GFAP and DAPI nucleic dye, the comparison of control condition (images A - D) and further 24 h treatment conditions in the following lines. First, images E - H display 24 h treatment with ErbB4

ligand NRG4. GFAP and ErbB4 expression seems to be upregulated. The processes appear to be thicker and more dense when compared to control. After 24 h EGF treatment (I - L) there seems to be a higher cell number with higher DAPI signal, and a higher GFAP upregulation compared to ErbB4. Morphologically, the number, volume and length of processes seems to be increased.

Images M - P from treatments with proinflammatory $\text{TNF}\alpha$ display a stressed cytoarchitecture with long and branched processes, with GFAP and ErbB4 upregulation. On the last row (Q - T) with $\text{TNF}\alpha$ and NRG4 treatments, ErbB4 upregulation seems to be highest, with lower GFAP expression compared to $\text{TNF}\alpha$ treatment only.

The stressed cells with even longer and branched processes stretch almost over half of the image. Not all of the ErbB4⁺ cells are positive for GFAP. Interestingly, strong nucleic ErbB4 signal as observed for human brain samples in control (e.g. figure 3.1) does not appear to be present here, and seems to be expressed equally along the cell membrane, without preference, although picture A in control condition shows a slight accentuated cell soma, with reactivity along the processes.

In EGF and NRG4 conditions, the cells appear less stressed with shorter processes and a more organized, less chaotic cell arrangement. Further, the expression for GFAP and ErbB4 seem to be less upregulated and seems to be higher after $\text{TNF}\alpha$. Overall, in increasing order, GFAP and ErbB4 expression rates range from NRG4 to EGF to $\text{TNF}\alpha$ or $\text{TNF}\alpha$ + NRG4 treatments with less GFAP upregulation after EGF treatment.

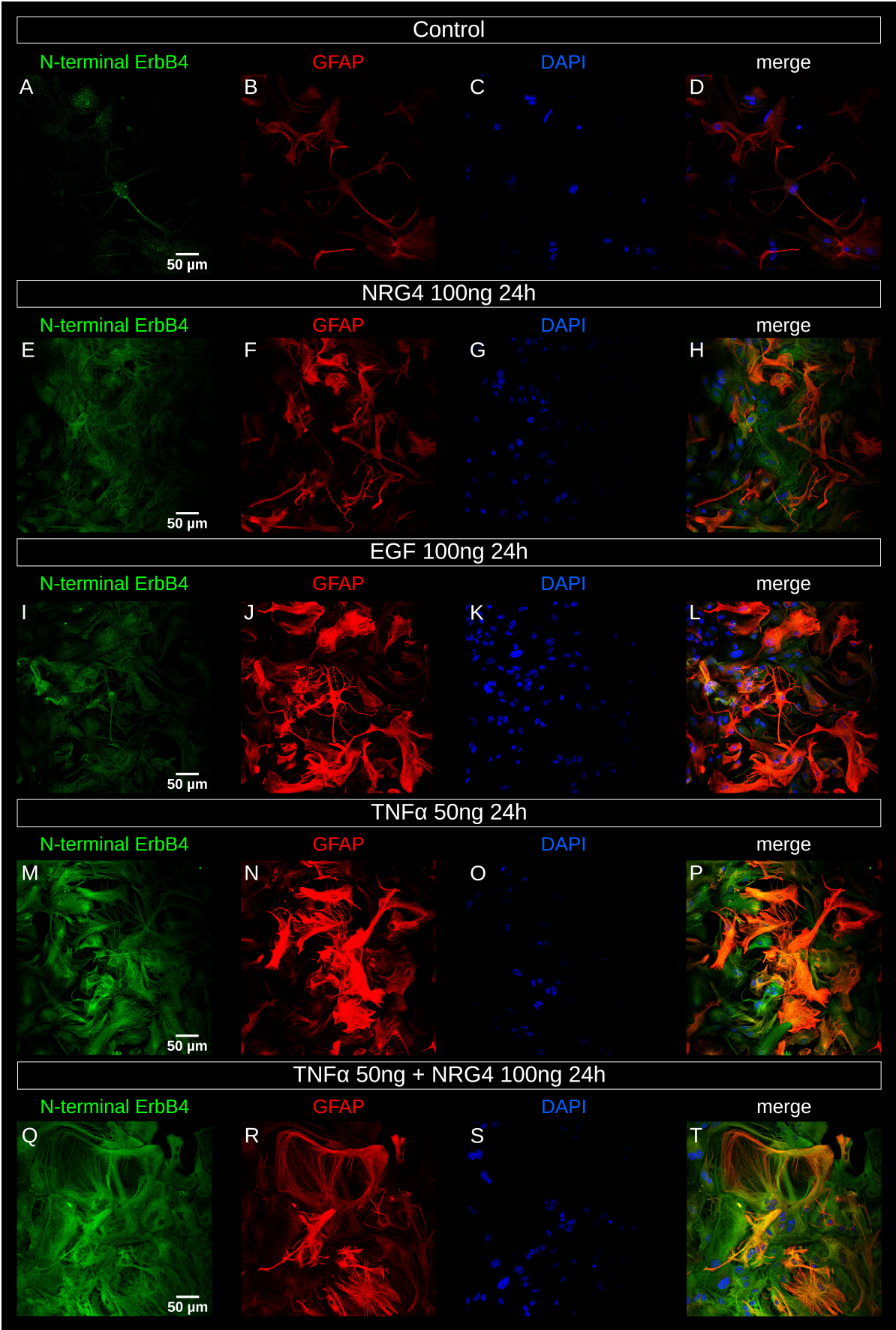


Figure 3.13: Primary astrocyte cell culture, 24 h treatments.

3.4.3 Human iPSC astrocyte culture

The human iPSC culture experiments could not provide reliable results, due to a unfortunate high cell death rate. Therefore, no treatments with receptor ligands and subsequent immunohistochemical analysis was performed. In figure 3.14 a preliminary snapshot through a bright-field microscope of a few human astrocytes can be seen.

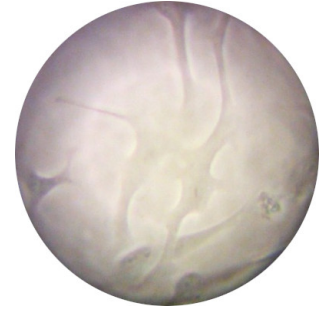


Figure 3.14: Human iPSC astrocytes

3.5 Quantitative analysis

A quantitative analysis, using the scale from table 2.5, has been performed. There was no statistically significant difference in the frequency of a nuclear-like expression of ErbB4 between AD (Mean=3.6) and control (Mean=4), $U=87.00$, $Z=-1.331$, $p=.183$. There were statistically significant differences of ErbB4 being expressed in the cell body or the proximal processes between AD (Mean=4.41) and CTL (Mean=2.14), $U=33$, $Z=-3.606$, $p<.001$, as well as between medians (AD Mdn=4, CTL Mdn=2.5) for colocalization of ErbB4 with GFAP, $U=28.5$, $Z=-3.705$, $p<0.001$, as between medians (AD Mdn=4, control=3) for intensity of GFAP fluorescence, $U=16.50$, $Z=-4.321$, $p<.001$.

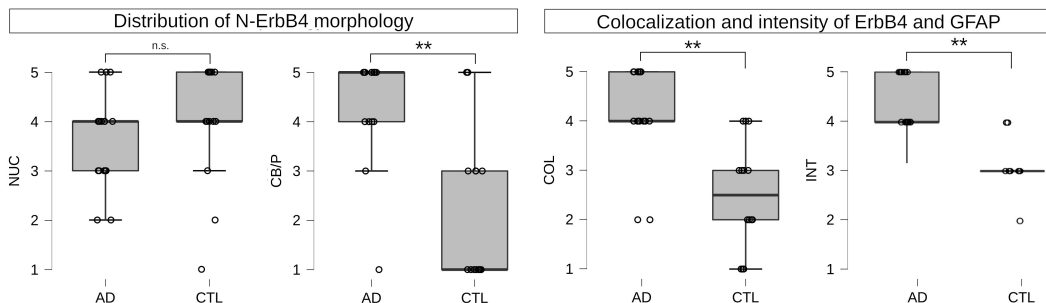


Figure 3.15: Boxplots of semiquantitative analysis, abbreviations: NUC=nuclear-like, CB/P=cell body/processes, COL=colocalization, INT=intensity, n.s.=non significant, p values: ** = $<.001$.

3.5.1 Digital fluorescence analysis on human samples

Unpaired t-test was conducted for testing difference in GFAP and ErbB4 intensities between AD and control groups. The precondition for a t-test is a Gaussian normal distribution of the data, which was recommended to be confirmed with a Shapiro-Wilk test (small sample size $n < 30$) on a significance level of $\alpha = .05$, which was not significant for all conditions, therefore the analyzed data is normally distributed (confirmed normality assumption): GFAP Control ($p = .334$), GFAP AD ($p = .654$), ErbB4 Control ($p = .425$), ErbB4 AD ($p = .918$). Results of t-test show there was a statistically significant difference in ErbB4 values between AD and control, $t(14) = 5.854$, $p < .001$, $d = 2.95$. For GFAP values between AD and control $t(14) = 3.355$, $p < .005$, $d = 1.69$. There was a strong correlation between groups ErbB4 and GFAP throughout all samples (Control + AD samples, $n = 16$), $r = .606$, $p < .013$, with $\alpha = .05$ for two sided t-test. The correlation factor of $r = .606$ shows a correlation between ErbB4 and GFAP values.

Protein	Group	Mean	SD
ErbB4	Control	132.3	89.83
	AD	542.05	154.04
GFAP	Control	538.95	264.16
	AD	1270.75	449.92

Table 3.1: Mean pixel intensity under areas: AD vs. Control samples. Intensities as pixel value in AU (arbitrary units).

3.5.2 Western blot

In Western blot analyses of total protein extractions from primary and immortalized astrocyte cell cultures, ErbB4 bands at molecular weights of ~60 kDa and ~260 kDa were detected. As this differs from the manufacturers' specifications in the data sheet (~80/180 kDa) and other published results of ErbB4 protein in astrocyte cell culture, different materials and methods were tested for error diagnostics.

Different antibodies (Phospho-, C-term, 2x N-term), HRP or immunofluorescent secondary antibodies, semidry or wet transfer for high/medium molecular weight, sonication of the pellet, with no effects on the result. Clean bands for α -Tubulin, GFAP, β -Actin, P-Erk show good migration and transfer conditions and approximately equal amounts of pipetted total proteins.

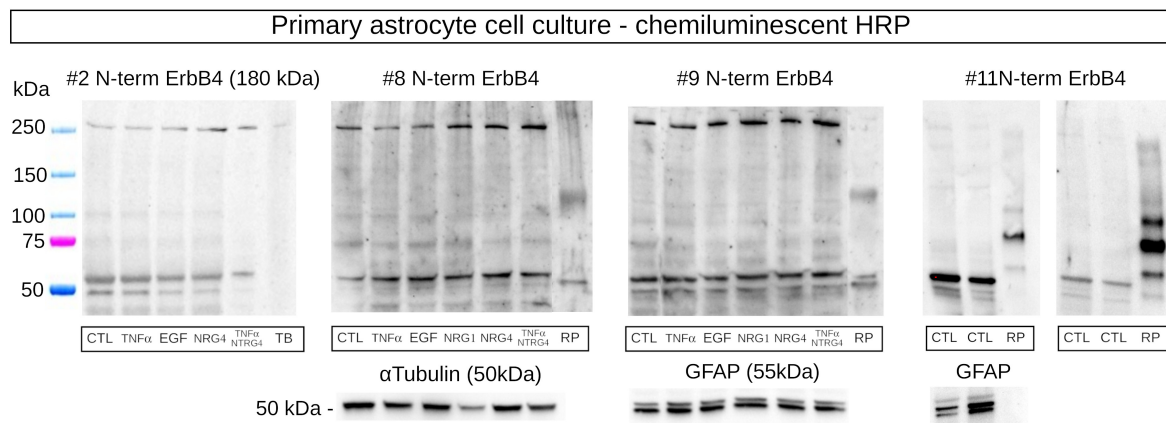


Figure 3.16: Western Blots of primary astrocyte cultures (see table 6.1), after 24 h treatments. TB: Total mouse brain, RP: Recombinant protein.

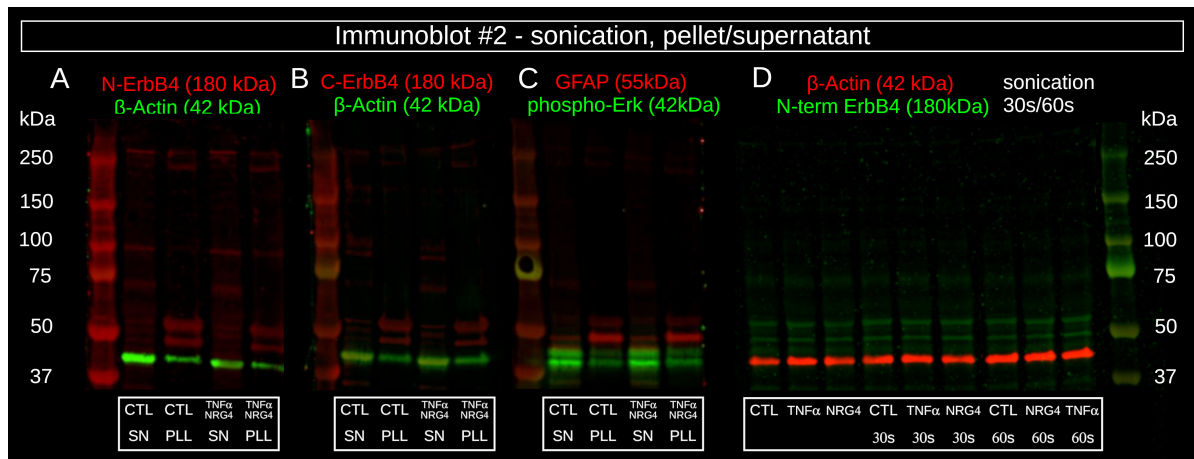


Figure 3.17: Western Blots of primary astrocyte culture (see table 6.1, after 24 h treatments, conditions: pellet/supernatant separated and 30s/60s sonicated. SN: Supernatant, PLL: Pellet.

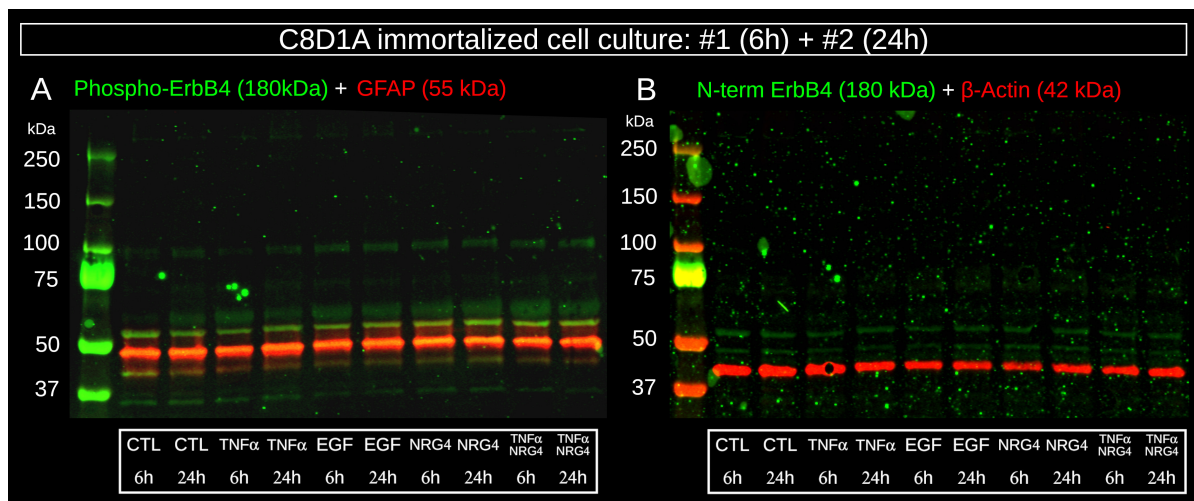


Figure 3.18: Western Blots of C8D1A immortalized cell culture with different treatments

3.5.3 qPCR

The scatterplot shows the distribution of individual $\Delta\Delta Ct$ values for each technical replicate. Depending on the qPCR experiment with either two for ErbB4 and ErbB1 primers or three data points. The \log_2 fold change of expression (y-axis) with different cell culture treatments (24 h) (x-axis) and explanations

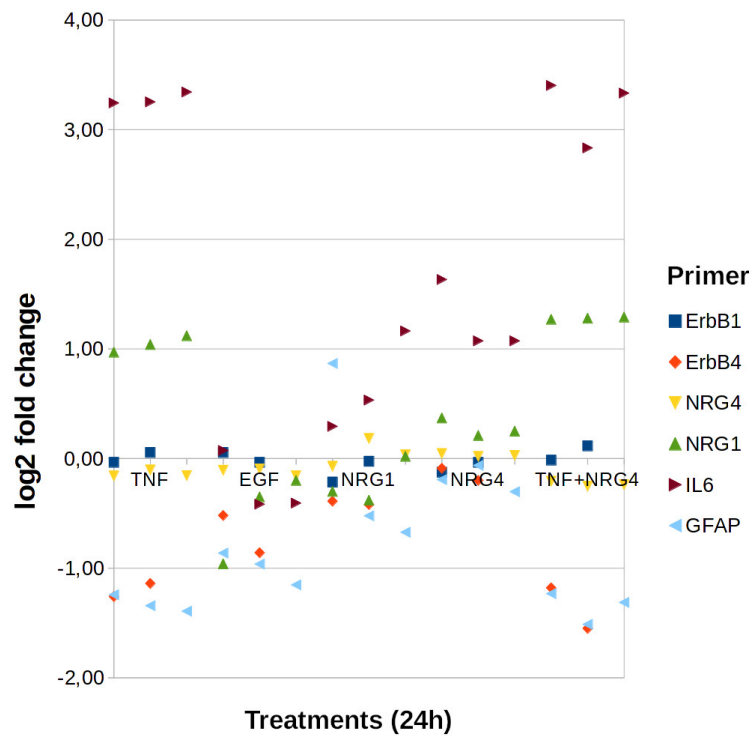


Figure 3.19: qPCR $\Delta\Delta Ct$. values for primers on cDNA of primary astrocyte culture after 24 h treatments

for each gene/primer with different symbols on the right. As expected, high values for IL6 expression after $TNF\alpha$ administration were measured, as an inflammatory response. NRG1 seems to be upregulated in $TNF\alpha$ and $TNF\alpha+NRG4$ conditions. Surprisingly, GFAP and ErbB4 are downregulated in inflammatory conditions with similar range of values for different treatments. Concerning potential anti-inflammatory effects after ErbB4 activation, the administration of ErbB4 specific ligand NRG4 lead to an 2-fold increase of IL6 expression.

4 Discussion

4.1 ErbB4 overexpression in reactive astrocytes

The induction of reactive astrogliosis, as a common hallmark of different neurological diseases is accompanied by the upregulation of GFAP. The primarily observed expression of ErbB4 in reactive astrocytes in immunostainings on samples of human AD hippocampi, as addressed in question No.#1, demonstrated the upregulation of ErbB4 in inflammatory conditions. ErbB4 expression was also present in putative neurons in human control hippocampus samples in GFAP negative, pyramidal-like cells. This finding of ErbB4 positive neurons in control was confirmed in the immunofluorescence of control cortex of mouse and rat, with ErbB4 positivity for NeuN⁺ neurons, but not for GFAP⁺ astrocytes. This points to a possible relationship between the induction of the reactive state and the expression of ErbB4. The colocalization of GFAP⁺ and ErbB4⁺ astrocytes confirms the previous finding of ErbB4⁺ astrocytes around neuritic plaques by Chaudhury et al. [70].

Interestingly, ErbB4 negative but GFAP positive astrocytes were spatially not associated with plaque-like structures, as demonstrated in figure 3.7. This finding of a subpopulation around putative plaques, suggests a possible link to a number of pathways that are involved e.g. in processing of APP or degradation of the plaque. The γ -secretase complex is both involved in ErbB4 cleavage of the intracellular domain E4ICD [82] and APP. In AD conditions, the excessive accu-

mulation of APP leads to higher concentrations of the intracellular domain AICD which is cleaved by the γ -secretase complex. The accumulation of AICD could in turn lead to a comparatively lower E4ICD concentration in the nucleus. In neurodevelopmental studies on mice, the regulation of the E4ICD unit was involved in the inhibition of GFAP expression, as observed during astrocytogenesis [48].

As a potential hypothesis, the AICD unit could antagonize the E4ICD on a competitive transcriptional level, resulting in a combined GFAP and ErbB4 overexpression. In short, the interaction of ErbB4 and APP processing could fail to inhibit GFAP upregulation, resulting in GFAP overexpression as observed in this thesis. This assumption would describe the observed GFAP and ErbB4 positive astrocytes in a subpopulation of astrocytes in the hippocampus of human AD samples around plaque-like structures. The involvement of the presenilin pathway could therefore serve as a potential molecular link between the observed altered GFAP and ErbB4 signalling of reactive astrocytes in AD pathology.

Additionally, the observation of a subpopulation of astrocytes expressing ErbB4, might be associated with paracrine signalling. As a potential mechanism, previous studies demonstrated astrocyte cultures overexpressing and secreting NRG1 after LPS treatment [78] or around induced traumatic sites after in-vitro forskolin treatment as an inductor of astrogliosis [79]. As cAMP is able to induce elevated NRG1 and GFAP expression it could constitute an additional link between ErbB4 and GFAP pathways. A further investigation of the ErbB4 activity around plaques, together with an immunostaining against on ErbB ligands (NRG1, NRG6, NRG4) as potential agents could elucidate a possible paracrine mechanism behind subpopulational ErbB4 activity.

Concerning the ErbB4 expression patterns in reactive (AD) vs. resting (CTL) astrocytes in human hippocampus, the observations ranged from homogeneously nuclear-like (for CTL cases), to a more pronounced membranous signal along the cell soma and the processes (for AD cases). The strong nuclear-like staining in control conditions was not expected, as the applied N-terminal antibody is supposed to target the extracellular part of the transmembranous ErbB4 protein and should therefore result in a more membrane targeted signal. Possibly, the nuclear expression pattern is due to the internalization and translocation of membrane to the nucleus.

Concerning AD condition, the observation of ErbB4 upregulation in the cell body showed less pronounced nuclear-like signal in inflammatory conditions of human hippocampal samples. This could be reproduced for astrocyte culture treatments with receptor ligands and proinflammatory $\text{TNF}\alpha$, to address question No.#7 of this study.

Regarding primary cell cultures, treatments with pro-inflammatory molecule $\text{TNF}\alpha$ alone, as well as in combination with NRG4, lead to a 2-fold elevation of NRG1 expression in qPCR experiments. This would confirm the observation of a upregulation for the ErbB4-NRG1 axis of reactive astrocytes. Interestingly, ErbB4 and GFAP expression is downregulated after $\text{TNF}\alpha$ treatment, possibly due to a shorter incubation time (24 h) compared to chronic reactive states of astrocytes in AD. Nevertheless, the qPCR experiment is limited to only one technical replicate which limits the explanatory power of these observations. Unfortunately, no comparative experiments or publications as have been performed yet.

4.2 Correlation of ErbB4 and GFAP

The measured correlation factor of ErbB4 and GFAP expression through AD and CTL samples is $r=0.606$ ($p<.013$, $\alpha=.05$). Therefore, the question of No.#1 concerning a potential correlation of ErbB4 and GFAP applies for low GFAP/ErbB4 values in control and for higher values in AD condition. It confirms the morphological observation of ErbB4 positive reactive astrocytes, as GFAP is upregulated in reactive astrogliosis. Hence, a correlation of two proteins does not necessarily imply a causal effect. The upregulation of ErbB4 can be induced by a multitude of different causes, through different pathways and transmitters. Whereas ErbB4 overexpression seems to be associated with GFAP upregulation, ErbB4⁻ cells with no proximity to plaque-like structures seem to be GFAP negative.

Assumptions from this study with a comparatively small number of cases and observations, are potentially prone to a lack of representability. Therefore, conclusions deduced from this data should be carefully drawn, as they only reflect results from small populations of cells. To investigate whether the observed correlation of GFAP and ErbB4 can be confirmed, a comparison to larger scale analyses from online available sequencing atlases (R2, Ben Barres and scREAD) will be described in the following part of the discussion.

On R2, a large-scale sequencing database with microarray data from AD dataset gse48350 includes a high number of samples ($n=253$, age 20-99 years), extracted from four brain regions (hippocampus, entorhinal cortex, superior frontal cortex, post-central gyrus), see figure 4.1.

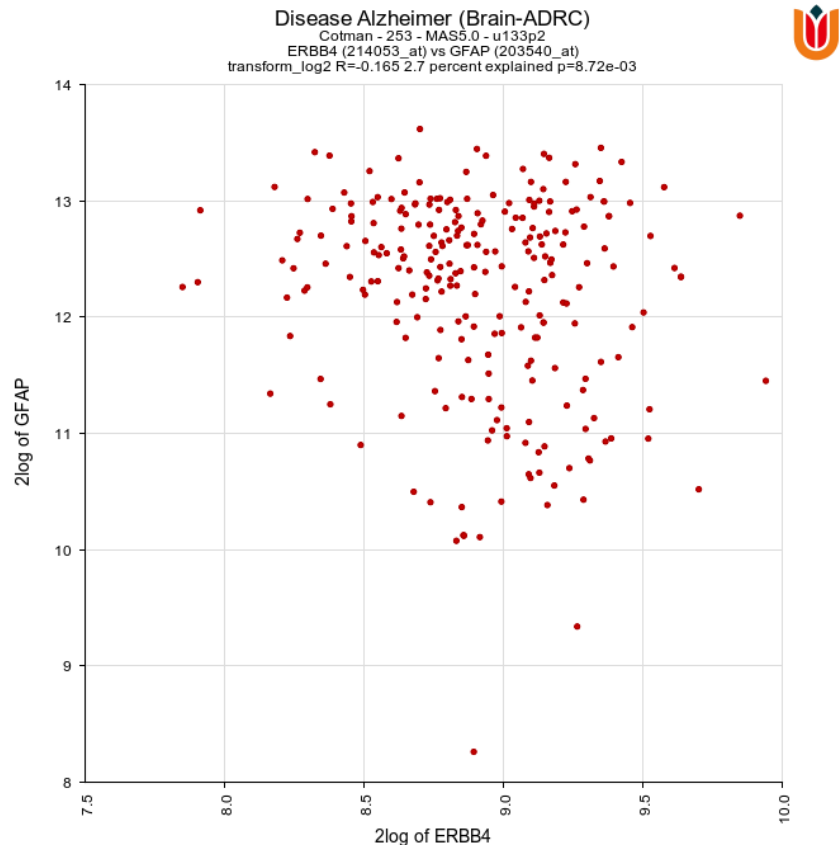


Figure 4.1: Results from R2 online sequencing atlas: Relation for ErbB4 and GFAP expression a 2log scale from RNA extraction from human AD brain samples from the Cotman dataset. Sample size is $n=253$. Each dot represents a sample. ARDC: Alzheimer disease research center, University of Washington. Cotman: Carl Cotman, University of Illinois, MAS5.0: gene expression detection algorithm. u133p2: GeneChip Human Genome U133 Plus 2.0 Array, $r=-0.165$, $p<0.01$ [87]

Each dot represents sequencing data from one case, including all four brain regions. On the y-axis, the 2log scaled expression of GFAP is displayed, whereas on the x-axis the respective 2log scaled expression of ErbB4 is shown. Overall, this sample set demonstrates a significant inverse relation of ErbB4 and GFAP expression ($r=-.165$, $p>.001$). Although this data is more reliable due to its larger scale, it still needs to be cautiously interpreted, as it might be inaccurate due to

obliterated expressional differences of different cell types and subpopulations as well as due to different brain areas that were sequenced together.

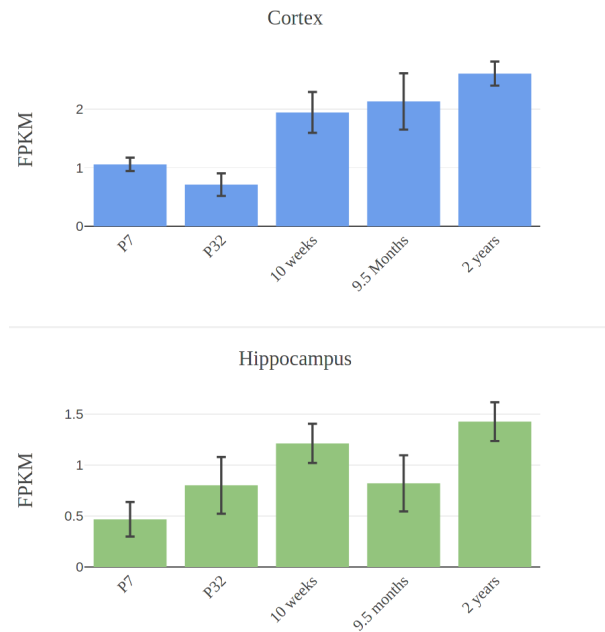


Figure 4.2: ErbB4 expression of aged mice, Ben Barres sequencing database. Y-axis, FPKM: Fragments per kilobase of transcript per million fragments mapped. x-axis, age of mice: P7 = 7 days, P32 = 32 days. Black strokes indicate the range of standard deviation [73].)

From another sequencing database of Ben Barres, the murine ErbB4 expression in the hippocampus and cortex is demonstrated for different ages [73]. On the y-axis the expression rate, as indicated with fragments per kilobase of transcript per million fragments mapped (FPKM), displays different levels of ErbB4 for aged mouse hippocampus and cortex. The y-axis illustrates the different ages of included mice. Concerning ErbB4 expression, it is

interesting to see that ErbB4 expression is increasing continuously with the age.

Concerning the relation to AD and the connection to ErbB4, it should be noted that aged mice were reported to contain elevated levels of astrocyte reactivity [73]. Therefore, aged mice that are known to express elevated levels of pro-inflammatory molecules like C1q, TNF α and Il1 β , correlate with higher ErbB4 expression levels. This correlation is consistent with the results from the current thesis revealing higher ErbB4 expression around inflammatory regions like AD related plaques and after TNF α administration. Prospectively, further analyses

on the cases from this study regarding a potential correlation of ErbB4 and age or AD staging need to be performed.

Hence, the interpretation of the results of this study with larger sequencing atlases R2 and Ben Barres has to be done with some caution. As this sequencing atlas is not cell specific, different expression levels of different cells are omitted. Possibly, the ErbB4 expression in (inter-)neurons is diminished in AD which will further lower the global expression level. Thus, these analyses do not provide a solid basis to analyse ErbB4 expression specifically in astrocytes.

Moreover reactive astrocytes in AD condition that surround the neuritic plaques in the hippocampus were shown to become hypertrophic, whereas in other regions they tend to become atrophic [88]. This demonstrates cell specific differences in different brain areas, that are not respected in the R2 sequencing atlas. Single cell analyses (e.g. astrocytes in AD vs. CTL) from astrocytes in entorhinal cortex in AD could show that astrocytes change their gene expression profile in coordinated ways compared to other cell types highly dependent on the microenvironment [89], [90]. Therefore the authors suggest the differentiation of different groups of astrocytes (e.g. brain region/anti-/inflammatory) to improve earlier differentiations for reactive astrocytes like A1/A2 that did not respect the diverse interaction with the environment. This could include the observation of coordinated groups of astrocytes that interact with each other e.g. around plaques to express the observed ErbB4⁺/GFAP⁺ feature. For example, scREAD, an online single cell database was conducted, (n=73, multiple brain regions) where ErbB4 is upregulated in subpopulations of astrocytes in the entorhinal cortex [91].

4.3 Digital image analysis

Standardizing the settings for the acquisition of scientific images with the confocal microscope can be a challenging procedure due to a multitude of parameters. This can range from the different quality and post mortem times of the tissue up to large sizes of micrographs (see figure 3.4) as well as the difficulty of precise horizontal alignments of the focal plane. Next, one seeks to minimize a potential observer bias by clear experimental designs with defined settings like prefixed laser strength for all samples. Additionally, predefined but at the same time randomly picked areas and z-levels of analysis make it difficult to provide micrographs suitable for further quantification. However, for control samples with lower cell number and lower immunoreactivity and correspondingly lower GFAP signal it was necessary to search for regions with preferably higher cell number. Therefore, the selected regions are dependent on the observer. For future analyses, multiple areas from each region should be included for each sample to increase the power of the image analysis.

The utilized Fiji macro, programmed to analyze z-stacks from multiple samples provides an effective and largely unbiased tool for quantification and comparison of IHC images with the differentiation of cell regions from background to specify the region of interest (ROI). In contrast to supervised algorithms, no user based preselection of areas had to be made. On the other hand, the unsupervised algorithm failed to reliably detect all ROIs/cells. Due to the large differences of cell density and fluorescence intensity in the acquired images between AD and CTL, a first effort to apply one fixed setting for segmenting failed to succeed for all samples. The preselection randomly assigned seeds, the average deviation of the

ROI from the center of the seed and number of iterations were therefore adjusted for each sample, with better segmentational results. Unfortunately, with impact to the initial idea of an unsupervised algorithm. Nevertheless, the major part of the segmentation still equally applies to all samples and can therefore be regarded as unbiased. Still, the adjustments of the mentioned parts of the mentioned algorithm led to significant differences concerning the results and should be improved with non-user controlled thresholds to regain the advantages of unsupervised segmentation.

For future acquisitions, a merged three dimensional analysis of voxels instead of pixels would permit the calculation of a more cell based representation of cellular protein expression. Through the acquisition of large z-stacks, a higher amount of whole cell bodies could be included in such analyses. This would save the time-consuming step of stack-wise separation and demanding iterative ROI generation. In addition, potential calculations regarding the number of cells e.g. forming a cluster as a subpopulation around a plaque could be performed. Subsequently, comparisons of average fluorescence intensities could be done. This spatial comparison would also allow to detect potential similar distribution patterns of protein expression throughout the tissue in a more precise manner.

As higher fluorescence levels and larger sizes of ROI create higher average values, small cell regions in control condition create low values and large clusters for AD create high values. Therefore, this analysis reflects hypertrophic astrocytes that form clusters, but should not be seen as an average value for each cell. High values for standard deviations therefore are due to larger areas that are summed together, and cannot be reduced to differences in fluorescence intensity. However,

this is not contradictory to the assumption of ErbB4/GFAP upregulation, as each mask that was created from the GFAP channel of the image is used for the measurements for both channels. Accordingly the analysed area under mask is spatially and nominally equal for both channels for each image. Therefore, it can be assumed that this pair-wise relation of the measurements of ErbB4 and GFAP under a defined mask can be compared as a correlation between samples by appropriate statistical calculations.

4.4 ErbB4 and inflammatory pathways

Results from immunofluorescence experiments demonstrated the colocalization of ErbB4 with proinflammatory markers C1q, COX2 and the inductor of apoptosis Cleaved-Caspase 3. This indicates a possible correlation of ErbB4 with inflammatory pathways, but does not determine whether ErbB4 activation leads to further pro- or antiinflammatory effects.

Concerning the colocalization with apoptotic marker Cleaved-Caspase-3, ErbB4 is able to induce pro-apoptotic signalling via the translocation of the E4ICD unit as well as programmed cell death via cytochrome c efflux [76].

In contrast to the observed strong GFAP/ErbB4 correlation, findings from the neurodegenerative mouse model of middle cerebral artery occlusion (MCAO) and chronic cerebral hypoperfusion mouse model, ErbB4 correlated with neuronal apoptosis, but not with glial activation [80]. GFAP upregulation of activated astrocytes in periinfarct regions (penumbra) did not lead to the upregulation of ErbB4. This is in contrast to the present documentation of observations of reac-

tive astrocytes around plaque-like structure overexpressing GFAP together with ErbB4 and C1q or COX2. Nevertheless, studies from MCAO mouse model do not necessarily reflect the different levels of impaired signalling nor the profound global changes in expression from AD. Possibly, the diverging expression levels of ErbB4 in inflammatory conditions, it is possible that due to the involvement of the γ -secretase and the proteolytic cleavage of APP, the interference with AICD for example leads to the activation of ErbB4.

Moreover, the administration of NRG1 in the left lateral ventricle of mice reduced GFAP expression [92], leading to reduced levels of neuronal apoptosis and inflammatory markers [93]. In addition, administration with ErbB4 specific ligand NRG4 induced apoptosis in activated human macrophages and is therefore regarded as antiinflammatory [94].

Possibly, different ErbB4 isoforms are expressed in different subpopulations. This may lead to the activation of different downstream pathways that are not able to promote the cleavage of the 4EICD domain that leads to inhibition of GFAP expression [48]. The preliminary results from the current qPCR expression analysis of primary astrocyte cultures showing upregulation of NRG1 after $\text{TNF}\alpha$ treatment, partially confirm the theory of a changed NRG1-ErbB4 axis in astrocytes in AD. However, the downregulation of ErbB4 after $\text{TNF}\alpha$ administration is not in agreement with this theory. Instead, we expected that the observed ErbB4 overexpression of human samples in AD hippocampi with high $\text{TNF}\alpha$ levels could be reproduced by $\text{TNF}\alpha$ administration in-vitro. Concerning antiinflammatory effects, administration of ErbB4 ligand NRG1 or NRG4 led to a 2-fold increase of IL6 expression. As no expression analyses of e.g. IL10 or Arginase-1 were per-

formed, question No.#2 (concerning antiinflammatory effects) remains an open issue. Therefore, conclusive statements cannot be made on the basis of the current study.

Unfortunately, not all human AD brain samples were neuropathologically staged according to the ABC method as recommended by established guidelines. Therefore, a correlation to the proteopathic load could apparently not be established. In future experiments, the regulation of ErbB4 in astrocytes and its effects on the expression of pro-/antiinflammatory as well as inhibitory pathways that are involved in AD should be investigated. As a first approach, an ELISA detecting the upregulation of different (anti-)inflammatory pathways on extracted total protein of treated cells could result in a valuable method for screening possible downstream targets.

4.5 ErbB4 cell specificity and distribution

To address the question #3 of the study, the tile scans displayed in figures 3.5 and 3.4 of whole hippocampus images provide a detailed overview on the expression pattern of ErbB4 in AD. Furthermore, the descriptive characterization of the ErbB4 expression in AD throughout the different hippocampal sectors revealed that ErbB4 and Phospho-ErbB4 are mainly expressed in a nuclear-like morphology of putative neurons in the dentate gyrus. In addition, ErbB4 seems to be expressed in astrocytes close to histopathological hallmarks like putative β -Amyloid plaques throughout the different CA sectors preferentially in CA1 and CA3.

Unfortunately, a double staining of ErbB4 with established neuronal markers (NeuN, MAP2 and others) were not able to provide specific results. Likewise, markers for GABAergic interneurons (GAD67, SST) did not reveal a reliable IHC staining, limiting further analyses regarding the colocalization of ErbB4 with interneurons to parvalbumin⁺ cells. A factor contributing to the technical limitation could be high post mortem intervals of aged brains containing partially destroyed epitopes/proteins with unfavorable signal to noise ratio. This technical constraint limited conclusions of this study.

Nevertheless, the dentate-granular layer that mostly contains neurons, turned out to be Phospho-ErbB4⁺, which indicates a putative expression of ErbB4 in neurons. Apart from the dentate granule layer, ErbB4 seems to be expressed in the nuclei of interneurons (Parvalbumin⁺/SST⁺). Furthermore, in some samples the ErbB4 expression appears to be present in pyramidal-like cells observed in CA1, CA4 and DG sectors (figures 3.5 and 3.1) and showed co-expression with NeuN in the control rat brain (figure 3.3). This demonstrates that pyramidal cells indeed express ErbB4 and therefore the finding of a selective expression limited to interneurons, as it was reported by Vullhorst et al. [57], could not be confirmed.

In contrast to Chaudhury et al. [70] microglia did not show any immunoreactivity using phospho-/N-/ or C-terminal antibodies. In other studies on inflammatory conditions after induced MCAO, penumbra-associated microglia expressed ErbB4 whereas neighbouring astrocytes were ErbB4 negative [93]. From murine anatomical studies on the distribution of ErbB receptors throughout the different brain areas, ErbB4 was ubiquitously expressed in glia cells [95]. However, as it is challenging to find clear statements in the literature concerning cell specificity

of ErbB4 expression, it is challenging to draw conclusive comparisons with the current study.

A more systematic experimental design for IHC and confocal investigation on each sample would allow to investigate the distribution of different expression patterns of astrocytes and different neuronal subtypes in different CA sectors of the hippocampus. Therefore, multiple images of CA1, CA4 and DG of human samples with higher number of z-stacks would provide deeper insight regarding the distribution of ErbB4⁺ in distinct cell types.

4.6 Regulation of ErbB4 inhibitory signalling

As NRG1 and ErbB4 is presumably expressed by inhibitory interneurons [57], the expression of ErbB4 mainly for GFAP⁺ astrocytes in the majority of the observed cases from this study was unexpected. At the same time, it is difficult to make statements regarding ErbB4 expression of neurons from post mortem samples, as the majority of the established neuronal markers failed to work. Regarding the functional implication of ErbB4 signalling, the impaired neuronal inhibitory network in the hippocampus of AD patients could lead to disturbed LTP and further neurological symptoms [96]. As the majority of neuroscientific research on ErbB4 focusses on schizophrenia, it is important to understand that the impairment of inhibitory signalling is a potential common mechanism for different neurodegenerative diseases that share dysrhythmic signalling (e.g. impaired gamma oscillation) and concordant expressional changes also for AD. More specifically, reactive astrocytes in AD condition potentially secrete inhibitory neurotransmitters like GABA

which might interfere with ErbB4 activation via NRG1 [97]. Moreover, astrocytes exert some functions of inhibitory neurons to act as GABAergic cells [98].

A possible factor of NRG1 accumulation and further activation of astrocytes, is that the proinflammatory conditions lead to the secretion of different molecules like e.g. EGF or NRGs to stimulate cell growth related pathways. Due to the ability of astrocytes to secrete Neuregulins after injury, the changes in ErbB4 expression in cell body/processes could be due to a para-/autocrine signalling that could be amplified in clusters of cells [51]. High levels of NRGs through different stimulating factors could then contribute to impairment of important memory-related circuits [66]. Further, increased neuronal apoptosis could also diminish the level of NRG uptake by neurons. This could lead to higher extracellular levels of NRG which subsequently could lead to the observed ErbB4 activation of astrocytes.

Next, experiments with rodents on ErbB4 and $A\beta$ will be described. Interestingly, ErbB4 is able to interact with $A\beta$. The ablation of ErbB4 receptor in transgenic $A\beta$ overexpressing mice in Parvalbumin⁺ interneurons led to the restoration of LTP, spatial memory and synaptic plasticity [99]. Obviously, the expression of the ErbB4 receptor in astrocytes is regulated by $A\beta$ accumulation. Recently, Zhang et al. demonstrated that APP cleaved by the γ -secretase leads to the intracellular accumulation of the AICD intracellular unit, that migrates to the nucleus to regulate transcription of EGFR by binding to the respective promoter [100]. As ErbB4 is able to dimerize with EGFR, ErbB4 signalling is potentially affected. Furthermore, $A\beta$ could also activate the ErbB4 promoter directly. Further exper-

iments should be done to better understand the target of $A\beta$ regarding regulation of ErbB4 expression.

To get a better picture of ErbB4 distribution in inter-(neurons), additional stainings with neuronal markers e.g. in tissue with preserved epitopes e.g. in AD-related mouse models would help to better differentiate between cells. This could lead to a superior understanding of affected interneurons to draw a more specific conclusions on the involvement of ErbB4 in inhibitory pathways. A more functional study design focussing inhibitory signalling e.g. with ErbB4 receptor activation and patchclamp stimulation could also provide further insight into the functional implication of ErbB4 dysregulation.

4.7 Growth factor receptors and Glioblastoma

To address the question No.#5, the expression of ErbB4 in Glioblastoma tissue has been analyzed. Subsequently, the observation of ErbB4 upregulation in reactive astrocytes in human AD hippocampi has been to the expression in reactive astrocytes in Glioblastoma brain tumors. The observed expression of reactive astrocytes with GFAP⁺/ErbB4⁺ in some GB cases provided further evidence of reactive astrocytes expressing ErbB4 in AD condition. In principle, the observed expression of ErbB4 in astrocytes in GB brain tumor confirms previous publications that reported ErbB4 overexpression in GB, where ErbB4 activation or phosphorylation level was linked to increased proliferation [75], [101]. In contrast, other studies proposed ErbB4 to be a tumor suppressor being associated with prolonged survival in astrocytic glioma cells [76], [102].

The discrepancy between studies regarding ErbB4 activation and further oncogenic or tumor suppressing effects, may be related to the GB specific type of expression of different splice variants. This could explain the low expression of ErbB4 in most of the samples and cases in this study. Specifically, the isoform JM-A CYT-1 and isoform JM-A CYT-2 but not isoform JM-B CYT-1 nor isoform JM-B CYT-2 can be cleaved by the γ -secretase ADAM17 also called TACE, therefore only CYT-1/CYT-2 which are able to induce pro-apoptotic effects via E4ICD [41].

As GB cells are diverse concerning protein expression, a profound conclusion - in this context ErbB4 activation - it would be necessary to characterize the different ErbB4 isoforms of the tissue . This heterogeneity of GB expression profile and at the same time complexity of ErbB signalling reflects the difficulty regarding causal relationships e.g. concerning results of immunofluorescence. Methodologically, the antigen retrieval on GB paraffine embedded tissue remains a major challenge in this context.

4.8 ErbB4 in dementia with Lewy bodies

In DLB the neuropathological changes of accumulation of α -synuclein as so called Lewy bodies with concordant inflammatory states of the CNS and reactive tissue were expected to confirm ErbB4 upregulation in astrocytes similar to AD. The observed ErbB4 expression in astrocytes of DLB samples appeared more nuclear-like with a comparatively low signal in the proximal cell body. Next, Parvalbumin positive interneurons turned out to be ErbB4 negative. Noteworthy,

the regulation of ErbB4 in DLB has not been studied before, to the best of our knowledge. As there is no publication on DLB and ErbB4 for astrocytes neither for concordant NRG ligands nor putative expression changes, it is therefore difficult to contextualize the inconsistency with AD. As a possible hypothesis, the missing activation of the γ -secretase through APP and further internalization and proteolytic cleavage with translocation of the AICD unit does not occur in DLB. This may result in a lower activation or level of cleavage of ErbB4. Results from investigations on potential impaired EGFR pathways have thus been published for other diseases with Lewy body accumulation, like PD [103], [104]. Regarding the current finding of a more nuclear-like expression of ErbB4 in astrocytes of DLB cases, only one study on idiopathic PD reported a reduced serum level of NRG1 [103]. However, in the current sample, the low number of included DLB cases (n=5) with no further histopathological staging regarding the severity and Lewy body distribution of the cases make it difficult to draw a conclusion. As a potential future experiment, the stimulation of astrocytes with α -synuclein with subsequent analysis of ErbB4 expression, compared to $A\beta$ stimulation would contribute to a better understanding of the observed differences.

4.9 Astrocyte culture and 24 h treatments

Addressing question No.#6 in order to provide a more mechanistic insight, in-vitro experiments with astrocyte cultures have been conducted. Is the upregulation of ErbB4 in reactive astrocytes - as observed in human AD hippocampi - reproducible with pro-inflammatory treatments on astrocyte cultures? Results from Immunofluorescence on primary astrocyte cell culture treatments showed an in-

crease of GFAP and ErbB4 intensity after treatment with inflammatory TNF α molecule and ErbB4 ligand NRG4, compared to control. This corroborates our observed results of immunofluorescence on human AD hippocampus samples, with colocalization of proinflammatory markers C1q and COX2.

Interestingly, the expression pattern for phospho-ErbB4 appeared more membrane associated - rather than nuclear - as observed in human samples, where it appeared strictly nuclear-like for astrocytes. Further, the ErbB4 expression of astrocyte cultures of C8D1-A as well as primary murine cell lines in control condition appeared to be more pronounced in the membrane. In comparison to the expression observed in human CTL hippocampi samples, where it appeared more nuclear-like.

Subsequent Western blot analysis aimed to investigate whether the potentially increased expression level changes are reproducible. This repeatedly led to the revelation of bands for ErbB4 (50 kDa, 260 kDa) outside of the spectre of known and published molecular weights (80 kDa, 180 kDa). Therefore, further modification of applied methods with different antibodies and e.g. a ponceau red staining to investigate a possible transfer problem is required. The true nature of the size of the unexpected bands (260 kDa) remains to be further defined. For example a possible dimerization of different parts of the protein could be possible, as different receptor subunits could bind to each other. In order to prevent this potential formation denaturated conditions prior the migration and sonication of samples were performed, however with no obvious impact on the result. Control bands for α -Tubulin, GFAP, β -Actin, phospho-Erk showed apparently good migration and transfer conditions.

At the gene expression level, the qPCR analysis showed strong NRG1 upregulation after TNF α treatment, with similar range of GFAP and ErbB4 gene expression throughout different treatments. This confirms and extends the expected result that astrocytes upregulate NRG expression in pro-inflammatory conditions along with higher GFAP levels [79]. The current findings must be replicated by a higher number cell culture experiments. In addition, the optimization of primers has to be improved, as this step in the qPCR analysis is error-prone. Further, detailed analysis of different NRG isoforms has to be done, as this has a huge impact on subcellular location (membrane vs. nuclear), expression (cell specific) and the type of secretion [105]. Therefore, low NRG expression in cell culture treatments could be due to the specificity of the isoform to a certain other cell type.

For profound additional statements regarding the comparison of the different expression levels after treatments, the application of the digital segmentation algorithm - as performed in human samples - should be applied. This would allow a more unbiased approach to test for significant differences between control and treatment. According to the low number of performed technical replicates (n=1, for primary and C8D1A cultures) to date, it would thus not lead to significant results.

A high cell death rate for iPSC derived astrocytes, as indicated in table 6.1, where no treatments have been performed, led to contacting the manufacturer for error diagnostics. For future experiments with iPSC derived astrocytes, it was recommended to strictly comply with the data sheets. It is important to stick to the recommended number of cells per well, the centrifugation time, and

to leave out an additional PBS washing after laminin coating as this may cause detachment of cells.

4.10 Open questions for future ErbB4 expression analyses

The broad methodological scope of this study, investigating different fields of cell growth and cancer, neuroinflammation and neurodegeneration, can only provide a preliminary approach towards the complexity of the ErbB4 network. Different diseases of the central nervous system can share similar symptoms with each other and are therefore suspected to share common cellular response mechanism. In particular, the vast number of connections of the ErbB4 signalling to different intra- and extracellular pathways, made it difficult to narrow the observed ErbB4 overexpression in reactive astrocytes down to a potential cause and/or effect.

To provide a more mechanistic insight into the ErbB4 signalling it is necessary for future studies to focus on comprehensive quantification of a single pathway. As one of the most intensively studied receptor networks, ErbB signalling serves as a hub for a huge amount of different external stimuli that are further distributed in a broad number of different intracellular pathways. Therefore, future studies regarding ErbB4 should focus preferentially on one of the questions stated in the aim of the current thesis (see section 1.12).

5 Summary

Morbus Alzheimer is characterized by $A\beta$ plaques, neurofibrillary tangles and different inflammatory conditions that finally lead to neuronal death and neurological symptoms of dementia. Monocausal therapeutic approaches that target amyloid or NFT could not improve clinical symptoms nor the overall outcome and progression of the disease. Accumulation of protein is common for ageing and is not regarded to be necessarily linked to symptoms of dementia. Furthermore, glial response mechanisms to proteopathic load are suspected to have a higher correlation to final clinical stages than load of NFT or Amyloid- β . Therefore, it is crucial to characterize changes of receptor protein expression in glial cells which are able to interact between different pathways of inflammation, cell death and brain circuitry. Specifically, the ErbB4 receptor, a member of the epidermal growth factor receptor family, is suspected to be involved in AD associated pathways.

For the characterization of ErbB4 expression in astrocytes, brain tissue from human (hippocampus, Glioblastoma) and murine samples (whole brain) in control and disease were investigated. Additionally, cultures from murine astrocytes (primary, C8D1A immortalized) and human astrocytes (iPSC derived) were treated with receptor ligands and inflammatory molecule $TNF\alpha$ for 24 h. Subsequently, immunohistochemistry on coverslips, Western Blot and qPCR were performed to detect changes of expression. Immunofluorescent analysis of ErbB4, GFAP, Cleaved-Caspase 3, COX2, C1q and interneuronal markers was performed on postmortem PFA-fixed human samples of hippocampus in AD (n=17) and controls (n=14). The spatial distribution and morphological characteristics of ErbB4 was then analyzed and quantified. In addition a digital segmentation and measurement of fluorescence of ErbB4 and GFAP was performed with ImageJ. Immunofluorescence analysis of astrocytes in the CA1 sector of the human hippocampi indicated that the ErbB4 expression correlated with GFAP throughout all samples. Higher intensities for ErbB4/GFAP in AD condition compared to controls were measured on qualitative and quantitative analyses. Astrocytes in resting state showed ErbB4 expression limited to the nucleus with no expression

in the somatic cytoplasm or processes, in contrast to ErbB4 expression found in astroglial processes in AD samples. Different pathological conditions (Glioblastoma, dementia with Lewy bodies) showed similar ErbB4 expression patterns in somata and proximal astroglial processes. In addition, analysis of whole human hippocampal sections showed ErbB4 expression in the dentate gyrus and CA4 sector with triangular shaped cell bodies for ErbB4 and Phospho-ErbB4 in the nuclei and somata of neurons and interneurons. The observation of neuronal ErbB4 expression could be reproduced by NeuN/ErbB4 double positive stainings from controls (rat and mouse). Immunofluorescence on primary and immortalized astrocyte cultures showed higher intensities for ErbB4 and GFAP after TNF α treatment. The previously reported selective expression of ErbB4 limited to interneurons [57] could not be confirmed, as pyramidal neurons also expressed ErbB4. Likewise, in contrast to previous studies, microglia was immunonegative for ErbB4. Preliminary results from total RNA extraction/RT/qPCR of primary astrocyte cultures after TNF α administration (24 h) demonstrated upregulation of the ErbB4 ligand NRG1. Unexpectedly, the Western Blot showed bands for ErbB4 at 50 kDa and 230 kDa, reproducible with Phospho- and C-terminal ErbB4 antibodies, not reported in previous studies. Accordingly, these bands were excluded from further quantification.

The current thesis also documents a codistribution of ErbB4 with inflammatory markers C1q, Cleaved-Caspase 3 and COX2, indicating a possible induction of inflammatory pathways. This putative neuroinflammatory response may lead to the release of cell growth and neuroprotective molecules suggestive for an anti-inflammatory response. For future experiments, analyses at RNA and protein levels of different anti-/proinflammatory molecules after treatments would help to further understand the effects of ErbB4 activation. Additional stainings with different neuronal markers would allow a deeper understanding on cell specific upregulation of ErbB4. Finally, more comprehensive image analysis including multiple scans from all hippocampal areas could provide a more detailed pattern of ErbB4 expression. Taken together, the increased ErbB4 expression revealed in the current thesis is in agreement with previous studies, highlighting the potential relevance of ErbB4 signalling pathway as a potential therapeutic target in AD.

6 Supplemental materials

6.1 Primary murine culture treatments

#	Cell-type Date	cells / well		Experimental conditions in ng/ μ L					Analysis
1	C8D1A 24.10.18	700.000	Control	TNF α 50	EGF 50	/	NRG4 100	TNF α + NRG4	Proteins (6 h)
2	P2 24.10.18	700.000	Control	TNF α 50	EGF 50	/	NRG4 100	TNF α + NRG4	Proteins (24 h)
3	P2 07.11.18	700.000	Control	TNF α 50	EGF 50	/	NRG4 100	TNF α + NRG4	Coverslips (24 h)
4	P2 13.03.19	800.000	Control	TNF α 50	EGF 50	NRG1 100	NRG4 100	TNF α + NRG4	Proteins (24 h)
5	P2 21.03.19	800.000	Control	TNF α 50	EGF 50	NRG1 100	NRG4 100	TNF α + NRG4	RNA (24 h)
6	P2 07.05.19	800.000	Control	TNF α 50	EGF 50	NRG1 100	NRG4 100	TNF α + NRG4	Coverslips (24 h)
7	P2 26.02.20	800.000	Control	hTNF α 50	hEGF 50	hNRG1 100	hNRG4 100	hTNF α + hNRG4	RNA (24 h)
8	P2 26.02.20	800.000	Control	hTNF α 50	hEGF 50	hNRG1 100	hNRG4 100	hTNF α + hNRG4	Proteins (24 h)
9	P2 01.07.20	800.000	Control	hTNF α 50	hEGF 50	hNRG1 100	hNRG4 100	hTNF α + hNRG4	Proteins (24 h)
10	P2 01.07.20	700.000	Control	hTNF α 50	hEGF 50	hNRG1 100	hNRG4 100	hTNF α + hNRG4	Coverslips (24 h)
11	iCell [®] 16.07.20	100.000/ 15.000	Control (MW12)	Con- trol (MW96)	/	/	/	/	Proteins (72 h) + coverslips
12	P2 27.07.20	450.000	Control	hTNF α 50/100	hEGF 50	hNRG1 100	hNRG4 100	hTNF α + hNRG4 / + hNRG1	Proteins (24 h) + RNA (6 h)
13	P2 28.07.20	450.000	Control	hTNF α 50/100	hEGF 50	hNRG1 100	hNRG4 100	hTNF α + hNRG4 / + hNRG1	RNA (24 h)
14	P2 08.10.20	600.000	Control	hTNF α 50	hEGF 50	hNRG1 100	hNRG4 100	hTNF α + hNRG4 / + hNRG1	RNA (24 h)
15	P2 08.10.20	600.000	Control	hTNF α 50	hEGF 50	hNRG1 100	hNRG4 100	hTNF α + hNRG4 / + hNRG1	RNA (24 h)

Table 6.1: Overview of cell culture experiments.

6.2 ImageJ Macro

```

1 // 1) Split stack to single images
2
3 // 1.1 Settings
4
5 filetype = ".czi"; // Set your image file
  ⇨ type here
6 print("\\Clear");
7 setBatchMode(true);
8 MainDir = getDirectory("Choose starting
  ⇨ directory...");
9 checkFiles(MainDir);
10
11 // 1.2 List array of all files to be
  ⇨ split inside folder
12
13 function checkFiles(dir) {
14     list = getFileList(dir);
15     for (i=0; i<list.length; i++) {
16
17         if (endsWith(list[i], "/")) {
18             checkFiles(""+dir+list[i]);
19         }
20
21         else {
22
23             if (endsWith(list[i], filetype)) {
24                 open(dir + list[i]);
25                 split();
26                 run("Close All");
27             }
28             else {
29                 print("NO IMAGE: " + dir +
  ⇨ list[i]);
30                 print("-----");
31             }
32         }
33     }
34 }
35
36 // 1.3 Create folder for each stack and
  ⇨ save split images with file name
  ⇨ according to original file
37
38 function split(){
39     ImageTitle = getTitle();
40     ImageDir = getInfo("image.directory");
41
42     getDimensions(w,h,channels,slices,f);
43     print("Channels: "+channels+" Slices:
  ⇨ "+slices);
44     print ("ImageDir: "+ImageDir);
45     print ("ImageTitle: "+ImageTitle);
46
47     if (channels+slices > 1) {
48         File.makeDirectory(ImageDir+ImageTitle+"#");
49         saveDir = ImageDir+ImageTitle+"#/";
50         File.setDefaultDir(saveDir);
51         run("Image Sequence... ",
  ⇨ "format=TIFF digits=2
  ⇨ name=img");
52         images = getFileList(saveDir);
53
54         if (slices>1) {
55             for (i=0;i<images.length;i++) {
56                 tempdir =
  ⇨ substring(images[i],0,7);
57
58                 ⇨ File.makeDirectory(saveDir+tempdir);
59                 File.copy(saveDir+images[i],
  ⇨ saveDir+tempdir+"/"+images[i]);
60                 t = File.delete(saveDir+images[i]);
61             }
62             else {
63                 print("File does not contain
  ⇨ layers: No operation
  ⇨ performed.");
64             }
65         }
66     }
67     print("Finished.");
68
69 // 2) Preprocessing of GFAP channel
70
71 // 2.1 Settings and "choose folder"
  ⇨ dialogue for measurement
72
73 extension = ".tif";
74 showimages = true;
75 print("\\Clear");
76 macro "Density measurement" {
77     dirin = getDirectory("Choose input
  ⇨ directory..."); //
  ⇨ /chosen-folder/stack-number/acquisition.czi

```

```

77     start = getTime();
78     list = getFileList(dirin);
79
80     if (!showimages) setBatchMode(true);
81     print("Number of files:" +
82         ↪ list.length);
83
84     for (n = 0; n<list.length; n++) {
85         print(list[n]);
86         k = 0;
87         title = list[n];
88         print(title + " scanning...");
89         roiManager("reset");
90         actualFolder = dirin + list[n];
91         actualList =
92             ↪ getFileList(actualFolder);
93         print("Ordner "+n + " -- " +
94             ↪ actualFolder);
95
96     // 2.2. Go to each stack folder and open
97     ↪ GFAP and ErbB4 acquisition
98
99     // Open GFAP acquisition for GFAP mask
100    ↪ creation
101
102    for (i=0; i<actualList.length; i++) {
103        open(actualFolder+actualList[i]);
104        GFAPmask = getTitle();
105        print(GFAPmask);
106
107    // Open GFAP acquisition for GFAP
108    ↪ measurement
109
110    open(actualFolder+actualList[i]);
111    GFAPmeasure = getTitle();
112    print(GFAPmeasure);
113
114    // Open ErbB4 acquisition Image for
115    ↪ measurement
116    i++;
117    i++;
118    open(actualFolder+actualList[i]);
119    ErbB4 = getTitle();
120    print(ErbB4);
121
122    // 2.3 Preprocessing steps
123    selectWindow(GFAPmask);
124    run("Subtract Background...",
125        ↪ "rolling=50 sliding");
126
127    setMinAndMax(3, 255);
128    run("Apply LUT");
129    run("Despeckle");
130    run("Median...", "radius=2");
131
132    // 3) k-means clustering
133
134    run("k-means Clustering ...",
135        ↪ "number_of_clusters=5
136        ↪ cluster_center_tolerance=700
137        ↪ enable_randomization_seed
138        ↪ randomization_seed=1000
139        ↪ show_clusters_as_centroid_value");
140    setThreshold(6, 255);
141
142    // 4) Create mask
143
144    run("Convert to Mask");
145    run("Analyze Particles...",
146        ↪ "size=800-20000
147        ↪ circularity=0.0-1.00 show=Nothing
148        ↪ add");
149
150    // 5) Apply mask on original images
151
152    // 5.1 GFAP acquisition
153
154    selectWindow(GFAPmeasure);
155    setMinAndMax(10, 255);
156    run("Apply LUT");
157    roiManager("Show All without
158        ↪ labels");
159    if (showimages) waitForUser("Klicken,
160        ↪ um fortzufuehren");
161
162    // 5.2 ErbB4 acquisition
163
164    selectWindow(ErbB4);
165    setMinAndMax(10, 255);
166    run("Apply LUT");
167    roiManager("Show All without
168        ↪ labels");
169    if (showimages) waitForUser("Klicken,
170        ↪ um fortzufuehren");
171
172    // 6) Measure density under mask
173
174    run("Set Measurements...", "mean
175        ↪ integrated redirect=None
176        ↪ decimal=3");
177    for(j=0; j<roiManager("count"); j++)
178        ↪ {

```

```
153     roiManager("select", j);
154     IntDen = getValue("IntDen");
155     setResult(title + "IntDen", k,
156     ↪ IntDen);
156     k++;
157     updateResults();
158     }
159     }
```

```
160     roiManager("Reset");
161     run("Close All");
162     }
163     scripttime = (getTime() -
164     ↪ start)/1000;
164     print ("Script execution time:
165     ↪ "+scripttime+"s");
165     }
```

List of Figures

1.1	Three phases of AD [14].	8
1.2	The hippocampus during cerebral development [30].	12
1.3	Archicortex of the hippocampus [31].	13
1.4	EGFR receptor family	15
2.1	Exemplary CA1 sector as included for the digital measurements of fluorescence.	40
2.2	Sequence of image segmentation and analysis with Fiji macro . . .	42
3.1	Immunofluorescence with ErbB4, proinflammatory and interneu- ronal marker, human control hippocampus cases No.#23, #25, #32, #33	43
3.2	Immunofluorescence with ErbB4, proinflammatory and microglia marker, human control hippocampus case No. #29	45
3.3	Immunofluorescence with ErbB4 and neuronal and astroglial mark- ers, control rat and mouse neocortex	46
3.4	Immunofluorescence, whole human AD hippocampus case No.#15, large tile scan overview on CA1 to CA4 sectors including DG #1	47
3.5	Immunofluorescence, whole human AD hippocampus case No.#7, large tile scan overview on CA1 to CA4 sectors including DG #2	48
3.6	Immunofluorescence with ErbB4, Cleaved-Caspase 3 and microglial marker, human CA1 hippocampus case No.#2	49
3.7	Immunofluorescence inflammatory markers, human CA1 hippocam- pus cases No.#16, #7, #6, #2	51
3.8	Immunofluorescence with interneuronal and other ErbB markers, human CA1 hippocampus cases No.#15, #5, #1	53
3.9	Immunofluorescence with ErbB4 and interneuronal markers, hu- man DLB hippocampus cases No.#22, #19	54
3.10	Nissl staining overview, Immunofluorescence with ErbB4 and GFAP, human GB case No.#37	55

3.11	Nissl staining overview, Immunofluorescence with ErbB4 and GFAP, human GB case No.#38	56
3.12	Immunofluorescence, C8-D1A immortalized astrocyte culture . . .	58
3.13	Immunofluorescence, primary astrocyte culture	61
3.14	Human iPSC astrocytes	62
3.15	Boxplots of semiquantitative analysis	62
3.16	Western Blots of primary astrocyte cultures (see table 6.1), after 24 h treatments. TB: Total mouse brain, RP: Recombinant protein.	64
3.17	Western Blots of primary astrocyte culture (see table 6.1, after 24 h treatments, conditions: pellet/supernatant separated and 30s/60s sonicated. SN: Supernatant, PLL: Pellet.	65
3.18	Western Blots of C8D1A immortalized cell culture with different treatments	65
3.19	qPCR $\Delta\Delta C_t$ values for primers on cDNA of primary astrocyte culture after 24 h treatments	66
4.1	Results from R2 online sequencing atlas: Relation for ErbB4 and GFAP expression a 2log scale from RNA extraction from human AD brain samples from the Cotman dataset.	71
4.2	ErbB4 expression of aged mice, Ben Barres sequencing database .	72

List of Tables

1.1	ABC score for neuropathological changes in AD	9
1.2	Specificity of ErbB receptors and ligands	18
2.1	Primary & secondary antibodies	25
2.2	Cell culture materials	26
2.3	Protein and RNA quantification materials	27
2.4	Human brain samples	30
2.5	Semiquantitative grading scale	31
2.6	Nucleotide sequences of used primers	39
3.1	Mean and SD of ErbB4/GFAP in AD and control condition . . .	63
6.1	Overview of cell culture experiments	90

Bibliography

- [1] B. Winblad, P. Amouyel, S. Andrieu, *et al.*, “Defeating Alzheimer’s disease and other dementias: A priority for European science and society,” *The Lancet Neurology*, vol. 15, no. 5, pp. 455–532, Apr. 2016, ISSN: 14744422. DOI: 10.1016/S1474-4422(16)00062-4.
- [2] DGPPN – DGN, Ed., *S3-Leitlinie Demenzen*. Berlin, Heidelberg: Springer Berlin Heidelberg, 2017, ISBN: 978-3-662-53874-6 978-3-662-53875-3. DOI: 10.1007/978-3-662-53875-3.
- [3] H. W. Querfurth and F. M. LaFerla, “Alzheimer’s Disease,” *New England Journal of Medicine*, vol. 362, no. 4, pp. 329–344, Jan. 28, 2010, ISSN: 0028-4793, 1533-4406. DOI: 10.1056/NEJMra0909142.
- [4] W. Hacke, Ed., *Neurologie*, ser. Springer-Lehrbuch. Berlin, Heidelberg: Springer Berlin Heidelberg, 2016, ISBN: 978-3-662-46891-3 978-3-662-46892-0. DOI: 10.1007/978-3-662-46892-0.
- [5] K. F. Winklhofer, J. Tatzelt, and C. Haass, “The two faces of protein misfolding: Gain- and loss-of-function in neurodegenerative diseases,” *The EMBO Journal*, vol. 27, no. 2, pp. 336–349, Jan. 23, 2008, ISSN: 0261-4189, 1460-2075. DOI: 10.1038/sj.emboj.7601930.
- [6] B. Frost and M. I. Diamond, “Prion-like mechanisms in neurodegenerative diseases,” *Nature Reviews Neuroscience*, vol. 11, no. 3, pp. 155–159, Mar. 2010, ISSN: 1471-003X, 1471-0048. DOI: 10.1038/nrn2786.
- [7] M. Ingelsson, H. Fukumoto, K. L. Newell, *et al.*, “Early A accumulation and progressive synaptic loss, gliosis, and tangle formation in AD brain,” *Neurology*, vol. 62, no. 6, pp. 925–931, Mar. 23, 2004, ISSN: 0028-3878, 1526-632X. DOI: 10.1212/01.WNL.0000115115.98960.37.
- [8] A. B. Reiss, H. A. Arain, M. M. Stecker, N. M. Siegart, and L. J. Kaselman, “Amyloid toxicity in Alzheimer’s disease,” *Reviews in the Neurosciences*, vol. 29, no. 6, pp. 613–627, Aug. 28, 2018, ISSN: 2191-0200, 0334-1763. DOI: 10.1515/revneuro-2017-0063.

- [9] F. P. Chong, K. Y. Ng, R. Y. Koh, and S. M. Chye, “Tau Proteins and Tauopathies in Alzheimer’s Disease,” *Cellular and Molecular Neurobiology*, vol. 38, no. 5, pp. 965–980, Jul. 2018, ISSN: 0272-4340, 1573-6830. DOI: 10.1007/s10571-017-0574-1.
- [10] K. Iqbal, F. Liu, and C.-X. Gong, “Tau and neurodegenerative disease: The story so far,” *Nature Reviews Neurology*, vol. 12, no. 1, pp. 15–27, Jan. 2016, ISSN: 1759-4758, 1759-4766. DOI: 10.1038/nrneuro1.2015.225.
- [11] P. Giannakopoulos, F. R. Herrmann, T. Bussiere, *et al.*, “Tangle and neuron numbers, but not amyloid load, predict cognitive status in Alzheimer’s disease,” *Neurology*, vol. 60, no. 9, pp. 1495–1500, May 13, 2003, ISSN: 0028-3878, 1526-632X. DOI: 10.1212/01.WNL.0000063311.58879.01.
- [12] L. M. Ittner, Y. D. Ke, F. Delerue, *et al.*, “Dendritic Function of Tau Mediates Amyloid- β Toxicity in Alzheimer’s Disease Mouse Models,” *Cell*, vol. 142, no. 3, pp. 387–397, Aug. 2010, ISSN: 00928674. DOI: 10.1016/j.cell.2010.06.036.
- [13] S. Forner, D. Baglietto-Vargas, A. C. Martini, L. Trujillo-Estrada, and F. M. LaFerla, “Synaptic Impairment in Alzheimer’s Disease: A Dysregulated Symphony,” *Trends in Neurosciences*, vol. 40, no. 6, pp. 347–357, Jun. 2017, ISSN: 01662236. DOI: 10.1016/j.tins.2017.04.002.
- [14] B. De Strooper and E. Karran, “The Cellular Phase of Alzheimer’s Disease,” *Cell*, vol. 164, no. 4, pp. 603–615, Feb. 2016, ISSN: 00928674. DOI: 10.1016/j.cell.2015.12.056.
- [15] H. Braak and E. Braak, “Neuropathological staging of Alzheimer-related changes,” *Acta Neuropathologica*, vol. 82, no. 4, pp. 239–259, Sep. 1991, ISSN: 0001-6322, 1432-0533. DOI: 10.1007/BF00308809.
- [16] T. J. Montine, C. H. Phelps, T. G. Beach, *et al.*, “National Institute on Aging–Alzheimer’s Association guidelines for the neuropathologic assessment of Alzheimer’s disease: A practical approach,” *Acta Neuropathologica*, vol. 123, no. 1, pp. 1–11, Jan. 2012, ISSN: 0001-6322, 1432-0533. DOI: 10.1007/s00401-011-0910-3.
- [17] D. R. Thal, U. Rüb, M. Orantes, and H. Braak, “Phases of A β -deposition in the human brain and its relevance for the development of AD,” p. 11,

- [18] R. S. Wilson, E. Segawa, P. A. Boyle, S. E. Anagnos, L. P. Hizel, and D. A. Bennett, “The natural history of cognitive decline in Alzheimer’s disease,” *Psychology and Aging*, vol. 27, no. 4, pp. 1008–1017, Dec. 2012, ISSN: 1939-1498, 0882-7974. DOI: 10.1037/a0029857.
- [19] R. Briggs, S. P. Kennelly, and D. O’Neill, “Drug treatments in Alzheimer’s disease,” *Clinical Medicine*, vol. 16, no. 3, pp. 247–253, Jun. 2016, ISSN: 1470-2118, 1473-4893. DOI: 10.7861/clinmedicine.16-3-247.
- [20] H. I. L. Jacobs, T. Hedden, A. P. Schultz, *et al.*, “Structural tract alterations predict downstream tau accumulation in amyloid-positive older individuals,” *Nature Neuroscience*, vol. 21, no. 3, pp. 424–431, Mar. 2018, ISSN: 1097-6256, 1546-1726. DOI: 10.1038/s41593-018-0070-z.
- [21] C. H. Andrade-Moraes, A. V. Oliveira-Pinto, E. Castro-Fonseca, *et al.*, “Cell number changes in Alzheimer’s disease relate to dementia, not to plaques and tangles,” *Brain*, vol. 136, no. 12, pp. 3738–3752, Dec. 1, 2013, ISSN: 0006-8950, 1460-2156. DOI: 10.1093/brain/awt273.
- [22] D. S. Bouvier and K. K. Murai, “Synergistic Actions of Microglia and Astrocytes in the Progression of Alzheimer’s Disease,” *Journal of Alzheimer’s Disease*, vol. 45, no. 4, pp. 1001–1014, Apr. 13, 2015, ISSN: 18758908, 13872877. DOI: 10.3233/JAD-143156.
- [23] S. A. Liddelow, K. A. Guttenplan, L. E. Clarke, *et al.*, “Neurotoxic reactive astrocytes are induced by activated microglia,” *Nature*, vol. 541, no. 7638, pp. 481–487, Jan. 2017, ISSN: 0028-0836, 1476-4687. DOI: 10.1038/nature21029.
- [24] L. Rajendran and R. C. Paolicelli, “Microglia-Mediated Synapse Loss in Alzheimer’s Disease,” *The Journal of Neuroscience*, vol. 38, no. 12, pp. 2911–2919, Mar. 21, 2018, ISSN: 0270-6474, 1529-2401. DOI: 10.1523/JNEUROSCI.1136-17.2017.
- [25] A. M. Arranz and B. De Strooper, “The role of astroglia in Alzheimer’s disease: Pathophysiology and clinical implications,” *The Lancet Neurology*, vol. 18, no. 4, pp. 406–414, Apr. 2019, ISSN: 14744422. DOI: 10.1016/S1474-4422(18)30490-3.

- [26] A. Panatier and R. Robitaille, “Astrocytic mGluR5 and the tripartite synapse,” *Neuroscience*, vol. 323, pp. 29–34, May 2016, ISSN: 03064522. DOI: 10.1016/j.neuroscience.2015.03.063.
- [27] C. Escartin, E. Galea, A. Lakatos, J. P. O’Callaghan, G. C. Petzold, and C. Steinhäuser, “Reactive astrocyte nomenclature, definitions, and future directions,” *Nature Neuroscience*, vol. 24, no. 3, pp. 312–325, Mar. 2021, ISSN: 1097-6256, 1546-1726. DOI: 10.1038/s41593-020-00783-4.
- [28] T. Beach, R. Walker, and E. McGeer, “Patterns of gliosis in alzheimer’s disease and aging cerebrum,” *Glia*, vol. 2, no. 6, pp. 420–436, 1989, ISSN: 0894-1491, 1098-1136. DOI: 10.1002/glia.440020605.
- [29] C. E. G. Leyns and D. M. Holtzman, “Glial contributions to neurodegeneration in tauopathies,” *Molecular Neurodegeneration*, vol. 12, no. 1, p. 50, Dec. 2017, ISSN: 1750-1326. DOI: 10.1186/s13024-017-0192-x.
- [30] H. M. Duvernoy, *The Human Hippocampus: Functional Anatomy, Vascularization, and Serial Sections with MRI*, 3rd ed. Berlin ; New York: Springer, 2005, 232 pp., ISBN: 978-3-540-23191-2.
- [31] M. Trepel, *Neuroanatomie: Struktur und Funktion*, 7. Auflage. München: Elsevier, 2017, 419 pp., ISBN: 978-3-437-41288-2 978-3-437-18009-5.
- [32] E. Pastalkova, “Storage of Spatial Information by the Maintenance Mechanism of LTP,” *Science*, vol. 313, no. 5790, pp. 1141–1144, Aug. 25, 2006, ISSN: 0036-8075, 1095-9203. DOI: 10.1126/science.1128657.
- [33] L. Mei and K.-A. Nave, “Neuregulin-ERBB Signaling in the Nervous System and Neuropsychiatric Diseases,” *Neuron*, vol. 83, no. 1, pp. 27–49, Jul. 2014, ISSN: 08966273. DOI: 10.1016/j.neuron.2014.06.007.
- [34] J. Downward, Y. Yarden, E. Mayes, *et al.*, “Close similarity of epidermal growth factor receptor and v-erb-B oncogene protein sequences,” *Nature*, vol. 307, no. 5951, pp. 521–527, Feb. 1984, ISSN: 0028-0836, 1476-4687. DOI: 10.1038/307521a0.
- [35] Y. Yarden and M. X. Sliwkowski, “Untangling the ErbB signalling network,” *Nature Reviews Molecular Cell Biology*, vol. 2, no. 2, pp. 127–137, Feb. 2001, ISSN: 1471-0072, 1471-0080. DOI: 10.1038/35052073.

- [36] X. Zhang, J. Gureasko, K. Shen, P. A. Cole, and J. Kuriyan, “An Allosteric Mechanism for Activation of the Kinase Domain of Epidermal Growth Factor Receptor,” *Cell*, vol. 125, no. 6, pp. 1137–1149, Jun. 2006, ISSN: 00928674. DOI: 10.1016/j.cell.2006.05.013.
- [37] M. Vecchi, J. Baulida, and G. Carpenter, “Selective Cleavage of the Heregulin Receptor ErbB-4 by Protein Kinase C Activation,” *Journal of Biological Chemistry*, vol. 271, no. 31, pp. 18 989–18 995, Aug. 1996, ISSN: 00219258. DOI: 10.1074/jbc.271.31.18989.
- [38] A. Sorokin and L. K. Goh, “Endocytosis and intracellular trafficking of ErbBs,” *Experimental Cell Research*, vol. 315, no. 4, pp. 683–696, Feb. 2009, ISSN: 00144827. DOI: 10.1016/j.yexcr.2008.07.029.
- [39] D. K. Giri, M. Ali-Seyed, L.-Y. Li, *et al.*, “Endosomal Transport of ErbB-2: Mechanism for Nuclear Entry of the Cell Surface Receptor,” *Molecular and Cellular Biology*, vol. 25, no. 24, pp. 11 005–11 018, Dec. 15, 2005, ISSN: 0270-7306, 1098-5549. DOI: 10.1128/MCB.25.24.11005-11018.2005.
- [40] C.-Y. Ni, “Gamma -Secretase Cleavage and Nuclear Localization of ErbB-4 Receptor Tyrosine Kinase,” *Science*, vol. 294, no. 5549, pp. 2179–2181, Dec. 7, 2001, ISSN: 00368075, 10959203. DOI: 10.1126/science.1065412.
- [41] C. Rio, J. D. Buxbaum, J. J. Peschon, and G. Corfas, “Tumor Necrosis Factor- α -converting Enzyme Is Required for Cleavage of erbB4/HER4,” *Journal of Biological Chemistry*, vol. 275, no. 14, pp. 10 379–10 387, Apr. 2000, ISSN: 00219258. DOI: 10.1074/jbc.275.14.10379.
- [42] Z. Wang, “ErbB Receptors and Cancer,” in *ErbB Receptor Signaling*, ser. Methods in Molecular Biology, Z. Wang, Ed., vol. 1652, New York, NY: Springer New York, 2017, pp. 3–35, ISBN: 978-1-4939-7218-0 978-1-4939-7219-7. DOI: 10.1007/978-1-4939-7219-7_1.
- [43] “UniProtKB - Q15303 (ERBB4_HUMAN).” (), [Online]. Available: <https://www.uniprot.org/uniprot/Q15303>.
- [44] Y. Z. Huang, S. Won, D. W. Ali, *et al.*, “Regulation of Neuregulin Signaling by PSD-95 Interacting with ErbB4 at CNS Synapses,” *Neuron*, vol. 26, no. 2, pp. 443–455, May 2000, ISSN: 08966273. DOI: 10.1016/S0896-6273(00)81176-9.

- [45] G.-H. Tan, Y.-Y. Liu, X.-L. Hu, D.-M. Yin, L. Mei, and Z.-Q. Xiong, “Neuregulin 1 represses limbic epileptogenesis through ErbB4 in parvalbumin-expressing interneurons,” *Nature Neuroscience*, vol. 15, no. 2, pp. 258–266, Feb. 2012, ISSN: 1097-6256, 1546-1726. DOI: 10.1038/nn.3005.
- [46] B. Linggi and G. Carpenter, “ErbB receptors: New insights on mechanisms and biology,” *Trends in Cell Biology*, vol. 16, no. 12, pp. 649–656, Dec. 2006, ISSN: 09628924. DOI: 10.1016/j.tcb.2006.10.008.
- [47] Y. Iwakura and H. Nawa, “ErbB1-4-dependent EGF/neuregulin signals and their cross talk in the central nervous system: Pathological implications in schizophrenia and Parkinson’s disease,” *Frontiers in Cellular Neuroscience*, vol. 7, 2013, ISSN: 1662-5102. DOI: 10.3389/fncel.2013.00004.
- [48] S. P. Sardi, J. Murtie, S. Koirala, B. A. Patten, and G. Corfas, “Presenilin-Dependent ErbB4 Nuclear Signaling Regulates the Timing of Astrogenesis in the Developing Brain,” *Cell*, vol. 127, no. 1, pp. 185–197, Oct. 2006, ISSN: 00928674. DOI: 10.1016/j.cell.2006.07.037.
- [49] O. B. Kwon, D. Paredes, C. M. Gonzalez, J. Neddens, L. Hernandez, D. Vullhorst, and A. Buonanno, “Neuregulin-1 regulates LTP at CA1 hippocampal synapses through activation of dopamine D4 receptors,” *Proceedings of the National Academy of Sciences*, vol. 105, no. 40, pp. 15 587–15 592, Oct. 7, 2008, ISSN: 0027-8424, 1091-6490. DOI: 10.1073/pnas.0805722105.
- [50] M. Skirzewski, I. Karavanova, A. Shamir, *et al.*, “ErbB4 signaling in dopaminergic axonal projections increases extracellular dopamine levels and regulates spatial/working memory behaviors,” *Molecular Psychiatry*, vol. 23, no. 11, pp. 2227–2237, Nov. 2018, ISSN: 1359-4184, 1476-5578. DOI: 10.1038/mp.2017.132.
- [51] A. Sharif, V. Duhem-Tonnelle, C. Allet, *et al.*, “Differential erbB signaling in astrocytes from the cerebral cortex and the hypothalamus of the human brain,” *Glia*, vol. 57, no. 4, pp. 362–379, Mar. 2009, ISSN: 08941491, 10981136. DOI: 10.1002/glia.20762.

- [52] M. Yamada, T. Ikeuchi, and H. Hatanaka, “The neurotrophic action and signalling of epidermal growth factor,” *Progress in Neurobiology*, vol. 51, no. 1, pp. 19–37, Jan. 1997, ISSN: 03010082. DOI: 10.1016/S0301-0082(96)00046-9.
- [53] M. A. Anderson, J. E. Burda, Y. Ren, *et al.*, “Astrocyte scar formation aids central nervous system axon regeneration,” *Nature*, vol. 532, no. 7598, pp. 195–200, Apr. 2016, ISSN: 0028-0836, 1476-4687. DOI: 10.1038/nature17623.
- [54] X. Hu, C. W. Hicks, W. He, P. Wong, W. B. Macklin, B. D. Trapp, and R. Yan, “Bace1 modulates myelination in the central and peripheral nervous system,” *Nature Neuroscience*, vol. 9, no. 12, pp. 1520–1525, Dec. 2006, ISSN: 1097-6256, 1546-1726. DOI: 10.1038/nn1797.
- [55] R.-S. Woo, J.-H. Lee, H.-S. Kim, C.-H. Baek, D.-Y. Song, Y.-H. Suh, and T.-K. Baik, “Neuregulin-1 protects against neurotoxicities induced by Swedish amyloid precursor protein via the ErbB4 receptor,” *Neuroscience*, vol. 202, pp. 413–423, Jan. 2012, ISSN: 03064522. DOI: 10.1016/j.neuroscience.2011.11.026.
- [56] M. Gassmann, F. Casagrande, D. Orioli, H. Simon, C. Lai, R. Klein, and G. Lemke, “Aberrant neural and cardiac development in mice lacking the ErbB4 neuregulin receptor,” *Nature*, vol. 378, no. 6555, pp. 390–394, Nov. 1995, ISSN: 0028-0836, 1476-4687. DOI: 10.1038/378390a0.
- [57] D. Vullhorst, J. Neddens, I. Karavanova, L. Tricoire, R. S. Petralia, C. J. McBain, and A. Buonanno, “Selective Expression of ErbB4 in Interneurons, But Not Pyramidal Cells, of the Rodent Hippocampus,” *Journal of Neuroscience*, vol. 29, no. 39, pp. 12 255–12 264, Sep. 30, 2009, ISSN: 0270-6474, 1529-2401. DOI: 10.1523/JNEUROSCI.2454-09.2009.
- [58] A. Shamir, O.-B. Kwon, I. Karavanova, D. Vullhorst, E. Leiva-Salcedo, M. J. Janssen, and A. Buonanno, “The Importance of the NRG-1/ErbB4 Pathway for Synaptic Plasticity and Behaviors Associated with Psychiatric Disorders,” *Journal of Neuroscience*, vol. 32, no. 9, pp. 2988–2997, Feb. 29, 2012, ISSN: 0270-6474, 1529-2401. DOI: 10.1523/JNEUROSCI.1899-11.2012.

- [59] C. G. Perez-Garcia, “ErbB4 in Laminated Brain Structures: A Neurodevelopmental Approach to Schizophrenia,” *Frontiers in Cellular Neuroscience*, vol. 9, Dec. 18, 2015, ISSN: 1662-5102. DOI: 10.3389/fncel.2015.00472.
- [60] AmJ Psychiatry 146:5, May 1989 577, Dilip V. Jeste, M.D., and Robin E. Wragg, M.D., “Overview of depression and psychosis in Alzheimer’s disease,” *American Journal of Psychiatry*, vol. 146, no. 5, pp. 577–587, May 1989, ISSN: 0002-953X, 1535-7228. DOI: 10.1176/ajp.146.5.577.
- [61] S.-A. Bacanu, B. Devlin, K. V. Chowdari, S. T. DeKosky, V. L. Nimgaonkar, and R. A. Sweet, “Heritability of Psychosis in Alzheimer Disease,” *The American Journal of Geriatric Psychiatry*, vol. 13, no. 7, pp. 624–627, Jul. 2005, ISSN: 10647481. DOI: 10.1097/00019442-200507000-00011.
- [62] R. C. P. Go, R. T. Perry, H. Wiener, S. S. Bassett, D. Blacker, B. Devlin, and R. A. Sweet, “Neuregulin-1 polymorphism in late onset Alzheimer’s disease families with psychoses,” *American Journal of Medical Genetics Part B: Neuropsychiatric Genetics*, vol. 139B, no. 1, pp. 28–32, Nov. 5, 2005, ISSN: 1552-4841, 1552-485X. DOI: 10.1002/ajmg.b.30219.
- [63] D. Li, D. A. Collier, and L. He, “Meta-analysis shows strong positive association of the neuregulin 1 (NRG1) gene with schizophrenia,” *Human Molecular Genetics*, vol. 15, no. 12, pp. 1995–2002, Jun. 15, 2006, ISSN: 1460-2083, 0964-6906. DOI: 10.1093/hmg/ddl122.
- [64] R. Gao, M.-h. Ji, D.-p. Gao, R.-h. Yang, S.-g. Zhang, J.-j. Yang, and J.-c. Shen, “Neuroinflammation-Induced Downregulation of Hippocampal Neuregulin 1-ErbB4 Signaling in the Parvalbumin Interneurons Might Contribute to Cognitive Impairment in a Mouse Model of Sepsis-Associated Encephalopathy,” *Inflammation*, vol. 40, no. 2, pp. 387–400, Apr. 2017, ISSN: 0360-3997, 1573-2576. DOI: 10.1007/s10753-016-0484-2.
- [65] J. Wang, J. Huang, Y.-Q. Li, *et al.*, “Neuregulin 1/ErbB4 signaling contributes to the anti-epileptic effects of the ketogenic diet,” *Cell & Bioscience*, vol. 11, no. 1, p. 29, Dec. 2021, ISSN: 2045-3701. DOI: 10.1186/s13578-021-00536-1.

- [66] C.-G. Hahn, H.-Y. Wang, D.-S. Cho, *et al.*, “Altered neuregulin 1–erbB4 signaling contributes to NMDA \gt receptor hypofunction in schizophrenia,” *Nature Medicine*, vol. 12, no. 7, pp. 824–828, Jul. 2006, ISSN: 1078-8956, 1546-170X. DOI: 10.1038/nm1418.
- [67] N. Gajendran, J. P. Kapfhammer, E. Lain, M. Canepari, K. Vogt, W. Wisden, and H. R. Brenner, “Neuregulin Signaling Is Dispensable for NMDA- and GABAA-Receptor Expression in the Cerebellum In Vivo,” *Journal of Neuroscience*, vol. 29, no. 8, pp. 2404–2413, Feb. 25, 2009, ISSN: 0270-6474, 1529-2401. DOI: 10.1523/JNEUROSCI.4303-08.2009.
- [68] Y. Abe, H. Nawa, and H. Namba, “Activation of epidermal growth factor receptor ErbB1 attenuates inhibitory synaptic development in mouse dentate gyrus,” *Neuroscience Research*, vol. 63, no. 2, pp. 138–148, Feb. 2009, ISSN: 01680102. DOI: 10.1016/j.neures.2008.11.005.
- [69] Y.-J. Chen, M. Zhang, D.-M. Yin, *et al.*, “ErbB4 in parvalbumin-positive interneurons is critical for neuregulin 1 regulation of long-term potentiation,” *Proceedings of the National Academy of Sciences*, vol. 107, no. 50, pp. 21 818–21 823, Dec. 14, 2010, ISSN: 0027-8424, 1091-6490. DOI: 10.1073/pnas.1010669107.
- [70] A. R. Chaudhury, K. M. Gerecke, J. M. Wyss, D. G. Morgan, M. N. Gordon, and S. L. Carroll, “Neuregulin-1 and ErbB4 Immunoreactivity Is Associated with Neuritic Plaques in Alzheimer Disease Brain and in a Transgenic Model of Alzheimer Disease,” *Journal of Neuropathology & Experimental Neurology*, vol. 62, no. 1, pp. 42–54, Jan. 2003, ISSN: 0022-3069, 1554-6578. DOI: 10.1093/jnen/62.1.42.
- [71] W. Cui, J. Tao, Z. Wang, *et al.*, “Neuregulin1beta1 Antagonizes Apoptosis Via ErbB4-Dependent Activation of PI3-Kinase/Akt in APP/PS1 Transgenic Mice,” *Neurochemical Research*, vol. 38, no. 11, pp. 2237–2246, Nov. 2013, ISSN: 0364-3190, 1573-6903. DOI: 10.1007/s11064-013-1131-z.
- [72] K. M. Gerecke, J. M. Wyss, and S. L. Carroll, “Neuregulin-1 β induces neurite extension and arborization in cultured hippocampal neurons,” *Molecular and Cellular Neuroscience*, vol. 27, no. 4, pp. 379–393, Dec. 2004, ISSN: 10447431. DOI: 10.1016/j.mcn.2004.08.001.

- [73] L. E. Clarke, S. A. Liddelow, C. Chakraborty, A. E. Münch, M. Heiman, and B. A. Barres, “Normal aging induces A1-like astrocyte reactivity,” *Proceedings of the National Academy of Sciences*, vol. 115, no. 8, E1896–E1905, Feb. 20, 2018, ISSN: 0027-8424, 1091-6490. DOI: 10.1073/pnas.1800165115.
- [74] U. Andersson, D. Guo, B. Malmer, A. Bergenheim, T. Brännström, H. Hedman, and R. Henriksson, “Epidermal growth factor receptor family (EGFR, ErbB2, ErbB4) in gliomas and meningiomas,” *Acta Neuropathologica*, vol. 108, no. 2, Aug. 2004, ISSN: 0001-6322, 1432-0533. DOI: 10.1007/s00401-004-0875-6.
- [75] J. F. Donoghue, L. T. Kerr, N. W. Alexander, *et al.*, “Activation of ERBB4 in Glioblastoma Can Contribute to Increased Tumorigenicity and Influence Therapeutic Response,” *Cancers*, vol. 10, no. 8, p. 243, Jul. 25, 2018, ISSN: 2072-6694. DOI: 10.3390/cancers10080243. pmid: 30044378.
- [76] A. Naresh, W. Long, G. A. Vidal, *et al.*, “The ERBB4/HER4 Intracellular Domain 4ICD Is a BH3-Only Protein Promoting Apoptosis of Breast Cancer Cells,” *Cancer Research*, vol. 66, no. 12, pp. 6412–6420, Jun. 15, 2006, ISSN: 0008-5472, 1538-7445. DOI: 10.1158/0008-5472.CAN-05-2368. pmid: 16778220.
- [77] X. Liu, R. Bates, D.-M. Yin, *et al.*, “Specific Regulation of NRG1 Isoform Expression by Neuronal Activity,” *Journal of Neuroscience*, vol. 31, no. 23, pp. 8491–8501, Jun. 8, 2011, ISSN: 0270-6474, 1529-2401. DOI: 10.1523/JNEUROSCI.5317-10.2011.
- [78] J. Kronenberg, L. Merkel, S. Heckers, V. Gudi, H. M. Schwab, and M. Stangel, “Investigation of Neuregulin-1 and Glial Cell-Derived Neurotrophic Factor in Rodent Astrocytes and Microglia,” *Journal of Molecular Neuroscience*, vol. 67, no. 3, pp. 484–493, Mar. 2019, ISSN: 0895-8696, 1559-1166. DOI: 10.1007/s12031-019-1258-8.
- [79] Y. Tokita, H. Keino, F. Matsui, S. Aono, H. Ishiguro, S. Higashiyama, and A. Oohira, “Regulation of Neuregulin Expression in the Injured Rat Brain and Cultured Astrocytes,” p. 8,

- [80] Y. Hei, R. Chen, X. Yi, L. Wei, Q. Long, and W. Liu, “The Expression of Hippocampal NRG1/ErbB4 Correlates With Neuronal Apoptosis, but Not With Glial Activation During Chronic Cerebral Hypoperfusion,” *Frontiers in Aging Neuroscience*, vol. 10, p. 149, May 23, 2018, ISSN: 1663-4365. DOI: 10.3389/fnagi.2018.00149.
- [81] A. Alizadeh, S. M. Dyck, H. Kataria, G. M. Shahriary, D. H. Nguyen, K. T. Santhosh, and S. Karimi-Abdolrezaee, “Neuregulin-1 positively modulates glial response and improves neurological recovery following traumatic spinal cord injury,” *Glia*, vol. 65, no. 7, pp. 1152–1175, Jul. 2017, ISSN: 08941491. DOI: 10.1002/glia.23150.
- [82] M. Hutton, “The presenilins and Alzheimer’s disease,” *Human Molecular Genetics*, vol. 6, no. 10, pp. 1639–1646, Sep. 1, 1997, ISSN: 14602083. DOI: 10.1093/hmg/6.10.1639.
- [83] J. Sacha. “ImageJ Plugins Toolkit v.2.2.0.” (Jan. 18, 2020), [Online]. Available: <https://github.com/ij-plugins/ijp-toolkit/>.
- [84] “ImageJ User Guide.” (Feb. 22, 2021), [Online]. Available: <https://imagej.nih.gov/ij/docs/guide/146-30.html#sub:Set-Measurements>.
- [85] N. De Francesco. “Mean gray intensity, Integrated density and Raw integrated density - Image Analysis,” Image.sc Forum. (Apr. 22, 2017), [Online]. Available: <https://forum.image.sc/t/mean-gray-intensity-integrated-density-and-raw-integrated-density/4983> (visited on 03/05/2021).
- [86] D. Arthur and S. Vassilvitskii, “K-Means++: The advantages of careful seeding,” ser. Proc. of the Annu. ACM-SIAM Symp. on Discrete Algorithms, vol. 8, Jan. 2007, pp. 1027–1035. DOI: 10.1145/1283383.1283494.
- [87] “R2 Genomics Analysis and Visualization Platform.” (Mar. 4, 2021), [Online]. Available: <http://hgserver1.amc.nl/cgi-bin/r2/main.cgi> (visited on 04/03/2021).
- [88] J. J. Rodríguez, M. Olabarria, A. Chvatal, and A. Verkhratsky, “Astroglia in dementia and Alzheimer’s disease,” *Cell Death & Differentiation*, vol. 16, no. 3, pp. 378–385, Mar. 2009, ISSN: 1350-9047, 1476-5403. DOI: 10.1038/cdd.2008.172.

- [89] A. Grubman, G. Chew, J. F. Ouyang, *et al.*, “A single-cell atlas of entorhinal cortex from individuals with Alzheimer’s disease reveals cell-type-specific gene expression regulation,” *Nature Neuroscience*, vol. 22, no. 12, pp. 2087–2097, Dec. 2019, ISSN: 1097-6256, 1546-1726. DOI: 10.1038/s41593-019-0539-4.
- [90] H. Mathys, J. Davila-Velderrain, Z. Peng, *et al.*, “Single-cell transcriptomic analysis of Alzheimer’s disease,” *Nature*, vol. 570, no. 7761, pp. 332–337, Jun. 2019, ISSN: 0028-0836, 1476-4687. DOI: 10.1038/s41586-019-1195-2.
- [91] J. Jiang, C. Wang, R. Qi, H. Fu, and Q. Ma, “scREAD: A Single-Cell RNA-Seq Database for Alzheimer’s Disease,” *iScience*, vol. 23, no. 11, p. 101769, Nov. 2020, ISSN: 25890042. DOI: 10.1016/j.isci.2020.101769.
- [92] Z. Xu, J. Jiang, G. Ford, and B. D. Ford, “Neuregulin-1 is neuroprotective and attenuates inflammatory responses induced by ischemic stroke,” *Biochemical and Biophysical Research Communications*, vol. 322, no. 2, pp. 440–446, Sep. 2004, ISSN: 0006291X. DOI: 10.1016/j.bbrc.2004.07.149.
- [93] Z. Xu and B. D. Ford, “Upregulation of erbB receptors in rat brain after middle cerebral arterial occlusion,” *Neuroscience Letters*, vol. 375, no. 3, pp. 181–186, Mar. 2005, ISSN: 03043940. DOI: 10.1016/j.neulet.2004.11.039.
- [94] M. A. Schumacher, M. Hedl, C. Abraham, *et al.*, “ErbB4 signaling stimulates pro-inflammatory macrophage apoptosis and limits colonic inflammation,” *Cell Death & Disease*, vol. 8, no. 2, e2622–e2622, Feb. 2017, ISSN: 2041-4889. DOI: 10.1038/cddis.2017.42.
- [95] K. M. Gerecke, J. M. Wyss, I. Karavanova, A. Buonanno, and S. L. Carroll, “ErbB transmembrane tyrosine kinase receptors are differentially expressed throughout the adult rat central nervous system,” *The Journal of Comparative Neurology*, vol. 433, no. 1, pp. 86–100, Apr. 23, 2001, ISSN: 0021-9967, 1096-9861. DOI: 10.1002/cne.1127.

- [96] G. M. Shankar, S. Li, T. H. Mehta, *et al.*, “Amyloid- β protein dimers isolated directly from Alzheimer’s brains impair synaptic plasticity and memory,” *Nature Medicine*, vol. 14, no. 8, pp. 837–842, Aug. 2008, ISSN: 1078-8956, 1546-170X. DOI: 10.1038/nm1782.
- [97] S. Jo, O. Yarishkin, Y. J. Hwang, *et al.*, “GABA from reactive astrocytes impairs memory in mouse models of Alzheimer’s disease,” *Nature Medicine*, vol. 20, no. 8, pp. 886–896, Aug. 2014, ISSN: 1078-8956, 1546-170X. DOI: 10.1038/nm.3639.
- [98] S. Mederos and G. Perea, “GABAergic-astrocyte signaling: A refinement of inhibitory brain networks,” *Glia*, vol. 67, no. 10, pp. 1842–1851, Oct. 2019, ISSN: 0894-1491, 1098-1136. DOI: 10.1002/glia.23644.
- [99] H. Zhang, L. Zhang, D. Zhou, *et al.*, “Ablating ErbB4 in PV neurons attenuates synaptic and cognitive deficits in an animal model of Alzheimer’s disease,” *Neurobiology of Disease*, vol. 106, pp. 171–180, Oct. 2017, ISSN: 09699961. DOI: 10.1016/j.nbd.2017.07.001.
- [100] Y.-w. Zhang, R. Wang, Q. Liu, H. Zhang, F.-F. Liao, and H. Xu, “Presenilin/ gamma-secretase-dependent processing of beta-amyloid precursor protein regulates EGF receptor expression.,” *Proceedings of the National Academy of Sciences of the United States of America*, vol. 104, no. 25, pp. 10 613–10 618, Jun. 19, 2007, ISSN: 0027-8424 1091-6490. DOI: 10.1073/pnas.0703903104. pmid: 17556541.
- [101] C. Y. Thomas, M. Chouinard, M. Cox, *et al.*, “Spontaneous activation and signaling by overexpressed epidermal growth factor receptors in glioblastoma cells,” *International Journal of Cancer*, vol. 104, no. 1, pp. 19–27, Mar. 10, 2003, ISSN: 0020-7136, 1097-0215. DOI: 10.1002/ijc.10880.
- [102] P. S. Ritch, S. L. Carroll, and H. Sontheimer, “Neuregulin-1 enhances survival of human astrocytic glioma cells,” *Glia*, vol. 51, no. 3, pp. 217–228, Aug. 15, 2005, ISSN: 0894-1491, 1098-1136. DOI: 10.1002/glia.20197.
- [103] Y. Hama, I. Yabe, K. Wakabayashi, *et al.*, “Level of plasma neuregulin-1 SMDF is reduced in patients with idiopathic Parkinson’s disease,” *Neuroscience Letters*, vol. 587, pp. 17–21, Feb. 2015, ISSN: 03043940. DOI: 10.1016/j.neulet.2014.12.024.

- [104] C. Depboylu, M. Höllerhage, S. Schnurrbusch, P. Brundin, W. H. Oertel, A. Schrattenholz, and G. U. Höglinger, “Neuregulin-1 receptor tyrosine kinase ErbB4 is upregulated in midbrain dopaminergic neurons in Parkinson disease,” *Neuroscience Letters*, vol. 531, no. 2, pp. 209–214, Dec. 2012, ISSN: 03043940. DOI: 10.1016/j.neulet.2012.10.050.
- [105] A. Sharif and V. Prevot, “ErbB receptor signaling in astrocytes: A mediator of neuron-glia communication in the mature central nervous system,” *Neurochemistry International*, vol. 57, no. 4, pp. 344–358, Nov. 2010, ISSN: 01970186. DOI: 10.1016/j.neuint.2010.05.012.

Curriculum vitae

PERSONALIEN

Vor- und Nachname: Simon Uwe Mangold

Geburtsdatum: 25.04.1989

Geburtsort: Villingen-Schwenningen

Familienstand: Ledig

SCHULISCHER WERDEGANG

1996 - 2000: Grundschule Vöhrenbach

2000 - 2008: Gymnasium Furtwangen

Abitur: 24.06.2008

UNIVERSITÄRER WERDEGANG

WS 2015/2016 Beginn des Studiums der Humanmedizin an der
Universität Heidelberg, Medizinische Fakultät Mannheim

14.09.2017 1. Abschnitt der Ärztlichen Prüfung

2017 - 2021 Hauptstudium

07.10.2021 2. Abschnitt der Ärztlichen Prüfung

Danksagung

Herrn Dr. David Bouvier und Herrn Dr. Tony Heurtaux danke ich für die hervorragende fachliche Einarbeitung, die praktische Unterstützung im Labor und die ausgezeichneten Möglichkeiten die Untersuchungen dort auszuarbeiten.

Besonderen Dank schulde ich Prof. Dr. med. Michel Mittelbronn der Universität Luxemburg, LNS, der mich auf besondere Art auf meinem Wege des Studiums und der akademischen Reife begleitet hat. Prof. Dr. med. Christian Schultz der Medizinischen Fakultät Mannheim der Universität Heidelberg danke ich für die Unterstützung vor Ort in Mannheim. Ich danke Dr. rer. nat. Julian Schlegel vom DKFZ Heidelberg und Gero Gothe für die fruchtbare Zusammenarbeit bei der Erstellung der digitalen Auswertung.

Für die motivierende, finanzielle Unterstützung durch das Promotionsstipendium möchte ich der medizinischen Fakultät Mannheim meinen Dank aussprechen.

Weiter möchte ich mich bei meinen Eltern, Freunden und meiner Partnerin für die fachliche und persönliche Unterstützung bedanken.